


# Recent advances in lithium-sulfur batteries using biomass-derived carbons as sulfur host

 The corrections made in this section will be reviewed and approved by a journal production editor.

Almudena Benítez<sup>a,\*\*</sup> [q62beta@uco.es](mailto:q62beta@uco.es), Juan Amaro-Gahete<sup>b</sup>, Yu-Chuan Chien<sup>c</sup>, Álvaro Caballero<sup>a</sup>, Julián Morales<sup>a</sup>, Daniel Brandell<sup>c,\*</sup> [daniel.brandell@kemi.uu.se](mailto:daniel.brandell@kemi.uu.se)

<sup>a</sup>Departamento de Química Inorgánica e Ingeniería Química, Instituto Universitario de Nanoquímica (IUNAN), Facultad de Ciencias, Universidad de Córdoba, 14071, Córdoba, Spain

<sup>b</sup>Departamento de Química Orgánica, Instituto Universitario de Nanoquímica (IUNAN), Facultad de Ciencias, Universidad de Córdoba, 14071, Córdoba, Spain

<sup>c</sup>Department of Chemistry - Ångström Laboratory, Uppsala University, Box 538, SE-751 21, Uppsala, Sweden

 \*Corresponding author.

\*\*Corresponding author.

## Abstract

While biomass waste is generated in abundance, these materials and their production processes are generally environmentally friendly, low cost, non-hazardous and easily scalable. These advantages position biomass materials as excellent candidates to solve problems of environmental pollution, primarily by substitution of less sustainable counterparts. This also applies to energy storage systems such as batteries, where several components have large environmental impacts. Lithium-Sulfur batteries have, in this context, been extensively researched to cope with the growing energy needs, and are expected to foresee a growing commercialization. Specifically, advances in the use of renewable cathode materials for Li-S batteries is a field that has been widely addressed in recent years, with carbonaceous materials (C) and/or activated carbons (AC), obtained from biomass, being intensively studied. We here reviewed this field through a classification and discussion of carbonaceous materials from natural waste according to the type of biomass: (1) woody, (2) herbaceous and agricultural, (3) aquatic, (4) animal and human, and (5) contaminated and industrial biomass waste materials. In addition, all porous carbons or activated carbons used as sulfur hosts have been exhaustively evaluated in terms of origin, synthesis parameters, physical properties, and electrochemical performance in Li-S batteries. The purpose is to provide a general description of the progress in the preparation of carbons from biomass resources, examine the textural and electrochemical properties of these materials focusing on the last decade, and also to present an outlook for future research in this developing area.

## Keywords:

Activated carbon, Biomass, Li-S batteries, Sustainable materials, Sulfur hosts, Bio-waste

## 1 Introduction

From the discovery of fire to modern civilization, energy has played a fundamental role in our lives. In fact, its importance has reached such an extent that in today's society, the availability of energy is strongly linked to well-being, economy, health, and even life expectancy. However, the global energy system is still dominated by non-renewable fossil fuels (oil, coal and natural gas) and nuclear energy [1] which are finite and have limited reserves. We must therefore consider how the next generations will sustain themselves energetically in the future. Although this has been known for centuries, humanity has not yet been able to develop new technologies with the same power as the traditional ones [2].

It should be noted that coal has generally been the resource that has come to the rescue for energy throughout modern civilizations. However, this resource is unsustainable since the amount of carbon that needs to be stored to meet current energy demands is enormous, and, so far, the Carbon Capture and Storage (CCS) is not an effective enough process [3]. The environmental problems associated with the use of these types of fossil fuels, due to their combustion, are well known: generation of pollutants such as sulfur oxides (SO<sub>x</sub>), nitrogen oxides (NO<sub>x</sub>), carbon monoxide, carbon dioxide (an important greenhouse gas or GHG), hydrocarbons, and particles that affect air quality, leading to photochemical smog, soot and acid rain, and therefore posing a risk to the health of humans, animals and plants [4]. Nuclear energy in turn, in addition to safety concerns exemplified by Chernobyl and Fukushima, presents the serious problem of the management of spent fuel, which has still to be resolved [5]. Consequently, development of renewable energy and energy savings are necessary to avoid environmental disasters.

During the next decade, Europe faces one of the greatest environmental and sustainability challenges to meet the 2030 agenda [6]. The European Commission, the Climate Change Convention (Paris Agreement) and the United Nations (Sustainable Development Goals – SDGs) have established different plans and actions to combat climate change more effectively than in the past 40 years [7,8]. The common objective of these associations is to eradicate persistent problems in both Europe and worldwide, such as energy dependence, loss of biodiversity, environmental impact, and health risks, amongst others. For all these reasons, the ecological transition is a key element to achieve the goals of 2030 and beyond. Specifically, ten years are available to reduce greenhouse gas emissions by more than 20 % compared to 1990, generate 70 % of electricity with renewable resources, ensure that at least 35 % of final energy consumption comes from renewables, and improve energy efficiency by 35 %. Additionally, in 2050 it is intended that gas emissions be reduced by 90 % compared to 1990, and that the electrical system is 100 % renewable.

Hence, one of the most important pillars of the ecological transition, but not the only one, is renewable energy. There is a wide spread of renewable resources in the local energy system in different EU member states. In 2018, for example, Sweden displayed a final gross energy consumption with around 55 % renewables, while several countries had less than 10 % [9]. Largely, the technologies used to fulfil the needs of energy services are determined by the availability of resources currently available. A more widespread electrification, and electricity generation from renewable resources, are critical for a more sustainable energy system. Complementary to this, making use of biomass resources in the form of materials or as energy sources will also serve to lower the carbon footprint of societies.

Biomass refers to the amount of living matter that organisms possess, including plants, animals, and microorganisms [10]. From a more fundamental point of view, biomass is composed of cellulose, hemicellulose, lignin, sugars, and proteins [11]. Overall, biomass energy comes from the sun and is therefore considered a renewable energy source. In the case of plants, their chlorophyll captures energy through the photosynthesis process and converts carbon dioxide (CO<sub>2</sub>) from the atmosphere and water from the ground into carbohydrates, to form organic matter. If these carbohydrates are burned, they return to carbon dioxide and water, while releasing the energy they contain. In this way, biomass in itself works as a kind of “battery” which stores solar energy. Every year, plants convert 4500 EJ of solar energy and 120 Giga-tonnes of carbon from the atmosphere into biomass - eight times as much as the global energy demand [12]. Meanwhile, animals and microorganisms decompose part of the plant biomass, return it to the atmosphere and thereby closing the carbon cycle [13], while the rest of the biomass can be used to satisfy human needs. Currently, biomass accounts for 8–15 % of the world energy supplies as heat, electricity and fuels for transportation [14].

If grown and harvested sustainably, biomass as an energy source can have multiple benefits for the environment in comparison to alternatives: mitigating climate change and the greenhouse effect, reducing acid rain, preventing soil erosion and contamination of water sources, reducing the pressure caused by urban waste, enriching wildlife habitats, and helping to maintain human health and ecosystem stability. However, the main problems of this resource are the relatively low power and energy efficiency obtained during conversion. Thereby, large volumes are necessary to produce power. This drawback is correlated to detriments such as deforestation, habitat degradation, and loss of biodiversity.


Globally, the continuous growth of CO<sub>2</sub> emissions remains a major concern in the transportation sector [15]. Thus, the efficient use of renewable energy sources and the replacement of internal combustion engines with electric motors for the development of sustainable vehicles, such as hybrid vehicles (HEV), plug-in hybrid vehicles (PHEV) and, ultimately, fully electric vehicles (EV), are crucial objectives for our society [16]. All these vehicles require an on-board power source for the electric engine [17]. Among the possible energy storage options, the most suitable today are rechargeable batteries, portable devices that can deliver the stored chemical energy as electrical energy with high conversion efficiency and without emissions. Lithium-based batteries are particularly attractive thanks to their merits such as high energy density, low self-discharge rate, and long lifespan [18,19]. While recent years have seen tremendous progress in the performance of commercial lithium-ion batteries (LIBs), they are still in many senses notable to compete with conventional fuel-based vehicles [20,21]. Moreover, the cost and environmental problems of some of the components of LIBs constitute drawbacks in the application of large-scale electric vehicles [22].

A very promising system constituting an alternative to LIBs is the lithium-sulfur battery (Li-S) [23–25], which possesses a theoretical specific capacity of 1672 mAh g<sup>-1</sup> and a working voltage of 2.1 V [26]. This technology leads to a high theoretical gravimetric energy density of 2552 Wh kg<sup>-1</sup>, which is almost one order of magnitude greater than conventional LIBs [27]. In addition to the high theoretical capacity that sulfur supplies, it is also an abundant element in nature and is considered an environmentally benign element compared to some transition metals used in the LIBs [28].

Li-S batteries operates by the electrochemical reactions of a Li-metal anode and a sulfur-based cathode. The ultimate reaction product during battery discharge is Li<sub>2</sub>S, but sulfur undergoes a cascade of complex reactions during its reduction, forming a range of lithium polysulfides. Some of these are highly soluble in the ether-based electrolytes (e.g., DME:DOL) normally employed, and which function comparatively well with the Li-metal electrode. However, the solubility of the cathode components leads to capacity degradation and rapid self-discharge through a so called “redox shuttle effect”. Due to that sulfur is electronically insulating, it also needs a carbon matrix for electronic conduction within the electrode. If tailoring this matrix properly, it can also retain the cathode material species, and thereby mitigating these problems – at least temporarily.

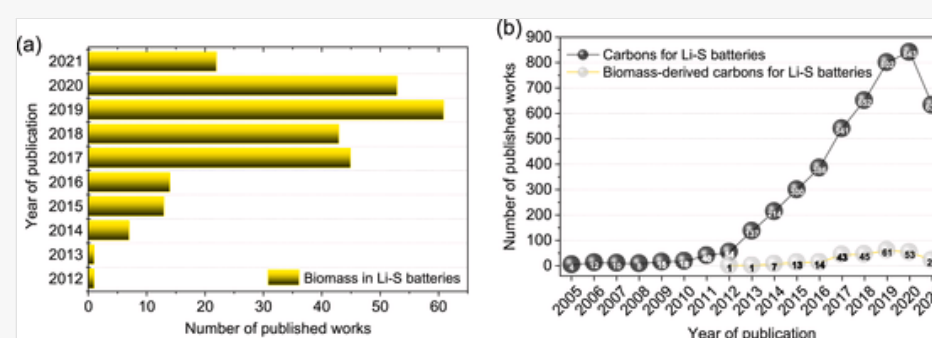
In recent years, Li-S batteries have received a great deal of attention, and significant advances having been made in their performance. However, the progress achieved has not yet been translated to an industrial scale, and large-scale commercialization has seen difficulties. Among the problems encountered, the most severe are the difficulty of operating at high current densities during a high number of cycles, limited values of S loading in the electrode, a coulombic efficiency far from 100 % (hardly above 98 %), and a strong dependence on LiNO<sub>3</sub> additives in the electrolyte to stabilize the Li-metal electrode. Moreover, there are only limited useful examples of utilizing commercially available carbon materials or easily synthesized such from abundant and sustainable sources, while more attention also needs to be paid to the safety issues of the batteries [29]. The use of biomass-derived carbons as sulfur hosts in the positive electrode of Li-S batteries began in 2011, in activated carbons obtained from pig bones [30]. A few years later, activated carbons obtained from agricultural residues began to be used [31,32].

In 2009, Nazar's group pioneered the development of highly ordered mesoporous carbons to encapsulate sulfur, thereby improving the capacity and life-span of these batteries [33]. Five years later, biomass began to be suggested as a first-class matrix to host sulfur and the number of publications in this line increased significantly. Fig. 1 (a) shows the growing trend in the study of materials derived from biomass into improving the conductivity of sulfur, trapping the polysulfides, enhancing the electrochemical performance in terms of both energy supplied and in the number of cycles, and advancing the scalability and sustainability of Li-S batteries. In Fig. 1 (b), the number of publications on carbons used in Li-S batteries is compared, grouped into two blocks: one related to biomass-derived carbons and the other to the rest of carbons. As is obvious, the number related to biomass-derived carbons is smaller than that dedicated to other sources of carbons, but it maintains a clear progressing trend.

 Images are optimised for fast web viewing. Click on the image to view the original version.

alt-text: Fig. 1

Fig. 1



(a) Bibliometric analysis of the topic 'biomass in lithium-sulfur batteries' and (b) comparison between the use of carbons and biomass-derived carbons for Li-S batteries, according to the Web of Science (WOS) database.

Replacement Image: Figure 1.tif

Replacement Instruction: Replace image requested

This increase in publications, especially outstanding in the last five years, has led to the appearance of several works focused on the synthesis of biomass-derived carbon materials as carbon hosts for sulfur [34,35], multi-functional separators and interlayers, and for the preparation of bio-derived polymers as binders and solid electrolytes [36]

in Li-S batteries. In other contributions, the influence of properties such as the porous structure [37,38], or doping with N [39] have been studied. The economic benefits of these approaches have also been pointed out [11]. Moreover, other reviews have pointed out the use of biomass in other energy storage systems such as Li/Na batteries [40] or supercapacitors [41], thus providing a wider overview.

The purpose of this review is to summarize the key aspects of biomass-derived activated carbons as sulfur hosts, and to analyse the latest advances of their application in Li-S batteries. Here we adopt a novel approach with the aim of facilitating access to information for researchers working in this field by a detailed classification of activated carbons from biomass based on their biological diversity, source, and origin. Special attention has been paid to the classification of biomass sources following the organization suggested by Vassilev [42–45]. We conclude with a perspective, highlighting the strategies and challenges in development of biomass-based Li-S batteries to achieve the optimization of these devices, and their long-awaited commercialization.

## 2 Biomass-derived activated carbons


Due to their merits of abundance, renewability, and low-cost properties, biomass and related by-products are considered as potential precursors for activated carbon materials in energy storage systems. This section will address the most important aspects of activated carbons obtained from biomass. First, a classification of biomass sources will be carried out, followed by a discussion of the manufacture of activated carbons. Next, the most used synthesis methods will be summarized as well as the main properties they present. Thereafter, we turn to the transformation of the materials based on activated carbons into suitable matrices to provide conductivity in the cathode of Li-S batteries, together with their ability to trap polysulfides (LiPSs) for mitigating the redox shuttle effect.

### 2.1 Biomass sources

Over the years, numerous efforts have been made to replace fossil fuels with biomass for energy conversion. As is well known, this alternative allows reducing the problems caused by greenhouse gases, while favouring the development of bioenergy. In addition to being renewable, natural, with huge availability, and a relatively cheap source of energy, bioenergy possesses benefits of being potentially CO<sub>2</sub> neutral in conversion and climate change. However, the composition of the biomass is highly variable depending on the nature of the chosen starting raw material, and this will ultimately determine the chemical composition and resulting properties of the carbon-based materials obtained from it.

Biomass are biogenic organic-inorganic resources produced by natural processes, which result in materials highly enriched in Mn > K > P > Cl > Ca > (Mg, Na) > O > moisture > volatile matter, and to a lesser extent in H, and with a much lower content of ash, Al, C, Fe, N, S, Si and Ti in comparison with coals [42]. Knowledge of the composition and physicochemical properties of the generated biofuels from natural biomass is essential for their environmentally safe use in a wide number of applications. Biomass varieties as solid fuels have been classified by Vassilev et al. [43] based on biological diversity, source, and phase-mineral composition (Fig. 2): (1) woody, (2) herbaceous and agricultural, (3) aquatic, (4) animal and human, (5) contaminated and industrial biomass wastes (semi-biomass), and (6) biomass mixtures.

- (1) Woody biomass from forestlands and extensive plantations is one of the most abundant organic sources in the world, whose sustainable production ( $5.64 \times 10^{10}$  tons of carbon per year) [46,47] may promote the development of key energy commodities through the advancement of modern biorefineries associated with a future bio-based economy [48]. These types of biomass resources, produced on a large scale and composed mainly of cellulose (30–50 %), hemicellulose (23–32 %) and lignin (15–25 %) [49], are considered candidates to potentially cover 10–40 % of the world's primary energy consumption in 30 years' time [50]. The chemical composition and the rigid physical structure of woody biomass makes it highly efficient in terms of production, transportation, and energy. As a second-generation biofuel, woody biomass has received special industrial attention for its cost-effective conversion and application in chemical production, agri-food and paper industry, construction materials, and other value added products, although currently only 5–10 % contributes to the global energy supply [51–53].
- (2) Agricultural residues (flowers, plants and straws) and agri-food waste (shells, husks, pits, sugars, vegetable oil and other edible compounds) constitute the group of herbaceous and agricultural biomass. This type of biomass represents the source with the highest content of lignocellulosic material with an annual production of 300 million tons per year in the United States and 250 million tons/year in Europe, which renders it a great potential for chemical, bioenergy, or biofuel conversion [54–56].
- (3) The marine or freshwater aqueous biomass is a group within second and third generations of biofuels, consisting mainly of easily biodegradable and non-toxic macro/microalgae that offer great efficiency for the production of biofuels and biogas compared to land crops [57–59]. Algae as a biomass resource can be produced continuously due to its high growth rate, reaching hundreds of tons per day from the natural environment, making it an organic matter source of interest in the bioenergy sector [45,60,61]. Microalgae are raw materials, extracted from seawater or wastewater, with photosynthetic properties to produce renewable biofuels, including anaerobic digestion of methane, and the generation of biodiesel or photoproduction of hydrogen [62]. The biomass from microalgae can be doubled after 24 h and is mainly enriched in lipids ( $4.5\text{--}7.5 \text{ ton ha}^{-1} \text{ y}^{-1}$ ), jatropha ( $4.1 \text{ ton ha}^{-1} \text{ y}^{-1}$ ), and soybeans ( $0.4 \text{ ton ha}^{-1} \text{ y}^{-1}$ ), with a low content of recalcitrant lignin, contributing to an environmentally and economically sustainable biorefinery [63].
- (4) The set of human and animal biomass refers to the remains of bones, fertilizers, faeces, silk or ashes that play an important role in the heterogeneity and contribution of nutrients within the ecosystem [64]. In this group, fungi and bacterial residues are included since they are microorganisms that can live in diverse environments. The estimate of animal biomass production worldwide is 2 Gt, which is a significantly lower figure compared to plants, bacteria and fungi (532 Gt) [65]. The animal biomass content varies between different terrestrial ecosystems from  $30.400 \text{ kg m}^{-3}$  in the East African savanna to  $20.000 \text{ kg m}^{-3}$  in the central Amazonian rainforest [66,67]. Although the percentage of this type of biomass is not very high, its contribution and implication in terms of quality, quantity, and distribution of nutrients within the biogeochemical cycle for the health and function of the ecosystem are of high importance.
- (5) Municipal solid waste, sewage, paper pulp sludge, waste papers, refuse-derived fuel, or household waste are considered as a semi-biomass within the group of industrial and contaminated biomass waste. The current exponential industrial growth has caused the generation of an enormous amount of industrial waste (more than 400 million tons per year in China), generally originating from sewage plants, pharmaceutical companies, or drug manufacturing [68]. It is not considered pure biomass due to organic and inorganic pollutants, and natural or industrial post-epigenetic components, such as dust particles, metals, plastics, charcoal, and glass or paints, which appear after the processing [69].
- (6) The additional category of biomass mixture is constituted by biomass whose composition is a blend of the previous varieties and, therefore, it is controversial to classify it in a specific group of biomasses such as those previously mentioned.

 Images are optimised for fast web viewing. Click on the image to view the original version.

alt-text: Fig. 2



Classification of the different sources of biomass for energy according to their origin.


Replacement Image: Figure 2.tif

Replacement Instruction: Replace image requested

## 2.2 Background of activated carbons

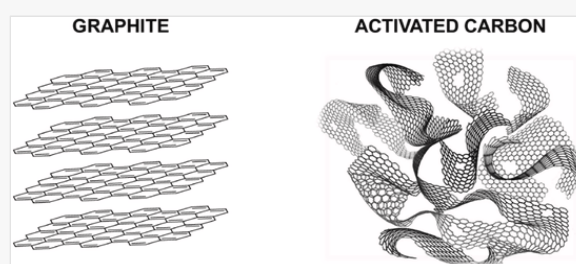
Activated carbon (AC) refers to a set of materials with a non-graphitic amorphous composition with a well-developed internal tridisperse pore structure of micro (<2 nm), meso (2–50 nm) and macro-pores (>50 nm), and a wide variety of surface chemical functional groups, making them highly versatile compounds that can be used in a multitude of applications [70]. According to its physical characteristics, AC can be classified as granulated (GAC), powdered (PAC), extracted (EAC), pellet, and other activated carbons. Regarding chemical properties, ACs are globally recognized as materials with high porosity, large surface area, enormous degree of surface reactivity, remarkable physicochemical stability, and high mechanical strength.

ACs are generated from combustion, partial combustion, or thermal decomposition of carbon-based precursor, but which undergoes structural changes both at the molecular and morphological levels. Although ACs are considered as processed amorphous carbon-based materials, they in fact possess a microcrystalline structure. However, they have a greater interlayer space and disorder of the aromatic sheet stacks compared to crystalline graphite (Fig. 3). Carbon is the element present in the highest proportion in ACs, contributing with a percentage of 85–95 % or above, while the remaining composition corresponds to inorganic ash constituents and heteroatoms such as hydrogen, nitrogen, sulfur and oxygen, derived from the starting raw material or from a subsequent activation process or other preparation procedures. Therefore, the degree of disorder in the microcrystallite layers is caused by the presence of these heteroatoms and the defects such as vacant lattice sites. Generally, all materials of a carbonaceous nature can be transformed into ACs, although the properties of the final product will depend on the chosen starting raw material as well as the conditions and type of activation process. During carbonization, the non-carbonaceous elements are eliminated as volatile compounds by decomposition of the raw material, leaving the residual carbon atoms grouped into stacks of aromatic sheets which become cross-linked in a random arrangement. Thus, free interstices between the sheets are created and could be filled with tarry matter and decomposition products as by-products of the pyrolysis process, or simply blocked by non-ordered carbon. These interstices are mainly responsible for the generation of pores in the AC structures, although the char generated post-carbonization has a poorly developed porous structure. The activation process of the char results in the interstices between the aromatic sheets being cleared, and in formation of randomly distributed pores with different shapes and sizes, providing ACs with an extended surface area [71,72].

 Images are optimised for fast web viewing. Click on the image to view the original version.

alt-text: Fig. 3

Fig. 3



Illustrative representation of three-dimensional crystal lattice of graphite and amorphous activated carbon.

Replacement Image: Figure 3.tif

Replacement Instruction: Replace image requested

ACs have been used for many centuries in the form of charcoal produced from wood carbonization. In fact, Egyptians and Sumerians already applied it for medical purposes and as a purifying agent as early as the period 3750 to 1500 BCE [73].

Based on their excellent performances and economic profitability, these materials have been applied in different industrial areas showing versatility for especially the effective adsorption of organic and inorganic pollutants in aqueous media, gaseous compounds to eliminate industrial volatile substances, or odours and impurities in municipal environments. The first large-scale AC applications for wastewater [74] took place in the mid-19th century when installations of wood charcoal filters were implemented in many sewer ventilation systems to remove residual odours, and similarly for the design of face masks in chemical industries to prevent inhalation of mercury vapours [75]. Currently, they are increasingly being used in the control of air pollution, gas separation and purification, energy storage/conversion, the pharmaceutical sector for the treatment of drugs, recovery of different metals in the hydrometallurgical industry, agri-food industry for food processing, and the field of catalysis as efficient supports for catalysts [76–82]. In fact, 12.800.000 tons of AC were consumed worldwide in 2015, mainly produced from mineral carbons and lignocellulose contained in wood and agricultural biomass [83].


Depending on the precursor used for the generation of AC, the existence of heteroatoms such as oxygen, nitrogen, sulfur or halogens, chemically bonded in the form of functional groups or individual atoms in the structure, is very common. Oxygen is the predominant element in these materials, existing as a surface carbon-oxygen group that in some cases contributes to acidic properties (carboxylic acid, carboxylic anhydride, lactone, and phenolic hydroxyl) and in other cases, basic characteristics (carbonyl,

ethers and quinones). However, the acidity and surface basicity of the AC can be modified by thermal or chemical methods in order to obtain higher performance for a specific function. AC acid treatments are generally based on chemical oxidations whose main purpose is the elimination of heavy metals in aqueous solutions due to the chelating capacity of the acidic functional groups, capable of forming complexes and retaining these species on the surface of the material. As a disadvantage, it should be mentioned that these procedures lead to a decrease in the specific surface area and pore volume, as well as the generation of toxic gases such as  $\text{SO}_2$  or  $\text{NO}_2$  when  $\text{H}_2\text{SO}_4$  or  $\text{HNO}_3$  are used. On the other hand, the basicity of AC is tied to the presence of resonant  $\pi$ -electrons on carbon aromatic rings, and basic surface functionalities that attract and bind protons. The incorporation of nitrogen-containing functional groups (amide, imide, pyrrolic, pyridinic, lactame) with activating reagents such as  $\text{NH}_3$ ,  $\text{HNO}_3$  or amines, is the best-known procedure to increase the basicity of ACs, showing high efficiency for the capture of organic compounds [84,85].

A wide variety of carbon precursors have been reported in the scientific literature which have been selected due to their availability, low economic cost, environmentally non-hazardous properties, low degradation upon storing, high content of fixed carbon, and minimal amount of ash produced. In addition, the physicochemical properties of the resulting AC may be influenced by the precursor used in the preparation, the activation methods, the synthesis time, the impregnation conditions and parameters used, the carbonization temperature, or inorganic impurities that will affect the textural, surface and structural properties.

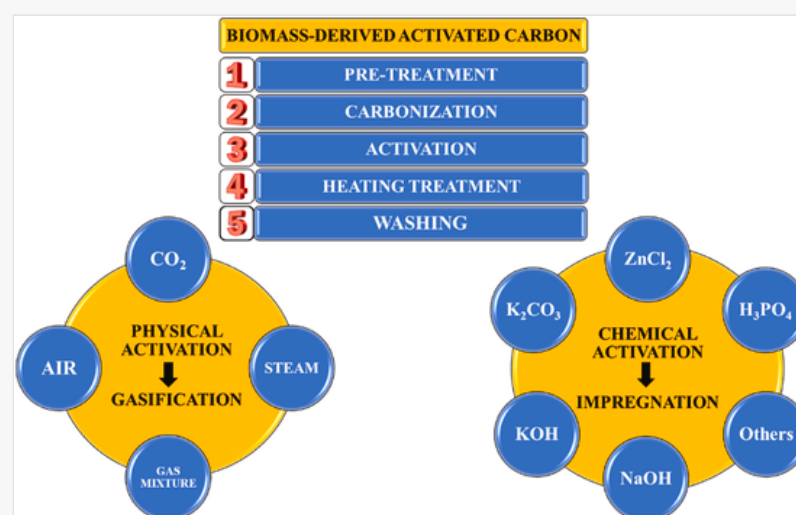
Biomass precursors for AC generation are the optimal choice from an environmental pollution point of view, as well as availability of raw materials at low-cost. The synthesis of AC from natural biomass is industrially scalable and has enormous benefits. These include the inhibition of carbon dioxide and methane production, renewability and ecological suitability, improved economic efficiency of the value-added process, and the possibility of designing environmental friendly materials that can easily be integrated into the carbon biological cycle with interesting and potentially applicable characteristics in different research areas [86–88].

The design of biomass-derived activated carbon with the desired pore network distribution, large pore volume, extensive surface area and high carbon content is based on the general synthesis process shown in Fig. 4, which consists of the following steps: 1) pre-treatment, 2) carbonization, 3) activation, 4) heat treatment, and 5) washing. Each of these stages can be carried out isolated, or together with another, to optimize the procedure and making it sustainable depending on the biomass precursor used, the structural capacity of the raw material to assimilate to the reaction conditions, and the desired physical-chemical properties of the resulting AC.

 Images are optimised for fast web viewing. Click on the image to view the original version.

alt-text: Fig. 4

Fig. 4



General preparation procedure and activation methods of biomass-derived activated carbons.

**Replacement Image:** Figure 4.tif

**Replacement Instruction:** Replace image requested

The pre-treatment of natural biomass refers to the preliminary stages carried out on the raw material. Crushing, milling and sieving are examples that influence the appropriate particle size of the AC, and that affect subsequent handling and the intended application. The commonly performed sieving generates particle sizes from a few microns to 1–2 mm that are suitable for further processing and activation of the material [89,90]. The effect of particle size on surface area and pore volume has been reported, demonstrating a trend regarding the increase in specific surface area and volume of mesopores with smaller particle size, together with incorporation of a slight percentage of microporosity in ACs [91,92].

Carbonization is a process for obtaining charcoal from a starting material by thermal decomposition that is carried out to eliminate volatile matter and non-carbonaceous species (H, N, O and S), thus enriching the fixed carbon content for activation purposes. Selected carbonization parameters such as temperature, heating rate, presence of inert atmosphere, and residence time play a significant role for the final product. The carbonization temperature renders the most significant effect, usually oscillating in an optimal range of 400–600 °C. An exponential temperature rise initially causes decomposition of the biomass precursor and then generation of the carbonaceous material. Normally, temperature values above 600–700 °C generate an increase in released liquids and gases, as well as production of a higher percentage of ash. High temperatures thus promote an increase in the content of fixed carbon and a lower amount of volatile matter, resulting in an improvement in char quality, but a reduction in the overall reaction yield. High char yield is achieved by establishing low heating rates that provide an increase in the dehydration capacity and stabilization of the polymeric components, although both these parameters are generally independent of the resulting microporous distribution [76,93,94]. During this process, moisture and low molecular weight volatile compounds are released first, followed by light aromatics, and lastly, hydrogen gas [95,96]. During carbonization, the carbon atoms are reorganized, progressively building up the fixed carbonaceous skeleton. The resulting carbonaceous material acquires a low porosity and surface area, while the formed pores are filled with tarry residues derived from the pyrolysis process, requiring a subsequent activation to increase the textural characteristics and become an active product [97].

The main purpose of the activation process is to increase the surface area and enhance the pore volume of the AC, so that specific textural properties are achieved by creating a desirable hierarchical porosity. The activation process consists of a first initial phase in which the disorganized carbon is eliminated, leading to the development of microporosity. In the second stage, the pores created are widened. If the walls between pores collapse due to combustion, which depend on the type of activation employed, it gives rise to large macropores and thus decreasing the volume of the micropores [76]. There are two widely known activation methods for the AC preparation with specific size and morphology [93,98,99]: physical and chemical activation.

Physical activation is generally considered a process carried out in two steps: carbonization under inert atmosphere ( $N_2$  or Ar) and activation. This method consists of taking the non-porous char obtained by pyrolysis from the biomass precursor during carbonization and subjecting it to a gaseous activating agent at high temperatures, up to 1200 °C, to develop porosity and a large specific surface area. The activation stage involves the reaction between the carbonaceous material and a gas phase ( $CO_2$ , steam, air or a mixture of gases with steam) resulting in the elimination of the tarry amorphous carbon from the interstitial layers of the carbonaceous structure. The development of pores during physical activation has been reported to occur in three distinct phases: the opening of previously inaccessible pores, the creation of pores by selective activation and the dimensional widening of existing pores [100,101]. This makes the internal porous structure accessible and generates microporosity in the AC produced [97,102,103]. The gases commonly used as physical activators of ACs are steam,  $CO_2$  and air, whose reaction mechanisms have been widely described in the literature [104,105]. In the case of activation with steam, two mechanistic reaction models could take place: oxygen exchange and hydrogen inhibition. Both involve an initial stage of adsorption/dissociation of water molecules at the active sites of the carbon surface, and a subsequent generation of carbon monoxide (CO) and hydrogen ( $H_2$ ) [83]. Therefore, steam oxidation requires an initial pre-oxidation step consisting of the dilution of air with inert nitrogen gas that reduces the oxygen concentration. Consequently, the increase of the exothermic reaction temperature between the oxygen and the coal is avoided, thereby preventing coal agglomeration phenomena during pyrolysis. Activation is then carried out by replacing the nitrogen flow with a 50 % mixture of water and nitrogen [106].  $CO_2$  is the most widely used activation gas because it is clean, easy to handle, and facilitates control of the activation process as a consequence of the slow reaction rate at high temperatures [107]. However, several studies have reported greater efficiency of steam compared to  $CO_2$ , producing ACs with an increased specific surface area in a faster activation time, yet reaching the same degree of conversion. Furthermore, the relatively small water molecule size enables improved diffusion within the porous structure of the AC, causing a continuous gradual increase during combustion that promotes an enlargement of the micropore size and the formation of a mesoporous surface [78,108–110]. Generally, inert gases are used alternatively in the activation process, although gasification with  $N_2$  is frequently carried out because it repels gaseous oxygen from the pyrolysis chamber, thereby avoiding burning the biomass. Additionally, the use of nitrogen gas facilitates the control of the activation stage and has several advantages such as environmental sustainability, easy handling, and low-cost availability [88].

Chemical activation is a commonly used method for the generation of AC based on the degradation/dehydration of the raw material, carbonization/aromatization of the carbonaceous skeleton, and the removal of tar from the biomass material to facilitate the development of the porous structure [78,93,111,112]. For this, a wide variety of chemical agents such as phosphoric acid ( $H_3PO_4$ ), sulfuric acid ( $H_2SO_4$ ), nitric acid ( $HNO_3$ ), zinc chloride ( $ZnCl_2$ ), potassium hydroxide (KOH), sodium hydroxide (NaOH), calcium oxide (CaO), calcium chloride ( $CaCl_2$ ), potassium carbonate ( $K_2CO_3$ ) and sodium carbonate ( $CaCO_3$ ), among others, can be used to impregnate the biomass precursor [83,97,99,113,114]. Subsequently, the resulting precursor-agent mixture is subjected to a heat treatment, generally in a range of 400–800 °C under controlled inert atmosphere ( $N_2$  or Ar), to develop a porous structure with a large specific surface area. The heating stage is conventionally carried out in a tube furnace, although microwave-assisted thermal processes have recently attracted great interest in the industrial sector due to their extensive commercial applicability and the higher performance compared to the conventional heating: reduction of treatment time, energy savings, possibility of large thermal gradients, uniform heating, lower gas consumption and smaller reactor size, etc. [115]. Finally, a washing process of the generated AC is carried out to eliminate the residual activating chemical agent. A strict control of parameters such as the precursor-agent ratio, the selection of the chemical activator, the impregnation time, the stirring speed, the set temperature, and the heating ramp during the AC formation process is crucial to achieve the desired pore size distribution as well as preventing tar and undesired product formation [71,83]. Chemical activation has some advantages over physical activation: simplicity of the process with the possibility of carrying out the carbonization and activation stage of the biomass precursor in a single step, lower activation temperatures, formation of a well-defined porous structure, an increased yield by up to 30 % by mass, less time required in the activation process, possibility of incorporating suitable functional groups, higher micropore volumes, and greater surface area of the resulting AC [76,94,103,116]. However, the main drawback of the chemical activation method is the cost and environmental effect of the activating chemical agents coupled with the need to incorporate an additional washing step [88]. Additionally, some studies have reported the combination of physical and chemical activation processes (physicochemical methods) for the effective activation of biomass precursors, widely using KOH as a chemical activator and a physical stream of  $CO_2$  [117–119].

Regarding the fundamental characterization of ACs, the textural properties such as surface area, pore size distribution, and pore volume, are crucial characteristics to categorize them into micro, meso or macro porous, and also for the evaluation of these materials in a specific application. The surface characterization, to study the surface functional groups and elemental composition of AC, is usually carried out by methods such as Raman spectroscopy, Fourier transform infrared spectroscopy (FTIR), X-ray Photoelectron Spectroscopy (XPS), CHNS elemental analysis, Energy-dispersive X-ray spectroscopy (EDX/EDS), Boehm titration, Temperature Programmed Desorption (TPD), or pH at the potential of zero-point charge (pHzpc). The ACs morphology can be obtained by Scanning Electron Microscopy (SEM), Field Emission Electron Microscopy (FESEM), Transmission Electron Microscopy (TEM), or High-Resolution Transmission Electron Microscopy (HRTEM). X-Ray Diffraction (XRD) is an instrumental technique used for extracting information on the amorphous structure and degree of graphitization of AC, where also Raman spectroscopy constitutes a useful complement. Furthermore, Thermogravimetric Analysis (TGA) has become very useful in the study of the starting biomass, since the TGA curves help provide the fundamental composition of the raw material, showing stages of weight loss that are the fingerprint of the selected precursor. The pore properties and surface area are evaluated from gas absorption measurements, generally with  $N_2$ , and Hg porosimetry. Nitrogen adsorption-desorption isotherms are widely used to evaluate the textural properties of activated carbons, with Brunauer, Emmett and Teller (BET) being the commonly used method for determining the carbon surface area and microporosity. Mercury intrusion porosimetry is used for the characterization of mesopores, and especially macropores.

## 3 Lithium–sulfur battery applications

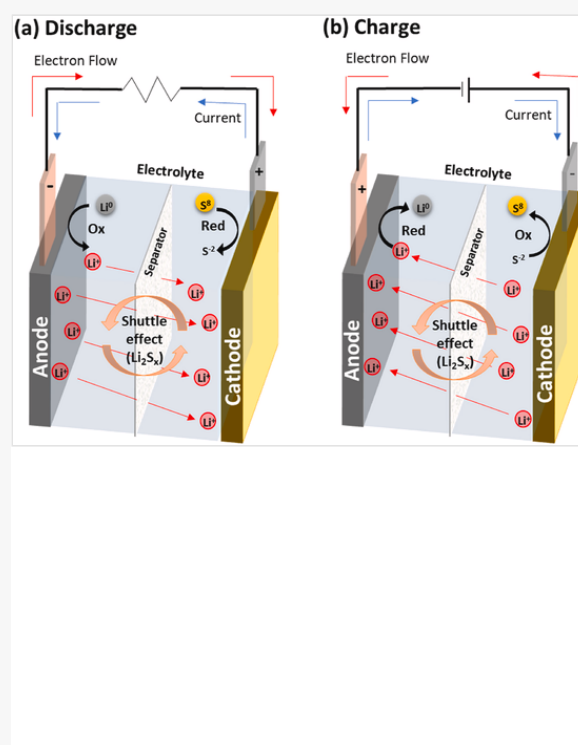
### 3.1 Electrochemical reactions

As mentioned in the *Introduction*, Li–S batteries are considered an alternative to current LIBs since they possess higher theoretical energy density; moreover, S is more abundant, cheaper and a less toxic element than some of the alternative redox-active elements present in Li-ion batteries, e.g. Co and Ni. However, the Li–S system has not been widely available on the commercial market due to several hurdles in its development: the poor conductivity of S, volume changes caused by the reversible  $S \rightleftharpoons Li_2S_x$  ( $x = 1, 2$ ) chemical transformations and the solubility of lithium polysulfides (LiPSs) in the electrolyte solvent. The LiPS diffuse to the anode, where they are reduced to short-chain polysulfides and diffuse back to the cathode where long-chain polysulfides are formed again (the redox shuttle effect). All these obstacles lead to a decrease in the delivered capacity, coulombic efficiency, and cycle life of the battery.

A schematic of the Li–S battery operation mode is shown in Fig. 5. During discharge, the reactions in the positive electrode start with the reduction of elemental sulfur into longer lithium polysulfides,  $Li_2S_x$  ( $x = 4–8$ ), which dissolve to different degrees in commonly used ether-based electrolytes [120–123]. Though the exact mechanism is still under debate, it is generally accepted that the subsequent reduction on the positive electrode shortens the chain length of the polysulfides [124]. At the end of discharge, insulating and insoluble lithium sulfide ( $Li_2S$ ) is precipitated. The charging process starts with the oxidation of  $Li_2S$  to polysulfides and ends with the precipitation of elemental sulfur. While operando X-ray diffraction (XRD) have detected  $Li_2S$  and S being formed around the same states of charge (SoC) upon both discharging and charging, indicating a uniform reversibility in the process [125], operando spectroscopic reports have suggested that the intermediate reactions are not exactly the same during charge and discharge [126]. At the negative electrode, metallic Li is oxidized to  $Li^+$  during discharge, which are reduced back to metallic Li upon charging. These processes are referred to as stripping and plating, and have been extensively studied in the literature beyond the Li–S field [127]. The inhomogeneous reactivity of the metallic Li during stripping and plating – associated with dendrite formation – is an issue for most systems pairing metallic Li with any kind of cathode, not only sulfur.

alt-text: Fig. 5

Fig. 5



Components and mode of operation in (a) discharge and (b) charge for a Li-S battery.

Replacement Image: Figure 5.tif

Replacement Instruction: Replace image requested

The insulating nature of the fully charged and discharged states requires a conductive matrix in the positive electrode to facilitate the electrochemical reactions. This is often realized by fabricating S/C composite electrodes with highly porous carbon [128]. The properties of the porous carbon are thus critical to the performance of the positive electrode, as well as the entire cell, due to the mobility of the soluble polysulfides. Indeed, one of the crucial criteria for the porous carbon host is the ability to retain the dissolved polysulfides in the electrolyte within the positive electrode, the so called ‘catholyte’. The migration of sulfur species from the cathode results in loss of active materials and the redox shuttle between the electrodes [124,129,130]. Substantial efforts have been devoted to the search for porous carbon with the best polysulfide retention, among which a milestone would be improvements in capacity and cycle life achieved by highly ordered mesoporous carbon (CMK-3) [33]. In addition to porosity control [131], polar functional groups, and doping in the carbon matrix with elements such as boron [132], nitrogen [133], transition metals [134] and transition metal oxides [135], have been demonstrated to increase the composite's affinity to polysulfides when introduced into the carbon host, and/or different polymer binders used in the composite electrode fabrication [136–139].


Another motivation for the optimization of the porous carbon host is to enhance the utilization of the active materials in the cathode. Low sulfur utilization is responsible for the mismatch between the achieved and the theoretical specific capacity, which is then strongly related to the low practical energy density of the cell [140]. Since S and  $\text{Li}_2\text{S}$  are insulating, it has been proposed that one or both of their formation passivates the conductive surface of the porous carbon [141] and may block the pores in larger amounts [142,143]. These processes may make the remaining active material in the electrolyte inaccessible to the electronically conductive surface [144]. Consequently, the discharge or charge process ends with low reaction efficiency within a cycle. It is postulated that the insulating films or particles that cannot react to form soluble polysulfides are again responsible for the decreasing sulfur utilization as the cycle number increases [145–147]. To bring the sulfur utilization closer to the theoretical value, the carbon host plays an important role to maximize the conductive surface area and to speed up the reaction kinetics [128,148]. Such improvements will also allow a higher S-to-C ratio in the composite, which increases the specific capacity of the whole electrode (given the same specific capacity of the active material) [140,149]. Porous carbons synthesized with tailored porosity have been tested as the conductive matrix in S/C composite electrodes [131]. Introducing N-doping [133], transition metals [134], and their oxides [135] into the carbon host is a commonly reported method to improve sulfur utilization through their catalytic effects.

In general, composites between S and AC are prepared by a melting diffusion method, uniformly mixing S and AC in a 60:40 or 70:30 ratio, and then heating at 155 °C for 12 h inside a sealed autoclave or in the tube furnace under an inert gas flow (Ar or  $\text{N}_2$ ). Then, the cathodes are similarly prepared, in most cases, by using a slurry of 80 wt % as-prepared composite material, 10 wt % of the conductive agent (carbon black, Super P or acetylene black), and 10 wt % of the binding agent (polyvinylidene difluoride - PVDF) in a suitable amount of N-methyl pyrrolidone (NMP). Subsequently, the slurry is deposited on Al foil, the current collector most used.

In summary, the development of the S/C composite electrode has been focused on the retention of polysulfides and the enhancement of sulfur utilization by physical and/or chemical modifications of the carbon host. This is where the intrinsic properties of biomass-derived activated carbon can contribute to more straight-forward fabrication routes with, often, lower cost and higher environmental friendliness [35,150]. With the above-mentioned challenges facing the Li-S system, the biomass-derived carbon as the critical component of the S/C composite electrode will be evaluated in the following. It is worth noting that only issues related to the cathode are discussed. It is important to acknowledge other factors that strongly influence cell performance, such as the amount (thickness) of the metallic Li electrode or the amount and composition of electrolyte [151].

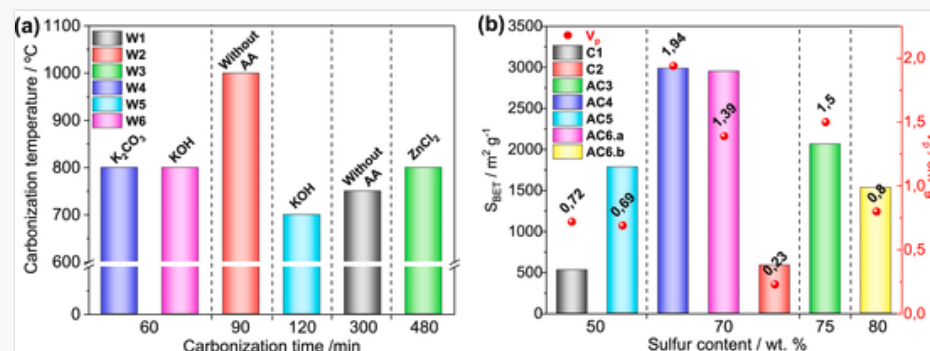
### 3.2 Preparation of Li-S cathodes using biomass-activated carbons

In this section, the main scientific contributions on biomass-derived carbons used in Li-S batteries are discussed and grouped according to the type of biomass from which they stem. For each group, the following carbon properties are considered: carbonization temperature and time, specific surface area ( $S_{\text{BET}}$ ), and pore volume ( $V_p$ ), and for composites their S content (in %). The activation agent is also included. The relationship between these properties is displayed in a number of figures (Figs. 6 and 7 and 9–11 and 13) which are split into **a** and **b**: the scale of the x axis of both figures is divided into blocks (60, 120 min for the carbonization time, and 50, 60 % for the S content). The temperature and time used for the preparation of the carbonaceous material together with the activating agent are included in Figs. **a**. In Figs. **b**, the other three properties have been included:  $S_{\text{BET}}$  and S content on the axes, and  $V_p$  indicated as a numerical value. Within each group, the waste type is labelled by **WN** (N is a whole number starting from 1) and **ACN** or **CN**, for the derived carbon being activated or non-activated, respectively. The composite name (which often appears as an abbreviation) used in the manuscript has been chosen to keep the nomenclature used by the authors of each article. The electrochemical properties discussed (cycling window, current density, initial and final capacity including cycle number and capacity retention) are summarized in Tables (Tables 1–6) together with the electrolyte used and the S loading of the electrode. The same symbols used by the respective authors have been used to identify the composites.


 Images are optimised for fast web viewing. Click on the image to view the original version.

alt-text: Fig. 6

Fig. 6

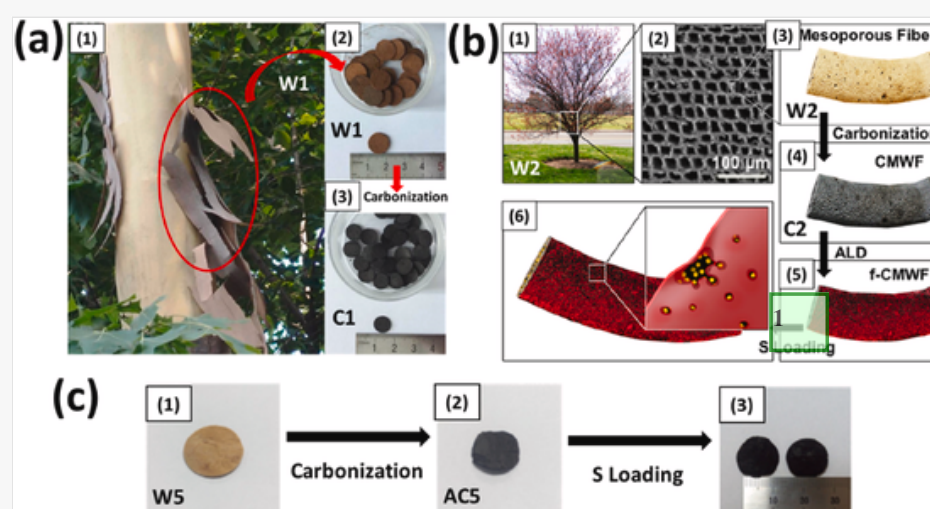


(a) Pyrolysis conditions set for different wastes (W) from woody biomass and the activating agent (AA) used [W1: Plane tree bark; W2: Wood microfiber; W3: Pinecone; W4: Sawdust; W5: Melaleuca bark; W6: Folium cymas] (b) Textural properties of activated carbons (ACs) obtained from the residues shown in Fig. 6 (a). From residue W6, the same authors prepared two activated carbons under different conditions: AC6-a and AC6-b. The values of  $S_{BET}$  and  $V_p$  were very different.

 Images are optimised for fast web viewing. Click on the image to view the original version.


alt-text: Fig. 7

Fig. 7



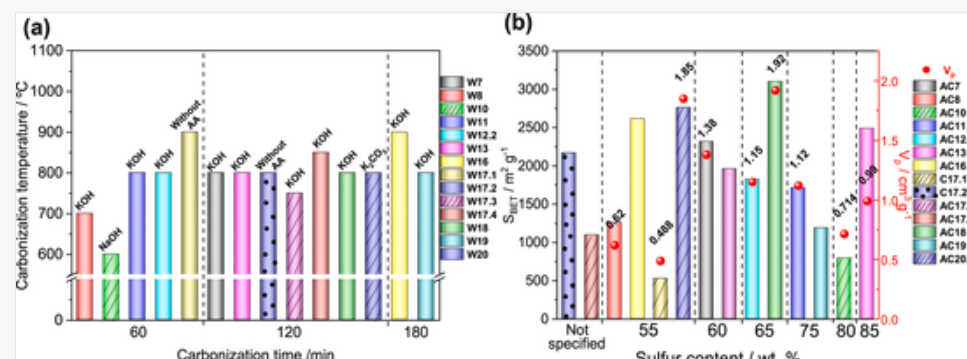
1 Figures 7 to 13 appear consecutively one after the other, sometimes quite some pages away from the text they refer to. This makes it very difficult for the reader, who wants to look at the Figure and read the text on the same page. Please move the Figures close to the text that discusses them

Schematic representation of the free-standing electrode preparation process from woody biomass: (a) W1: bark of plane tree (adapted from Ref. [152]. Copyright 2016 American Chemical Society), (b) W2: natural wood fiber (modified from Ref. [153]. Copyright 2017 American Chemical Society) and (c) W5: melaleuca bark (reproduced and modified from Ref. [159]).

 Images are optimised for fast web viewing. Click on the image to view the original version.


alt-text: Fig. 8

Fig. 8



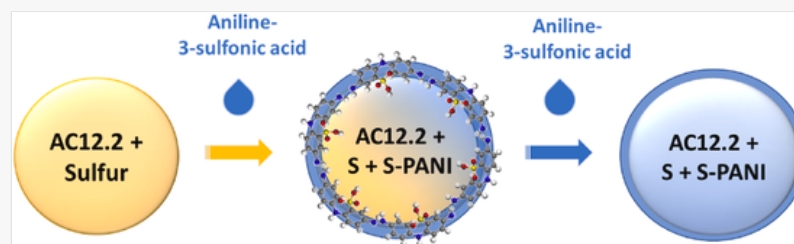
(a) Pyrolysis conditions set for different wastes (W) from agricultural residues and the activating agent (AA) used [W7: Camellia flower; W8: Poplar catkins; W9: Willow catkins; W10: Fluffy catkins; W11: Reed flower; W12: Bamboo; W13: Lotus plumule tea; W14: Luffa sponge; W15: Oil-tea shells; W16: Nodus nelumbis; W17: Rice husk; W18: Wheat straw; W19: Rice straw; W20: Sugarcane bagasse] (b) Textural properties of activated carbons (ACs) obtained from the residues shown in Fig. 8 (a).




 Images are optimised for fast web viewing. Click on the image to view the original version.

alt-text: Fig. 9

Fig. 9

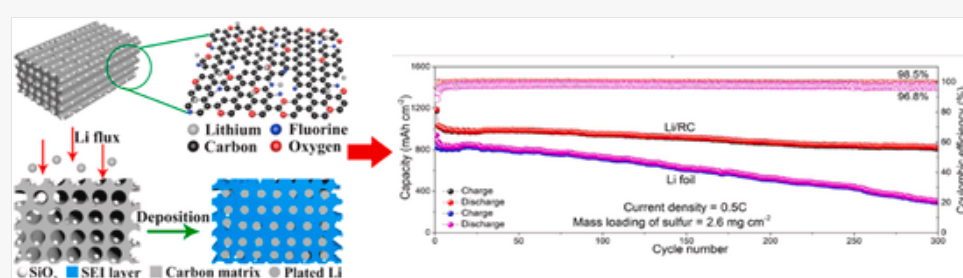


Schematic illustration of the morphological evolution process from obtained AC12.2/S to [\[Instruction: S-PANI@AC12.2/S is the name of the sample, it should not appear as links.\]S-PANI@AC12.2/S](#) composite. Adapted from Ref. [175].


 Images are optimised for fast web viewing. Click on the image to view the original version.

alt-text: Fig. 10

Fig. 10

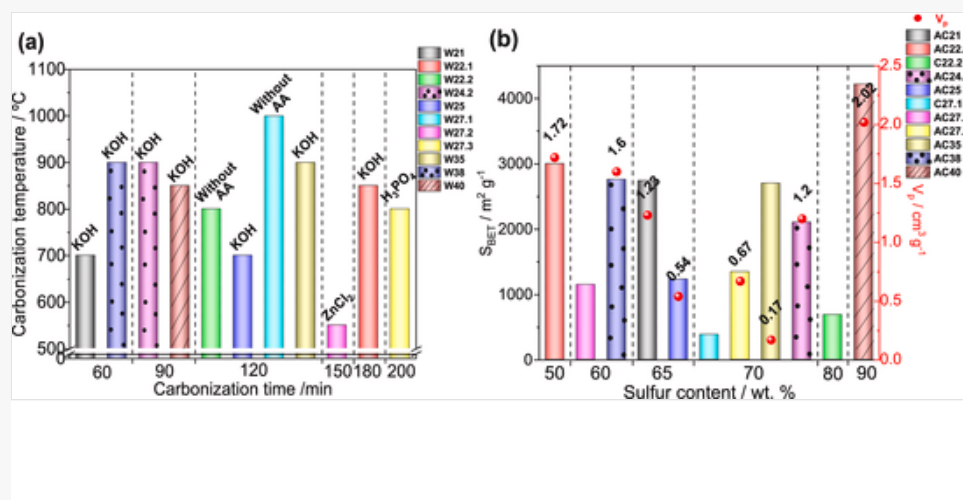


Schematic representation of the controllable Li deposition process and formation of SEI in the RC scaffold, and the favourable electrochemical behaviour of the Li/RC electrode thanks to its porous structure and the presence of SiO<sub>2</sub> and F-containing groups. (reprinted from Ref. [183] with permission from Elsevier).


 Images are optimised for fast web viewing. Click on the image to view the original version.

alt-text: Fig. 11

Fig. 11

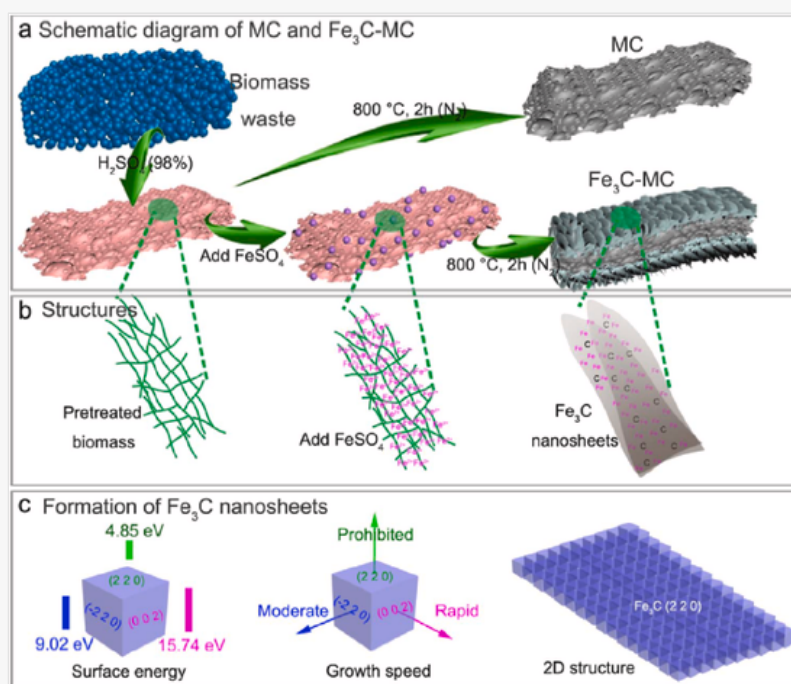


(a) Pyrolysis conditions set for different wastes (W) from non-edible agri-food residues and the activating agent (AA) used [W21: Banana peel; W22: Comcob; W23: Olive stones; W24: Coconut shell; W25: Soybean hull; W26: Oak tree fruit shell; W27: Pistachio shell; W28: Pomelo peel; W29: Almond shell; W30: Cherry pit; W31: Avocado shell; W32: Hickory shell; W33: Pomegranate residue; W34: Snake skin fruit peel; W35: Natura Okra shell; W36: Spent coffee; W37: Gingko nut; W38: Palm kernel shell; W39: Waste tea; W40: Garlic peel; W41: Peanut shell; W42: Rabutan peel; W43: Durian shell] (b) Textural properties of activated carbons (ACs) obtained from the residues shown in Fig. 11(a) and S content of the composite.

 Images are optimised for fast web viewing. Click on the image to view the original version.

alt-text: Fig. 12

Fig. 12



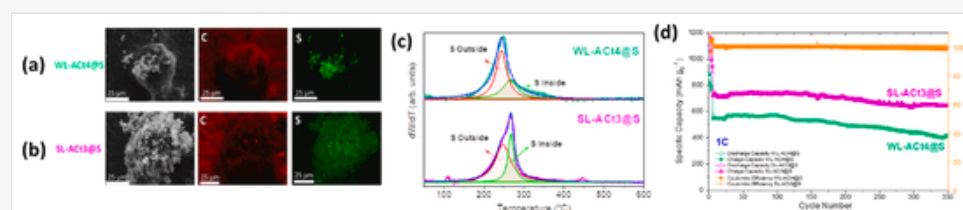
Schemes of the mesoporous carbon (MC) and Fe<sub>3</sub>C-MC composite synthesis (a), of the structure (b) and mechanism of Fe<sub>3</sub>C formation nanosheets (c) (reprinted from Ref. [211] with permission from Elsevier).

Images are optimised for fast web viewing. Click on the image to view the original version.

Q6

alt-text: Fig. 13

Fig. 13



(a and b) SEM images and elemental mapping of C and S; (c) Deconvolution of DTG curves; (d) electrochemical performance at 1C for WL-AC14@S and SL-AC13@S samples, respectively (reproduced and modifies from Ref. [218] with permission from John Wiley and Sons).

Replacement Image: Figure 13.jpg

Replacement Instruction: Replace image requested

alt-text: Table 1

Table 1

The table layout displayed in this section is not how it will appear in the final version. The representation below is solely purposed for providing corrections to the table. To preview the actual presentation of the table, please view the Proof.

Previous version

Expand

Electrochemical performance of carbons (C) or activated carbons (ACs) from woody biomass used as cathode in Li-S cells.

AC [Ref]	Cathode <sup>a</sup> (%S)	Electrolyte	Sulfur Loading/mg	Voltag	Current density	Initial Capacity/mAh	Final Capacity/mAh g <sup>-1</sup> (Cycle)	Capacity Retention (Fade rate/ %)
----------	---------------------------	-------------	-------------------	--------	-----------------	----------------------	--	-----------------------------------

Updated version

[Instruction: undefined][Instruction: Tables 1 to 6 appear consecutively one after the other. This makes it very difficult for the reader, who wants to look at the Table and read the text on the same page. Please move the tables close to the text that discusses them]

Electrochemical performance of carbons (C) or activated carbons (ACs) from woody biomass used as cathode in Li-S cells.

AC [Ref.]	Cathode <sup>a</sup> (%S)	Electrolyte	Sulfur Loading/mg cm <sup>-2</sup>	Voltag	Current density	Initial Capacity/mAh g <sup>-1</sup>	Final Capacity/mAh g <sup>-1</sup> (Cycle)	Capacity Retention (Fade rate/ %)
C1 [152]	C-S slice (48)	1 M LiTFSI + 0.1 M LiNO <sub>3</sub> (DOL:DME)	3.2-4.2	2.7-1.5	0.06 C (100 mA g <sup>-1</sup> )	1192	820 (10 <sup>th</sup> )	69 % (3.1)
						1159	608 (60 <sup>th</sup> )	52.5 % (0.79)
C2 [153]	S-CMWF (76)	1 M LiTFSI + 1 %wt	1.3	3.0-1.0	0.25 C (400 mA g <sup>-1</sup> )	1246	442 (450 <sup>th</sup> )	35.5 % (0.14)
	S-fCMWF		Not	3.0-1.0		1115	859 (450 <sup>th</sup> )	77 %

	(70)	LiNO <sub>3</sub> (DOL:DME)	specified						(0.046)
AC3 [157]	S-PCSC (54)	Not specified	Not specified	3.0–1.6	0.1 C	1606	1269 (100th)	79 % (0.21)	
	S-PCSC (68)					1370	1028 (100th)	76 % (0.24)	
	S-PCSC (73)					1145	891 (100th)	75 % (0.25)	
AC4 [158]	S- WWUPC (67)	1 M LiTFSI + 0.25 M LiNO <sub>3</sub> (DOL:DME) 5 μL mg <sup>-1</sup>	2.7	2.6–1.8	0.1C		980 (50th)	75 % (0.46)	
AC5 [159]	PCF-S (51)	1 M LiTFSI + 1 %wt LiNO <sub>3</sub> (DOL:DME) 25 μL mg <sup>-1</sup>	1.2	2.8–1.7	0.5 C	1120	701 (250th)	63 % (0.14)	
			1.8		0.2 C	1330	880 (100th)	66 % (0.34)	
			4.0			970	758 (100th)	78 % (0.22)	
			6.0			800	621 (100th)	78 % (0.22)	
AC6- a [160]	FCB-7-S (66.5)	1 M LiTFSI + 1 %wt LiNO <sub>3</sub> (DOL:DME)	Not specified	3.0–1.5	0.5 C	998	387 (200th)	39 % (0.3)	
	FCB-1-S (68)					1317	790 (200th)	60 % (0.068)	
AC6- b [161]	HPBC-S (Not specified)	1 M LiTFSI + 2 %wt LiNO <sub>3</sub> (DOL:DME) 36 μL mg <sup>-1</sup>	Not specified	3.0–1.5	0.5 C	907	436 (200th)	48 % (0.27)	
	HPBC/Ni-S (79)					907	610 (200th)	67 % (0.16)	

#### Table Footnotes

<sup>a</sup> Nomenclature used by the authors themselves.

alt-text: Table 2

Table 2

*i* The table layout displayed in this section is not how it will appear in the final version. The representation below is solely purposed for providing corrections to the table. To preview the actual presentation of the table, please view the Proof.

Previous version

Expand

Electrochemical performance of carbons (C) or activated carbons (ACs) from agricultural residues used as cathode in Li-S cells.

Type	AC [Ref.]	Cathode** (%S)	Electrolyte	Sulfur Loading/mg	Voltages/V	Current Density	Initial Capacity/mAh	Final Capacity/mAh g <sup>-1</sup> (Cycle)	Capacity Retention (Fade rate/ %)
------	-----------	----------------	-------------	-------------------	------------	-----------------	----------------------	--	-----------------------------------

Updated version

[Instruction: In the voltage column the width can be decreased by appearing "voltage" in the first line and the units "/ V" in the second line. In this way, the width of the first column (AC Ref.) Could be expanded so that the full names appear in the first line (Example: AC12.2-a) and the reference (Example: [174]) in the second line. Also, the text should always appear centered.]

Electrochemical performance of carbons (C) or activated carbons (ACs) from agricultural residues used as cathode in Li-S cells.


Type	AC [Ref.]	Cathode** (%S)	Electrolyte	Sulfur Loading/mg cm <sup>-2</sup>	Voltages/V	Current Density	Initial Capacity/mAh g <sup>-1</sup>	Final Capacity/mAh g <sup>-1</sup> (Cycle)	Capacity Retention (Fade rate/ %)
F L O W E R S	AC7 [162]	S@aNPCP3 <sup>a</sup> (60)	1 M LiTFSI + 1 %wt LiNO <sub>3</sub> (DOL:DME)	<1.0	3.0–1.5	1 C	740	580 (200 <sup>[Instruction: "th" must appear as a superscript]th</sup> )	78 % (0.11)
	AC8 [163]	S-HPC [Instruction: Sulfur percentages should appear centered on the second line] (56.5)	1 M LiTFSI (Tetraglyme)	Not specified	3.0–1.5	0.1 C	1318	850 (100th)	64.5 % (0.35)
	AC9 [164]	OAC-S [71]	1 M LiTFSI + 1 %wt LiNO <sub>3</sub> (DOL:DME) 90 μL mg <sup>-1</sup>	2.49	3.0–1.5	0.1 C	1365	590 (100th)	43 % (0.57)
	AC10 [165]	TACM-S [82.5]	1 M LiTFSI + 0.1 M LiNO <sub>3</sub> (DOL:DME) 20 μL mg <sup>-1</sup>	1.5	2.8–1.8	0.5 C	696.5	540 (500th)	77.5 % (0.045)
	AC11 [166]	BPC-S [74]	1 M LiTFSI (DOL:DME)	2.1	2.8–1.7	0.1 C	1557	908 (100th)	58 % (0.42)
		8.3	937	804 (50th)			85.8 %		

				2.1		1 C	877	663 (1000th)	75.5 % (0.024)
P L A N T S	AC12.1 [173]	T_BC-S (50)	1 M LiTFSI + 0.1 M LiNO <sub>3</sub> (DOL:DME)	Not specified	3.0–1.5	0.1 C	1295	756 (50th)	58 % (0.84)
						0.5 C	961	550 (150th)	57 % (0.29)
	AC12.2-a [174]	S/OBC (58.5)	1 M LiTFSI + 1 %wt LiNO <sub>3</sub> (DOL:DME)	Not specified	3.0–1.5	0.1 C	1453	711 (50th)	49 % (1)
						1 C	850	255 (500th)	30 % (0.14)
	AC12.2-b [175]	PANI@BDC/S-20 % (63.8)	1 M LiTFSI + 0.1 M LiNO <sub>3</sub> (DOL:DME) 32 μL mg <sup>-1</sup>	3.5	3.0–1.5	0.1 C	1185	585 (40th)	49 % (1.27)
							1463	683 (100th)	47 % (0.53)
				1.3–1.5		0.5 C	1270	366 (500th)	29 % (0.14)
	AC12.2-c [176]	SPANI@BDC/S (64)	1 M LiTFSI + 0.1 M LiNO <sub>3</sub> (DOL:DME) 29.5 μL mg <sup>-1</sup>	1.5–1.7	3.0–1.5	0.1 C	1484	853 (100th)	57.5 % (0.425)
						0.5 C After Rate	1500	298 (500th)	20 % (0.16)
						2 C	1484	496 (300th)	33 % (0.22)
	AC12.3 [177]	CER or CC-S (56.5)	1 M LiTFSI + 1 %wt LiNO <sub>3</sub> (DOL:DME) 15 μL mg <sup>-1</sup>	Not specified	2.8–1.7	1 C	737	526 (200th)	71 % (0.14)
	AC13 [178]	NSHPC-7/S (85)	1 M LiTFSI + 3 %wt LiNO <sub>3</sub> (DOL:DME) 10 μL mg <sup>-1</sup>	2.8	2.8–1.8	0.1 C	1453	1164 (150th)	80 % (0.13)
0.5 C						1285	952 (300th)	74 % (0.086)	
1 C						1204	496 (500th)	41 % (0.12)	
AC14 [179]	PCM650-S (63.6)	1 M LiTFSI + 3 %wt LiNO <sub>3</sub> (DOL:DME) 50 μL mg <sup>-1</sup>	1.2	2.6–1.7	0.2 C	1224	714 (300th)	58 % (0.14)	
					0.5 C	1130	797 (100th)	70.5 % (0.3)	
					1 C	1035	781 (100th)	75 % (0.25)	
AC15 [180]	NiAl@PAB-S (66)	1 M LiTFSI + 1 %wt LiNO <sub>3</sub> (DOL:DME) 40 μL mg <sup>-1</sup>	1.2	3.0–1.5	0.5 C	792	534 (200th)	67 % (0.165)	
					1 C	788	473 (300th)	60 % (0.13)	
AC16 [181]	NNH/PC/S (53)	1 M LiTFSI + 1 %wt LiNO <sub>3</sub> (DOL:DME) 40–50 μL mg <sup>-1</sup>	1.56	3.0–1.5	0.5 C	1203	521 (700th)	43 % (0.08)	
S T R A W S	C17.1 [182]	RHC/S (56)	1 M LiTFSI + 1 %wt LiNO <sub>3</sub> (DOL:DME)	1.0	2.8–1.7	0.5 C	834	600 (500th)	72 % (0.06)
		RHC-SiO <sub>2</sub> /S (56)					563	450 (500th)	80 % (0.04)
	AC17.2 [183]	Li-RC(SiO <sub>2</sub> )/S-RC (Not specified)	1 M LiTFSI + 0.1 M LiNO <sub>3</sub> (DOL:DME) 50 μL mg <sup>-1</sup>	2.6	2.6–1.8	0.5 C	820	300 (300th)	36 % (0.21)
		Li/S-RC (Not specified)					950	800 (300th)	84 % (0.05)
	C17.3 [184]	S@biocharRH (50)	1 M LiTFSI + 0.1 M LiNO <sub>3</sub> (DOL:DME)	Not specified	3.0–1.5	0.2 C	1005	567 (100th)	56 % (0.44)
		S@HPRH (60)					1534	739 (100th)	48 % (0.52)
	AC17.4 [185]	AC-S (Not specified)	1 M LiTFSI + 1 %wt LiNO <sub>3</sub> (DOL:DME)	Not specified	3.0–1.0	0.1 C	1230	200 (100th)	16 % (0.84)
						0.2 C	970	310 (100th)	32 % (0.68)
	AC18 [186]	NOSPC/S (63)	1 M LiTFSI + 0.1 M LiNO <sub>3</sub> (DOL:DME) 25 μL mg <sup>-1</sup>	1.0–1.2	2.8–1.7	0.2 C	1049	695 (100th)	66 % (0.34)
						1 C	810	455 (500th)	56 % (0.088)
	AC19 [187]	NHAC/S (76)	1 M LiTFSI + 1 %wt LiNO <sub>3</sub> (DOL:DME) 20 μL mg <sup>-1</sup>	5.8	2.8–1.6	1 C	1070	700 (100th)	65.5 % (0.34)
						1.2	2 C	755	584 (500th)
						3 C	680	270 (2000th)	40 % (0.029)
	ABT/S (Not specified)		1.2		2 C	400	280 (500th)	70 % (0.06)	
AC20.1 [188]	S/NDPC-1 (53)	1 M LiTFSI + 2 %wt LiNO <sub>3</sub> (DOL:DME) 20 μL mg <sup>-1</sup>	1.0	2.8–1.7	0.5 C	926	571 (400th)	62 % (0.095)	
					1 C	816	542 (500th)	66 % (0.067)	

\*\* Nomenclature used by the authors themselves; <sup>(a)</sup> aNPCP3-coated celgard@separator; \*Activation cycles at 0.2 C.

alt-text: Table 3

Table 3

 The table layout displayed in this section is not how it will appear in the final version. The representation below is solely purposed for providing corrections to the table. To preview the actual presentation of the table, please view the Proof.

Previous version

Expand

Electrochemical performance of carbons (C) or activated carbons (ACs) from agri-food residues used as cathodes in Li-S cells.

AC [Ref.]	Cathode** (%S)	Electrolyte	Sulfur Loading/mg	Voltages/V	Current density	Initial Capacity/mAh	Final capacity/mAh	Capacity retention (Fade rate/ %)
-----------	----------------	-------------	-------------------	------------	-----------------	----------------------	--------------------	-----------------------------------

Updated version

Electrochemical performance of carbons (C) or activated carbons (ACs) from agri-food residues used as cathodes in Li-S cells.

AC [Ref.]	Cathode** (%S)	Electrolyte	Sulfur Loading/mg cm <sup>-2</sup>	Voltages/V	Current density	Initial Capacity/mAh g <sup>-1</sup>	Final capacity/mAh g <sup>-1</sup> (Cycle)	Capacity retention (Fade rate/ %)
AC21 [209]	S-BPC-700 [Instruction: Sulfur percentages should appear centered on the second line](65)	1 M LiTFSI + 1 %wt LiNO <sub>3</sub> (DOL:DME) 4 μL mg <sup>-1</sup>	-	3.0-1.6	0.2 C	1227	870 (100[Instruction: "th" must appear as a superscript]th)	71 % (0.29)
					1 C	1227	775 (100th)	63 % (0.37)
	S-BPC-500 (65)				0.2 C	1179	752 (100th)	64 % (0.36)
					1 C	1143	522 (100th)	46 % (0.54)
	S-BPC-900 (65)				0.2 C	1143	595 (100th)	52 % (0.48)
					1 C	1143	509 (100th)	44.5 % (0.55)
AC22.1a [210]	NAC-800/50S (50)	1 M LiTFSI + 0.2 M LiNO <sub>3</sub> (DOL:DME) 25 μL mg <sup>-1</sup>	1.2	2.8-1.7	0.3 C	1080	720 (150th)	67 % (0.22)
AC22.1b [207]	NAC-800/50S (50)	0.5 M LiTFSI + 0.2 M LiNO <sub>3</sub> (DOL:DME)	0.8	2.8-1.7	0.3 C	1504	799 (200th)	53 % (0.235)
C22.2 [211]	Fe <sub>3</sub> C-MC/S (80)	0.5 M LiTFSI (DOL:DME) 6 μL mg <sup>-1</sup>	1.5	2.8-1.7	0.5 C	1465	920 (1000th)	63 % (0.037)
						9.0	960	699 (100th)
AC23a [212]	OSAC@TiO <sub>2</sub> /S (47)	1 M LiTFSI + 0.4 M LiNO <sub>3</sub> (DOL:DME)	Not specified	2.8-1.8	0.16 C	985	700 (100th)	71 % (0.29)
AC23b [213]	AC/MnO <sub>2</sub> /S@ht (58)	1 M LiTFSI + 0.4 M LiNO <sub>3</sub> (DOL:DME)	1.0	2.7-1.8	0.1 C	874	555 (100th)	63.5 % (0.36)
					0.5 C	1020	401 (100th)	39 % (0.61)
					1 C	1120	300 (100th)	27 % (0.73)
AC24.1 [217]	S@CSC (60)	1 M LiTFSI + 0.5 %wt LiNO <sub>3</sub> (DOL:DME)	0.78	3.0-1.0	0.5 C	1364 (3[Instruction: "rd" must appear as a superscript]rd)	1030 (100th)	75.5 % (0.25)
					1 C	1305 (3rd)	854 (200th)	65 % (0.18)
					2 C	1138 (3rd)	517 (400th)	45 % (0.145)
AC24.2 [218]	WL-Act4@S (60)	1 M LiTFSI + 0.4 M LiNO <sub>3</sub> (DOL:DME) 19 μL mg <sup>-1</sup>	2.0	2.8-1.8	0.5 C	653 <sup>d*</sup>	650 (150th)	99.5 % (0.003)
					1 C	570 <sup>d*</sup>	410 (350th)	71 % (0.08)
	SL-Act3@S (60)				0.5 C	871 <sup>d*</sup>	805 (150th)	92.4 % (0.05)
					1 C	750 <sup>d*</sup>	646 (350th)	85.4 % (0.04)
AC25 [219]	S/porous carbon (63.7)	1 M LiTFSI + 1 %wt LiNO <sub>3</sub> (DOL:DME)	1.5	2.8-1.7	0.5 C	1231	450 (200th)	36.5 % (0.32)
AC26 [220]	ACGFinterlayer	1 M LiTFSI + 0.1 M LiNO <sub>3</sub> (DOL:DME)	0.8-1.1	2.8-1.7	0.2 C	1321	906 (60th)	68.5 % (0.525)
C27.1 [214]	PC/S (70%)	1 M LiTFSI + 1 %wt LiNO <sub>3</sub> (DOL:DME)	Not specified	3.0-1.5	0.5 C	1060	480 (250th)	45 % (0.23)
	M-PC/S (MnO <sub>2</sub> ) (70)				0.5 C	1200	720 (250th)	60 % (0.16)
					1 C	930	730 (100th)	78.5 % (0.215)
AC27.2 [221]	C-AC/S (57)	1 M LiTFSI (DOL:DME)	0.84	3.0-1.5	0.2 C	980	380 (200th)	39 % (0.305)
AC27.3 [222]	PSAC@S (70)	1 M LiTFSI + 0.4 M LiNO <sub>3</sub> (DOL:DME) 50 μL mg <sup>-1</sup>	2.6	2.6-1.8	0.1 C	1193	570 (300th)	48 % (0.17)
AC28.1 [223]	PBG/S (GO) (63)	1 M LiTFSI + 0.1 M LiNO <sub>3</sub> (DOL:DME)	4.0	2.8-1.7	0.1 C	1053	459 (100th)	43 % (0.57)
	PBG/S (GO) (48)				1 C	1368	354 (600th)	26 % (0.12)
AC28.2 [224]	PCKH/S (54)	1 M LiTFSI + 0.2 M LiNO <sub>3</sub> (DOL:DME) 15 μL mg <sup>-1</sup>	1.2	2.8-1.7	0.2 C	1534 <sup>d*</sup>	717 (300th)	47 % (0.17)

AC28.3 [216]	S/CoFe@NC/PPC (20) (Co better than Mn, Ni and Fe)	1 M LiTFSI (DOL:DME)	Not specified	2.8-1.7	0.1 C	1049	409 (200th)	39 % (0.3)
					1 C	916	448 (500th)	49 % (0.1)
AC28.4 [225]	NB-PPCA interlayer	1 M LiTFSI + 0.1 M LiNO <sub>3</sub> (DOL:DME) 60 μL mg <sup>-1</sup>	1.1-1.4	2.8-1.7	1 C	1000	587 (500th)	59 % (0.082)
AC29 [226]	ASC/S (60)	1 M LiTFSI + 0.4 M LiNO <sub>3</sub> (DOL:DME)	2.0	2.7-1.7	0.06 C	916	665 (100th)	72 % (0.28)
AC30a [227]	C/S composite (57)	1 M LiCF <sub>3</sub> SO <sub>3</sub> + 0.4 M LiNO <sub>3</sub> (DOL:DME) 20 μL mg <sup>-1</sup>	0.77	2.7-1.8	0.06 C	1148	915 (100th)	80 % (0.2)
					0.2 C	950 <sup>*</sup> [Instruction: The symbol is not "d", the correct one would be an asterisk "*"]	707 (200th)	74.5 % (0.12)
					1 C	550 <sup>*</sup>	410 (200th)	74.5 % (0.12)
AC30b [228]	AC-H@S (75)	1 M LiTFSI + 1 M LiNO <sub>3</sub> (DOL:DME)	1.3	2.8-1.9	0.33 C	1350 <sup>*</sup>	800 (100th)	60 % (0.408)
AC31 [229]	AvS-N <sup>a</sup>	0.2 M Li <sub>2</sub> S <sub>8</sub> + 0.1 M LiTFSI + 1 M LiNO <sub>3</sub> (Catholyte)	5.0b	3.0-1.5	0.1 C	1300 [Instruction: "nd" must appear as a superscript]nd)	530 (100th)	41 % (0.59)
AC32 [230]	HKC-S (55)	1 M LiTFSI + 0.1 M LiNO <sub>3</sub> (DOL:DME)	1.5-2.0	3.0-1.5	0.2 C	1143	608 (300th)	53 % (0.156)
					0.5 C	995	429 (700th)	43 % (0.08)
					1 C	992	369 (1000th)	37 % (0.063)
AC33 [231]	HPC/S-600 (71.5)	Not specified 20 μL mg <sup>-1</sup>	Not specified	3.0-1.5	0.1 C	1010	550 (500th)	54 % (0.092)
					0.2 C	912	437 (500th)	48 % (0.104)
AC34 [232]	SFPC/S (63)	1 M LiTFSI + 0.1 M LiNO <sub>3</sub> (DOL:DME)	Not specified	3.0-1.5	0.1 C	945	619 (100th)	65.5 % (0.345)
					1 C	809	538 (100th)	66.5 % (0.335)
					2 C	718	466 (100th)	65 % (0.35)
AC35 [206]	N-OSC/S (70)	1 M LiTFSI + 0.2 M LiNO <sub>3</sub> (DOL:DME)	1.0	2.7-1.7	0.5 C	988	628 (100th)	63.5 % (0.365)
					2 C	750	416 (1000th)	55.5 % (0.05)
AC36 [233]	W-SPC-80/S (80)	1 M LiTFSI + 0.2 M LiNO <sub>3</sub> (DOL:DME)	Not specified	2.8-1.7	0.2 C	1458	474 (400th)	32 % (0.17)
AC37 [215]	GC-CoS <sub>2</sub> /S (63)	1 M LiTFSI + 0.1 M LiNO <sub>3</sub> (DOL:DME) 15 μL mg <sup>-1</sup>	2.2-2.5	3.0-1.5	0.1 C	1252	1019 (500th)	81.4 % (0.037)
					2 C	900	610 (1000th)	67.8 % (0.03)
					4 C	687	413 (1000th)	60.4 % (0.04)
AC38 [234]	PAC-S (60)	1 M LiTFSI (DOL:DME)	0.5-1.2	2.7-1.7	0.12 C	1045	870 (100th)	83 % (0.17)
		1 M LiTFSI + 1 %wt LiNO <sub>3</sub> (DOL:DME)			0.48 C	617	313 (1000th)	51 % (0.05)
					0.48 C	617	579 (200th)	94 % (0.03)
AC39 [235]	WTPK/S (60)	1 M LiTFSI + 0.1 M LiNO <sub>3</sub> (DOL:DME)	1.2	3.0-1.5	0.05 C	1048	627 (100th)	60 % (0.4)
					0.5 C	800	428 (100th)	53.5 % (0.465)
					2 C	560	300 (100th)	53.5 % (0.465)
AC40 [208]	GPC/HT-S (87.6)	1 M LiTFSI + 0.4 M LiNO <sub>3</sub> (DOL:DME) 18-20 μL mg <sup>-1</sup>	1.0	2.8-1.5	0.5 C	830 <sup>*</sup>	600 (400th)	72.2 % (0.07)
					1 C	680 <sup>*</sup>	400 (400th)	58.8 % (0.1)
					2 C	630 <sup>*</sup>	265 (400th)	42.06 % (0.15)
AC41 [236]	APS-B(W)/S (63)	1 M LiTFSI + 0.25 M LiNO <sub>3</sub> (DOL:DME) 40 μL mg <sup>-1</sup>	0.6	2.6-1.8	0.06 C	778	322 (100th)	41.3 % (0.59)
	BPS-B(W)/S (68.3)					720	335 (100th)	46.5 % (0.535)

AC42 [237]	RPC/S-4 (68.2)	1 M LiTFSI + 0.1 M LiNO <sub>3</sub> (DOL:DME) 40 μL mg <sup>-1</sup>	1.1	3.0–1.5	0.2 C	1275	936 (200th)	73 % (0.135)
AC43 [238]	4DPC-900/S (61.9)	1 M LiTFSI + 0.1 M LiNO <sub>3</sub> (DOL:DME) 20 μL mg <sup>-1</sup>	2.0	2.8–1.7	0.5 C	895.2	604 (100th)	67.5 % (0.325)

\*\*Nomenclature used by the authors themselves; [a] Catholyte; [c] Carbon loading; \*Activation cycles at lower C rate.

alt-text: Table 4

Table 4

The table layout displayed in this section is not how it will appear in the final version. The representation below is solely purposed for providing corrections to the table. To preview the actual presentation of the table, please view the Proof.

Previous version

Expand

Electrochemical performance of carbons (C) or activated carbons (ACs) from aquatic biomass used as cathode in Li-S cells.

AC [Ref]	Cathode <sup>a</sup> (%S)	Electrolyte	Sulfur Loading/mg cm <sup>-2</sup>	Voltages/V	Current Density	Initial Capacity/mAh	Final Capacity/mAh g <sup>-1</sup> (Cycle)	Capacity Retention (Fade rate/ %)
----------	---------------------------	-------------	------------------------------------	------------	-----------------	----------------------	--	-----------------------------------

Updated version

Electrochemical performance of carbons (C) or activated carbons (ACs) from aquatic biomass used as cathode in Li-S cells.

AC [Ref.]	Cathode <sup>a</sup> (%S)	Electrolyte	Sulfur Loading/mg cm <sup>-2</sup>	Voltages/V	Current Density	Initial Capacity/mAh g <sup>-1</sup>	Final Capacity/mAh g <sup>-1</sup> (Cycle)	Capacity Retention (Fade rate/ %)
C44 [242]	S-NPCM (65)	1 M LiTFSI (DOL:DME) 10 μL mg <sup>-1</sup>	1.1–1.3	3.0–1.7	0.16 C	1119	1031 (100 <sup>th</sup> )	91 % (0.09)
C45 [243]	S-NMPC (63)	1 M LiTFSI + 0.1 M LiNO <sub>3</sub> (DOL:DME) 75 μL mg <sup>-1</sup>	3.5	3.0–1.0	0.1 C	1327	757 (100th)	57 % (0.43)
C46 [244]	SWC-S (66)	1 M LiTFSI + 0.2 M LiNO <sub>3</sub> (DOL:DME)	Not specified	3.0–1.5	0.2 C	1221	855 (70th)	70 % (0.43)
					1 C	893.5	540.6 (300th)	60.5 % (0.13)
AC47 [241]	NPAC-S59 (59)	1 M LiTFSI + 2 % wt. LiNO <sub>3</sub> (DOL:DME)	Not specified	2.8–1.7	0.5 C	1182.5	667 (200th)	56.5 % (0.22)
						776	541 (300th)	67 % (0.11)
	NPAC-S72 (72)				1 C	750	517 (300th)	69 % (0.103)
	NPAC-S82 (82)				525	429 (300th)	82 % (0.06)	
AC48 [249]	CNHPC700G-S (40)	1 M LiPF <sub>6</sub> (EC:DMC)	~1.0	3.0–1.0	0.1 C	1555	734 (100th)	47 % (0.53)
AC49 [250]	NSC-S (75)	1 M LiTFSI (Not specified)	2.0	3.0–1.0	0.1 C	1387.8	823.5 (150th)	59 % (0.27)
C50 [245]	GNSCS/S (63)	1 M LiTFSI + 2 % wt. LiNO <sub>3</sub> (DOL:DME)	1.1 3.0	2.8–1.7	1 C	1140 <sup>b</sup>	548 (400th)	48 % (0.13)
					0.18 C	942	647 (110th)	68 % (0.3)
AC51 [248]	S/HPSCA-400 (80)	1 M LiTFSI + 0.25 M LiNO <sub>3</sub> (DOL:DME)	Not specified	2.8–1.7	1 C	~810	590 (400th)	73 % (0.07)

#### Table Footnotes

<sup>a</sup> Nomenclature used by the authors themselves.

<sup>b</sup> Activation cycles at 0.1 C.

alt-text: Table 5

Table 5

The table layout displayed in this section is not how it will appear in the final version. The representation below is solely purposed for providing corrections to the table. To preview the actual presentation of the table, please view the Proof.

Previous version

Expand

Electrochemical performance of carbons (C) or activated carbons (ACs) from animal and human waste biomass used as cathodes in Li-S cells.

AC [Ref]	Cathode <sup>a</sup> (%S)	Electrolyte	Sulfur Loading/mg	Voltages/V	Current Density	Initial Capacity/mAh	Final Capacity/mAh g <sup>-1</sup> (Cycle)	Capacity Retention (Fade rate/ %)
----------	---------------------------	-------------	-------------------	------------	-----------------	----------------------	--	-----------------------------------

Updated version

Electrochemical performance of carbons (C) or activated carbons (ACs) from animal and human waste biomass used as cathodes in Li-S cells.

AC [Ref.]	Cathode <sup>a</sup> (%S)	Electrolyte	Sulfur Loading/mg cm <sup>-2</sup>	Voltages/V	Current Density	Initial Capacity/mAh g <sup>-1</sup>	Final Capacity/mAh g <sup>-1</sup> (Cycle)	Capacity Retention (Fade rate/ %)
AC52 [30]	S/BHPC-850 (63)	1 M LiClO <sub>4</sub> (DOL:DME, 2:1)	Not specified	2.8–1.5	Not specified	1265	643 (50 <sup>th</sup> )	49 % (1.02)
AC53 [255]	Pure sulfur and FBPC as Interlayer (63)	Not specified	1.2–1.5	2.8–1.7	0.1 C	1300	1090 (50 <sup>th</sup> )	83.8 % (0.32)
					1 C	1171	600 (700 <sup>th</sup> )	51.2 % (0.07)
					0.2 C	1050	735 (100 <sup>th</sup> )	70 % (0.30)
AC54a [256]	rGO/GPC-2-S (70.1)	1 M LiTFSI + 1 % wt. LiNO <sub>3</sub> (DOL:DME)	1.5–1.6	3.0–1.7	0.1 C	1420	848 (200 <sup>th</sup> )	60 % (0.20)
					1 C	775	503 (500 <sup>th</sup> )	65 % (0.07)
AC54b [257]	S/NOPC-600 (54.3)	1 M LiTFSI + 1 % wt. LiNO <sub>3</sub> (DOL:DME)	1.3	3.0–1.7	0.2 C	921	489 (300 <sup>th</sup> )	53.1 % (0.16)
AC55 [253]	CHPC/S (75.8)	1 M LiTFSI + 1 % wt. LiNO <sub>3</sub> (DOL:DME) 20 μL mg <sup>-1</sup>	2.0	2.8–1.7	0.2 C	1076	699.6 (250 <sup>th</sup> )	65 % (0.14)
	CHPC/CoS <sub>2</sub> /S (75.8)					1231	1049 (250 <sup>th</sup> )	85.2 % (0.06)
C56 [254]	3DG/S (68)	1 M LiTFSI + 1 % wt. LiNO <sub>3</sub> (DOL:DME)	1.3	2.7–1.7	0.5	830	515 (200 <sup>th</sup> )	62 % (0.19)
AC57 [258]	NPPC/S (70.5)	1 M LiTFSI + 1 % wt. LiNO <sub>3</sub> (DOL:DME)	Not specified	3.0–1.7	0.1 C	1321.7	585.6 (100 <sup>th</sup> )	44 % (0.56)
					1 C	694.3 (2 <sup>nd</sup> )	372 (500 <sup>th</sup> )	53.5 % (0.09)
	0.1 C				1413	888.5 (100 <sup>th</sup> )	63 % (0.37)	
	1 C				757	526 (500 <sup>th</sup> )	69.5 % (0.06)	
AC58 [259]	55-PGC@SFPC/S (70)	1 M LiTFSI + 1 % wt. LiNO <sub>3</sub> (DOL:DME)	2.35	3.0–1.7	0.1 C	1354	757 (100 <sup>th</sup> )	56 % (0.44)
					2 C	975	700 (300 <sup>th</sup> )	72 % (0.09)
					3 C	641	414 (1000 <sup>th</sup> )	64.5 % (0.035)
AC59 [260]	g-C/S (69)	1 M LiTFSI + 2 % wt. LiNO <sub>3</sub> (DOL:DME)	1.2–1.5	2.8–1.8	0.2 C	1113.2	989.2 (300 <sup>th</sup> )	88.8 % (0.037)
					0.5 C	1066.1	870.3 (300 <sup>th</sup> )	81.6 % (0.061)
					1.0 C	737.8	705.3 (300 <sup>th</sup> )	95.6 % (0.014)
					2.0 C	606.7	574.2 (300 <sup>th</sup> )	94.6 % (0.018)

#### Table Footnotes

<sup>a</sup> Nomenclature used by the authors themselves.

alt-text: Table 6

Table 6

*i* The table layout displayed in this section is not how it will appear in the final version. The representation below is solely purposed for providing corrections to the table. To preview the actual presentation of the table, please view the Proof.

Previous version

Expand

Electrochemical performance of carbons (C) or activated carbons (ACs) from contaminated biomass and industrial wastes used as cathodes in Li-S cells.

Type	AC [Ref.]	Cathode** (%S)	Electrolyte	Sulfur Loading/mg	Voltages/V	Current density	Initial Capacity/mAh	Final Capacity/mAh g <sup>-1</sup> (Cycle)	Capacity Retention (Fade rate/ %)
------	-----------	----------------	-------------	-------------------	------------	-----------------	----------------------	--	-----------------------------------

Updated version

Electrochemical performance of carbons (C) or activated carbons (ACs) from contaminated biomass and industrial wastes used as cathodes in Li-S cells.

Type	AC [Ref.]	Cathode** (%S)	Electrolyte	Sulfur Loading/mg cm <sup>-2</sup>	Voltages/V	Current density	Initial Capacity/mAh g <sup>-1</sup>	Final Capacity/mAh g <sup>-1</sup> (Cycle)	Capacity Retention (Fade rate/ %)
H O U S E H O L D	C60 [261]	CSEM <sup>a</sup>	1 M LiCF <sub>3</sub> SO <sub>3</sub> + 0.1 M LiNO <sub>3</sub> 1 M Li <sub>2</sub> S <sub>6</sub> (DOL:DME) (Catholyte)	3.0–3.2	3.0–1.8	0.1 C	1327	1000 (100 <sup>th</sup> )	75 % (0.25)
	C61 [262]	APC-graphene/S (50)	1 M LiTFSI + 0.4 M LiNO <sub>3</sub> (DOL:DME) 15 μL mg <sup>-1</sup>	3.6	2.8–1.5	0.96 C	1083	754 (620 <sup>th</sup> )	69.6 % (0.05)
I N D	AC62 [263]	CF-6/S (69.7)	1 M LiTFSI + 1 % wt. LiNO <sub>3</sub> (DOL:DME) 20 μL mg <sup>-1</sup>	1.5	2.8–1.7	1 C	789	584.4 (500 <sup>th</sup> )	74 % (0.05)
						0.5 C	1200	700 (100 <sup>th</sup> )	58 % (0.42)



U S T R I A L	AC63 [264]	Act PyLs-Cap S + S (68)	1 M LiTFSI + 0.1 M LiNO <sub>3</sub> (DOL:DME) 40 μL mg <sup>-1</sup>	2.6	2.8–1.5	1 C	920	580 (100th)	63 % (0.37)
				3.1			580	395 (100th)	68 % (0.32)
				2.0			720	540 (200th)	75 % (0.14)
				3.6			510	410 (200th)	80 % (0.18)
	AC64 [265]	a-NOSPC/S (72)	1 M LiTFSI + 1 %wt. LiNO <sub>3</sub> (DOL:DME)	1.1	3.0–1.5	0.5	1122	754 (400th)	67.2 % (0.08)
				2.7		0.2	1074	745 (100th)	69 % (0.31)
	C65 [266]	ABW-C/S (70)	1 M LiTFSI + 0.4 M LiNO <sub>3</sub> (DOL:DME) 20 μL mg <sup>-1</sup>	1	2.7–1.8	1 C	1375	800 (450th)	58.2 % (0.09)
						2 C	1500	450 (625th)	30 % (0.11)
						3 C	900	270 (950th)	30 % (0.07)

\*\*Nomenclature used by the authors themselves; [a] Catholyte; [b] Carbon paper interlayer; [c] Carbon fiber@SiO<sub>2</sub> interlayer.

### 3.2.1 ACs from woody biomass

The five properties of all wastes from forestry biomass are included in Fig. 6 (a, b). Not all the employed carbons in Fig. 6a have been activated, and two different agents, KOH and ZnCl<sub>2</sub>, have been used for activation. Carbonization temperatures are also variable, ranging between 700 and 1000 °C. It seems reasonable that the non-activated carbons have significantly lower S<sub>BET</sub> values than the activated ones, Fig. 6b. More striking are the V<sub>p</sub> values, which are higher in one of the non-activated carbons: 0.72 cm<sup>3</sup> g<sup>-1</sup> (C1) as compared to that of an activated one, 0.69 cm<sup>3</sup> g<sup>-1</sup> (C2). Regarding the S content in the composite, it is very different, ranging 40–80 %. It is also noteworthy that the C2 composite with a low value of V<sub>p</sub> (0.23 cm<sup>3</sup> g<sup>-1</sup>) has a S loading greater than 70 %. [Instruction: Figure 6 should be moved to this section.]

The first bibliographic evidence on the use of activated carbons from forestry residues as cathodic matrices in Li–S batteries was reported in 2016. Xu et al. [152] used the bark of a plane tree (W1) carbonized at 750 °C under nitrogen atmosphere for 5 h to obtain a hierarchical architecture of micro- and mesopores (C1). The pyrolyzed bark slices were immersed in CS<sub>2</sub> and used directly as a free-standing cathode electrode, with a high sulfur loading between 3.0 and 4.0 mg cm<sup>-2</sup> (Fig. 7a). The study of the electrochemical performance of this material revealed modest capacity values during cycling. Specifically, at a current density of 0.125C a specific capacity of 1159 mAh g<sup>-1</sup> was achieved in the first cycle, and a retention capacity of 52.5 % after 60 charge/discharge cycles.

One year later, Luo et al. [153] described the use of natural wood microfibers (W2) as sulfur hosts. Its carbonized wood fibres (C2; CMWF) had a multi-channel structure of mesopores with a large pore size that allows incorporation in the CMWF-S composite of the highest amount of sulfur up to date (76 % S, Fig. 7b). However, the low capacity retention (35.5 %) obtained for this material at 0.25C rate after 450 cycles led the authors to propose a strategy for the functionalization of microfibers with Al<sub>2</sub>O<sub>3</sub> (f-CMWF) through atomic layer deposition (ALD), which would provide several advantages, the main one being the decrease in the pore size and volume of the carbonaceous matrix. Thereby, the sulfur percentage was reduced to 70 %, and the specific capacity increased to more than double that of the previous case without Al<sub>2</sub>O<sub>3</sub>. The prolonged stability shown during cycling for both materials should be noted, however, the capacity values indicated should be analyzed with caution since the voltage window used for galvanostatic measurements is generally considered too wide for Li–S cells, and would result in a sloping region below 1.6 V. Some authors assign this fact to the possible precipitation of Li<sub>2</sub>S<sub>2</sub> to Li<sub>2</sub>S [154], as in this case, and others to the reduction of LiNO<sub>3</sub> present in the electrolyte [155,156].

Pinecone derived porous carbon (W3) as a nitrogen and oxygen co-doped cathode material for Li–S batteries, was reported by Chulliyote et al. [157] for the first time, in 2017. This carbonaceous matrix (PC) had the heteroatoms inherent in its composition and, after an activation process with ZnCl<sub>2</sub> at 800 °C, it was able to reach high surface values (2065 m<sup>2</sup> g<sup>-1</sup>) and pore volume (1.5 cm<sup>3</sup> g<sup>-1</sup>). Therefore, it was postulated as an ideal material (AC3) to immobilize different amounts of sulfur (54, 68 and 73 % S) by the melt-diffusion method at 155 °C, giving rise to the C-S composite denoted as PCSC. The best electrochemical performance was observed for the PCSC cathode with 54 % sulfur, exhibiting a high initial discharge capacity of 1606 mAh g<sup>-1</sup> (close to the theoretical one) and after 100 cycles a reversible capacity of 1269 mAh g<sup>-1</sup> (79 % capacity) at 0.1C. Furthermore, during the rate capability test, this material managed to deliver capacity values of 923 mAh g<sup>-1</sup> at a high current density (2C). The better cycling is due to the uniform dispersion of sulfur within the pores which improves the ionic transport, and to the presence of heteroatoms that can chemically induce the adsorption of polysulfides in the PC matrix and mitigate the shuttle effect.

Subsequently, other authors used nitrogen-doped carbons derived from woody biomass for their research on Li–S batteries. In this respect, Schneidermann et al. synthesized nitrogen-doped biomass-derived carbon using sawdust (W4) as a carbon source, urea as a nitrogen source and potassium carbonate K<sub>2</sub>CO<sub>3</sub> as an activation agent [158]. After a high energy milling treatment (800 rpm), the powder sample was pyrolyzed at 800 °C (1 h), and finally washed with HCl and water. This process gave rise to activated carbon from forest biomass (AC4; WWUPC) with better textural properties and used as a matrix to host S. It is worth highlighting the high pore volume obtained, close to 2.0 cm<sup>3</sup> g<sup>-1</sup> with a microporosity of 30 %. Furthermore, a high nitrogen content of 7.0 wt % was determined by elemental analysis. In this study, it would be appropriate to know the behaviour of the material in a greater number of cycles; instead, the comparatively high quantity of sulfur in the electrode (2.7 mg cm<sup>-2</sup>) and the small volume of electrolyte (5 μL mg<sub>S</sub><sup>-1</sup>) used in the assembly of the cells are noteworthy. Furthermore, a free-standing nitrogen-doped porous carbon foam (PCF) electrode derived from natural melaleuca bark (W5) was studied in Li–S cells by Zhu et al. [159]. In this case, the activated carbon obtained from the melaleuca bark was used as a free-standing cathodic support after a simple carbonization process at 600 °C, a chemical activation with KOH, and another carbonization step at 700 °C in a nitrogen atmosphere for 2 h (AC5, Fig. 7c). Its high surface area (1785 m<sup>2</sup> g<sup>-1</sup>) and total pore volume (0.694 cm<sup>3</sup> g<sup>-1</sup>) allows the material to accommodate 51 wt % S after impregnation of the collector in a mixture of elemental sulfur, Ketjenblack, and multiwall carbon nanotubes in 1-methyl-2-pyrrolidone as a dispersant (S:KB:MWCNT in NMP; 90:5:5 wt ratio). In addition, the studied carbonaceous matrix had 2.21 at. % of nitrogen and 11.68 at. % of oxygen, which favours the absorption of the lithium polysulfides formed during cycling. Then, PCF/S electrodes were heat-treated at 155 °C for 12 h to improve the dispersion of sulfur in the PCF. In this study, the Li–S cells provided good electrochemical performance at 0.2 C for 100 cycles, increasing the sulfur load per electrode in a series of 1.8, 4.0 and 6.0 mg cm<sup>-2</sup>, and providing, in all cases, reversible capacity values greater than 600 mAh g<sup>-1</sup> and surprisingly good stability (capacity retention close to 75 %). [Instruction: Figure 7 should be moved to this section.]

Finally, the research group from Xiangtan University, led by Weixin Lei, have manufactured a porous activated carbon or ‘biochar’ from folium cycas (W6) by a chemical activation with KOH [160,161]. In both publications, the removal of the ash was carried out with dilute acid, either acetic acid (HAc) or hydrochloric acid (HCl). In the first study, a comparison was made between the behaviour of the carbonaceous matrix at neutral pH (FCB-7) and acid pH (FCB-1; AC6-a) with HAc, the latter being the one with best performance. In the second comparative study, it was confirmed that the presence of Ni nanoparticles in the matrix (AC6-b) was a beneficial factor since the addition of this transition metal favoured the reaction kinetics between Li and S and, at the same time, improved the cycling stability due to its strong affinity for polysulfides. However, the FCB-1/S electrode was the one that presented the best performance since it showed a high initial capacity, above 1300 mAh g<sup>-1</sup>, at a rate of 0.5C and stabilized at 790 mAh g<sup>-1</sup> after 200 cycles with an attenuation rate of only 0.068 % per cycle.

As a summary, Table 1 shows the numerical values of some of the electrochemical measurements discussed above. [Instruction: Table 1 should be moved to this section.]

### 3.2.2 ACs from herbaceous and agricultural biomass

In most publications whose main topic is the use of carbonaceous materials from biomass sources as a cathode in Li-S batteries, the activated carbons are prepared from herbaceous and agricultural biomass. Due to the large number of articles in this area, a subdivision is necessary to address the most relevant results. Agricultural residues will be discussed first, and then agri-food wastes.

### 3.2.2.1 Agricultural residues

The agricultural residues studied have been very varied, and can be classified into three sections: flowers, plants, and straws (Table 2). The five items of carbons are shown in Fig. 8. The carbonization time and temperature range remain wide, between 1 and 3 h and between 600 and 900 °C, respectively. More homogeneity is shown in the activating agent used; all of them have basic character with KOH dominating. Regarding the textural properties, a wide variation is also observed in both  $S_{\text{BET}}$ , between 3000 and 750  $\text{m}^2 \text{g}^{-1}$ , and pore volume, between 1.92 and 0.48  $\text{cm}^3 \text{g}^{-1}$ . It is difficult to establish relationships between these properties and the time and calcination temperature, as they seem poorly correlated. Furthermore, a non-activated carbon, C17.2, has an abnormally high specific surface area reported, more than 2000  $\text{m}^2 \text{g}^{-1}$ , greater than many activated carbons (Fig. 8b). Similarly, no relationship between pore volume and S content can be observed. In fact, the AC10 sample with the highest  $V_p$ , 1.92  $\text{cm}^3 \text{g}^{-1}$ , has less than 70 % S, but the AC18 sample, with only 0.71  $\text{cm}^3 \text{g}^{-1}$  more than 80 % S. [Instruction: Figure 8 should be moved to this section.]

In the *flower category*, carbon from biomass sources such as camellia (W7) or reed flowers (W11), and catkins of different types (W8 – W10) have been evaluated in Li-S cells [162–166]. Nitrogen-doped porous carbons (AC7) were fabricated from fallen camellia flowers by pyrolysis and activation with KOH [162]. Thanks to its doping and good textural properties, this matrix can help to delay the dissolution of polysulfides. This has been demonstrated by a simple absorption test and UV-visible measurements. The electrochemical performance exhibited using AC7 was striking, allowing cycling at high rates (1C) for a relatively high number of cycles (200), and providing a good cell stability with a small capacity decrease of 0.11 % per cycle. An unresolved issue in this work (and in many others on Li-S batteries) is the over-discharge observed for voltage values lower than 1.8 V; higher than 15 % of the total capacity. Its origin could be related to side reactions, e.g. reduction processes associated with electrolyte components. Hence, the voltage window in these batteries should be fixed, for example between 2.7 and 1.8 V, to avoid this problem and eliminate this factor in comparative studies. Moreover, the results in this study were provided by Li-S cells that instead of using a traditional Celgard separator (2300, 2400, 2500, etc.) employed a functionalized membrane by coating with the same activated carbon (AC7, aNPCP3). By incorporating this interlayer into the cell configuration, a physical barrier is being introduced, and consequently the electrochemical performance is improved.

Catkin-derived carbon has turned out to be a type of agricultural biomass that has adapted very well to Li-S technology. Its unique tubular morphology and porosity have made it a suitable cathodic matrix. Its first use in this context dates from 2017 when poplar catkins (W8) were subjected to an alkaline activation process (KOH) and hydrothermal carbonization [163]. The active carbon obtained (AC8) displayed a large presence of micropores in its structure, which was reflected in the shape of its nitrogen adsorption-desorption isotherm (type I without a hysteresis loop) [167]. This work also incorporated a novel approach in terms of the preparation of the electrolyte, using less common solvents such as tetraethylene glycol dimethyl ether (TEGDME). Although ether based solvents have not been widely used in Li-ion batteries due to the oxidative decomposition of ether at high potentials ( $\sim 4.0 \text{ V vs. Li/Li}^+$ ), they can operate in Li-S batteries at lower potentials ( $< 3.0 \text{ V vs. Li/Li}^+$ ) and are much more stable than carbonate-based ones with Li-metal [168]. Compared to low- $M_w$  ethers, glyme-based solutions are more suitable for Li-S batteries because they have high boiling and flash points, low or no flammability, and strong resistivity at high oxidative potentials. Barchasz et al. found that TEGDME solvent provided better electrochemical performance in these types of batteries [169]. This was argued to be because TEGDME contains a greater number of oxygen atoms in the glyme structure than other solvents; in other words, TEGDME solubilizes and dissociates lithium salts and polysulfide compounds better. In addition, its low flammability improves another important factor for the future commercialization of this type of battery: the safety of the cells manufactured. The low resistance of the electrode/electrolyte interface, driven by an improved electrode design and an adequate electrolyte, is considered one of the main reasons for the high performance that will foster break-through for commercial Li-S batteries [170–172].

Another interesting work using catkin (W10) as the carbon source has been published recently [165]. This mesoporous carbon (AC10) displayed a remarkable electrochemical performance, considering the high amount of sulfur contained in the TACM/S composite (82.5 % S) and the modest BET surface area (793  $\text{m}^2 \text{g}^{-1}$ ). Still, the S loading was not that high, around 1.5  $\text{mg cm}^{-2}$ . The TACM/S composite provides high discharge capacities at 0.1 C, and a satisfactory capacity retention close to 77.5 % after 500 cycles at 0.5 C, with a low fading rate (capacity loss around a 0.043 % per cycle). Moreover, the activation temperature was only 600 °C, the least severe as shown in Fig. 8 (a).

Reed flowers (W11) were transformed into a bimodal porous carbon (BPC, AC11) through a process in several steps: hydrothermal treatment of the residue, chemical activation using KOH and, finally, a two-stage carbonization strategy under successive medium (450 and 650 °C; mesopores formation) and high temperature (800 °C; micropore formation) treatment [166]. The BPC/S composite was prepared by melt-diffusion and managed to accommodate 74 % sulfur. Its electrochemistry was studied at appropriate conditions, and the charge/discharge profiles of the Li-S cells did not show anomalies in the range used (1.7–2.8 V) while different sulfur loadings (2.1 and 8.3  $\text{mg cm}^{-2}$ ) were tested. For the lower S content, good cycling properties at high current densities (663  $\text{mAh g}^{-1}$  at 1C after 1000 cycles and a capacity retention of 75.5 % with a low capacity fading rate of 0.025 % per cycle) and a remarkable electrochemical response at different currents (rate capability) was seen in the results. [Instruction: Table 2 should be moved to this section.]

Within the *plant category*, the residue most used has been bamboo culms (W12). Several works have been reported where bamboo is used to obtain a porous biochar with properties to act as a good sulfur host [173–177].

Yan et al. [174] pioneered the use of activated carbons from bamboo stems (AC12.2) since their inception with this by-product in 2018. The first studies of this group focused on the optimization of the production process of an AC with appropriate textural properties. To accomplish this, activated carbons by three different routes were prepared: (a) direct pyrolysis carbonization, (b) two-step activation and (c) one-step activation with KOH, the latter being the most appropriate due to the products large surface area (1824  $\text{m}^2 \text{g}^{-1}$ ) and total pore volume (1.15  $\text{cm}^3 \text{g}^{-1}$ ), with a dominating presence of micropores.

One year later, the same group added polyaniline (PANI) in the structure as a coating layer [175]. The use of PANI improved the electrochemical properties since it served to physically encapsulate the sulfur particles, minimized the volume changes experienced by the carbonaceous structure and increased the durability of the cycling. Furthermore, the migration of polysulfides was restricted with the N-doping introduced by the PANI backbone. Continuing on this route, the authors prepared a further improved cathode material based on a core-shell approach [176]. This time, the core consisted of a mixture of AC12.2-c and sulfur (containing about 64 % S) and the core-shell structure was developed by incorporating a soft coating of sulfonated polyaniline (S-PANI). A simple model scheme of the in-situ polymerization process is shown in Fig. 9. [Instruction: Figure 9 should be moved to this section.]

Other authors have focused their efforts on the transformation of bamboo through longer and more complex processes in which the biowaste undergoes both acid and alkaline treatments, activation with NaOH and carbonization at high temperatures [173–177]. Even enzymatic hydrolysis has been carried out in one of the steps [177].

Nevertheless, other wastes such as those stemming from lotus plumule tea (W13) or nodus nelumbinis rhizomatis (NNR; W16) have been converted into porous carbons derived from agricultural biomass using KOH as an activating agent and subsequently functionalized, providing electrochemical results that are competitive with those previously mentioned [178,181]. The first approach was based on the incorporation of thiourea ( $\text{CN}_2\text{H}_4\text{S}$ ) after obtaining activated carbon from lotus plumule tea (AC13). The functionalized material with N and S heteroatoms was prepared by a conventional hydrothermal treatment at 180 °C, thereby acquiring a unique honeycomb-like structure that favours the impregnation of the electrolyte (a small quantity of 10  $\mu\text{L mg}^{-1}$ ) and fast transport properties for both  $\text{e}^-$  and  $\text{Li}^+$ . The results obtained from the

nitrogen adsorption and desorption isotherms provided high BET surface area values close to  $2500 \text{ m}^2 \text{ g}^{-1}$  and pore volumes of approximately  $1.0 \text{ cm}^3 \text{ g}^{-1}$ , with dominating contribution from mesopores. The composite was prepared with a high S content, 85 %, and the electrode with a moderate S loading,  $2.8 \text{ mg cm}^{-2}$ . The Li-S cells exhibited high specific capacity values at the rates of 0.1C ( $1164 \text{ mAh g}^{-1}$  after 150th cycles), 0.5C ( $952 \text{ mAh g}^{-1}$  after 300th cycles), and 1C ( $496 \text{ mAh g}^{-1}$  after 500th cycles), i.e., with a capacity retention of 80 %, 74 % and 41 %, respectively. The good electrochemical properties of this material were attributed to both the special honeycomb-like structure that give it remarkable textural properties and to the double doping of hierarchical porous carbon derived from biomass that is related to the increase of active sites and the strong trapping capacity of polysulfides. These properties have generally shown to be beneficial for the development of high energy density Li-S batteries. Yan et al. [181] applied a somewhat different approach to the use of C obtained from NNR by adding a Ni-basic salt,  $\text{Ni}_3(\text{NO}_3)_2(\text{OH})_4$  (NNH) to reduce the shuttle effect. Specifically, the proposal to improve the immobilization of sulfur and polysulfides was to first prepare the mixture of porous activated carbon, assigned as **AC16**, with sulfur (PC/S) and continue by an encapsulation process through a mesh-like NNH layer coating in situ on the surface, to finally obtain an NNH/PC/S composite cathode for Li-S batteries. An impressive initial discharge specific capacity of  $1203 \text{ mAh g}^{-1}$  at 0.5 C and  $521 \text{ mAh g}^{-1}$  after 700 cycles, with a small capacity decay of 0.08 % per cycle, was obtained for this NNH/PC/S cathode. Furthermore, the cell exhibited good electrochemical response at high current densities in the range 0.2 C–5 C where it could maintain reversible capacity values of  $584 \text{ mAh g}^{-1}$ . These improvements are attributed to various factors: (1) better conductivity thanks to the use of activated carbons derived from biomass, (2) more active sites and stronger encapsulation of sulfur and its reaction intermediates due to the presence of nickel in the coating, providing a strong adsorption by Ni-S bonding, and (3) increasing number of cycles and prolongation of adequate capacity at high rates due to the decrease in both the dissolution of polysulfides in the electrolyte, and the loss of active material.

In the *straw category*, we have included carbons obtained from rice husks (**W17**, RH) used for Li-S batteries [182–185]. Other wastes collected are wheat straw (**W18**) [186], rice straw (**W19**) [187] and sugarcane bagasse (**W20**) [188,189]. Unlike other biomass carbons, that from rice husk (RH) has a significant content of  $\text{SiO}_2$  which can be modified, or even removed, by treatment with fluorinating agents, where HF [183] and  $\text{NH}_4\text{HF}_2$  [182] are the most used. There are some discrepancies regarding the role played by  $\text{SiO}_2$ . Rybarczyk et al. [182] obtained a non-activated carbon (**C17.1**) at  $900 \text{ }^\circ\text{C}$  under a flow of Ar. Although the resulting surface area was low compared to the rest of the waste analyzed, its total pore volume of  $0.5 \text{ cm}^3 \text{ g}^{-1}$  was appropriate to accommodate 56 % S in its structure. The presence of  $\text{SiO}_2$  in the electrode indicated a decrease in the capacity obtained: from  $834 \text{ mAh g}^{-1}$  to  $563 \text{ mAh g}^{-1}$  when the cell was cycled at 0.5 C. On the other hand, Jin et al. suggested a different role played by  $\text{SiO}_2$ , and found a positive effect of a moderate content of  $\text{SiO}_2$  on the stability of Li metal anode (**AC17.2**, Li/RC, Fig. 10). Control of the  $\text{SiO}_2$  content was carried out by a treatment with HF [183]. As a cathode, they also used a RH-derived carbon activated with KOH but without HF treatment, which was named RC. The use of the modified Li electrode (obtained by plating  $10 \text{ mAh cm}^{-2}$  lithium into the RC at  $1.0 \text{ mA cm}^{-2}$ ) improved the full cell performance. Finally, the works of Li et al. [184] and Chen et al. [185] should be commented in this context. In the first of these, a non-activated carbon (**C17.3**) was used, but in its preparation a  $\text{SiO}_2$  template agent was used. This rendered a significant effect on its textural properties, especially its content in mesopores, but therefore made it difficult to compare the electrochemical properties. Chen et al. [185] used an activated carbon (**AC17.4**) and employed a potential window between 3.0 and 1.0 V. The resulting discharge curve displayed a somewhat unorthodox profile, as well as over-discharge values (more than 50 %) below 1.8 V. [Instruction: Figure 10 should be moved to this section.]

As discussed in Section 3.1, the solubility of LiPSs ( $\text{Li}_2\text{S}_n$  with  $n > 2$ ) in the electrolyte and their diffusion through the separator and reaction with the Li anode is one of the main problems of Li-S batteries. Mitigating this by the immobilization of LiPSs in the C-S composites generally takes place due to a synergistic effect of physical absorption (PAB) and chemical adsorption (CAD). Weak van der Waals interactions are involved in the PAB processes, and are often correlated to the pore structure of the carbonaceous matrix. In the CAD process, the sulfur species are trapped through chemical interactions with the atoms located on the surface of the matrix C. Hence, the presence of functional groups or the substitution of C by other atoms can enhance the capture of polysulfides. As a result of the shuttle effect obstruction, the cell will perform better, with an increase in the specific capacity and lower capacity loss during cycling. Zhang was among the first to review the syntheses of heteroatom-doped carbons as well as their mechanisms and applications in the Li-S batteries [190]. One example relevant in this current context would be **AC18** prepared from wheat straw, which is a N-, O-, and S-tri-doped porous carbon (1.36 at % for N, 7.43 at % for O and 0.7 at % for S) with an uncommon value of BET surface area, higher than  $3000 \text{ m}^2 \text{ g}^{-1}$ , and a total pore volume of close to  $2.0 \text{ cm}^3 \text{ g}^{-1}$  (76 % microporosity) [186]. The capacity retention at 0.2C was moderate, around 66 % at 100 cycles, but displayed a rather impressive 56 % at 1C after 500 cycles, with a capacity loss of merely 0.088 % per cycle. However, some issues arise regarding the role played by the N impurity. This element is not present in the carbon matrix (WSC) obtained under the same conditions as NOSPC, but without activating with KOH its BET surface and pore volume are notably lower, around  $650 \text{ m}^2 \text{ g}^{-1}$  and  $0.3 \text{ cm}^3 \text{ g}^{-1}$ , respectively. The capacity of this non-activated carbon is also noticeably lower, around  $430\text{--}320 \text{ mA h g}^{-1}$  when cycled at 0.2C. Whether the cause is due to the role of N or the texture of the resulting carbon is still not known. Another example would be **AC19** derived from rice straw [187], which can be obtained in a similar way as the previous discussed with wheat straw [186]. Once the residue is thoroughly washed with distilled water, it is subjected to a pre-carbonization at  $800 \text{ }^\circ\text{C}$  in an inert atmosphere for 2 h. Subsequently, it is chemically activated by mixing C:KOH in a 1:2 ratio and finally, it is subjected to another pyrolysis step at the same conditions for 3 h. The presence of intrinsic heteroatoms in AC19 is also important for the composition of the raw material, which contains 1.07 at % for F, 0.86 at % for S and 4.99 at % for N. The tube-like morphology creates multifunctional carbon tunnels for electrolyte penetration and rapid ion transport. Moreover, the naturally doped heteroatoms generate catalytic sites on the surface of the tunnels which improves the polysulfide anchoring. Both factors contribute to improve the redox reaction kinetics and polysulfide anchoring. Finally, this synergistic effect translates into an improvement in electrochemical kinetics for high energy density Li-S batteries. The composite loaded with 76 wt % S exhibited a reversible capacity of  $260 \text{ mAh g}^{-1}$  after 2000 cycles at a high rate of 3C, displaying a capacity decay rate of only 0.029 % per cycle for electrodes with a sulfur loading of  $1.2 \text{ mg cm}^{-2}$ . Meanwhile, for electrodes with a higher sulfur loading ( $5.8 \text{ mg cm}^{-2}$ ), the electrochemical performance was also adequate, supplying an initial discharge capacity of  $1070 \text{ mAh g}^{-1}$  at 1C. After 100 charge-discharge cycles, the reversible capacity value recorded was still ca.  $700 \text{ mAh g}^{-1}$ . The explanation for the good behaviour observed for the NHAC/S composite [187], based exclusively on a combined effect of the presence of tunnels and heteroatoms in the structure, presents serious doubts if we compare the results with another composite, ABT/S where the ABT carbon is a physical mixture (mass ratio of 1:1) of KOH activated acetylene black with NHAC. The performance of this composite is clearly lower. This carbon also contains heteroatoms and tunnels, perhaps in low content, but the only property quantified is the BET surface that undergoes a drastic decrease from 1181 (NHAC) to  $191 \text{ m}^2 \text{ g}^{-1}$  (ABT), a property that is hardly considered by the authors.

In 2019, Wang et al. concentrated their efforts on studying the differences shown by the chemical mechanisms for  $\text{K}_2\text{CO}_3$  activation compared to KOH activation when urea is incorporated as a nitrogen doping agent [188]. Sugarcane bagasse was the waste chosen as the carbon precursor (**W20**). In order to obtain a high N-doping activated carbon (**AC20.1**), the treatment was carried out via a one-step activation process where the W20 residue was mixed with  $\text{K}_2\text{CO}_3$ , urea and water, and kept under stirring for 3 h. Afterwards, the water was evaporated in a rotary evaporator at  $70 \text{ }^\circ\text{C}$ , and finally, the sample was pyrolyzed at  $800 \text{ }^\circ\text{C}$  for 2 h under an Ar atmosphere. This gives rise to an **AC20.1** that contains 7.58 at % of N, and a large specific surface area and total pore volume of  $2762 \text{ m}^2 \text{ g}^{-1}$  and  $1.85 \text{ cm}^3 \text{ g}^{-1}$  (abundance of micropores: 63 %), respectively. In this work, it is worth highlighting the prolonged cycling of the Li-S cells, whose reversible discharge capacity values correspond to  $571 \text{ mAh g}^{-1}$  after 400 cycles and  $542 \text{ mAh g}^{-1}$  after 500 cycles at 0.5C and 1C, respectively. At the beginning of 2020, the same authors incorporated advances in the production process of AC from sugarcane bagasse by adding a greater amount of urea during the activation process (12.2 at % for N), and by manufacturing, in a simple way, an interlayer that allowed the functionalization of the polypropylene separator and efficiently improved the electrochemical performance of their Li-S batteries [189].

This chapter addresses a wide variety of scientific work on agricultural residues. For this reason, we classified these biomass residues into three categories: flowers, plants and straws. From this body of literature, a notable disparity both in the performance of the electrodes as well as in the experimental conditions used is seen. However, important improvements obtained both in the process of transformation of biomass into activated carbons, as well as in the electrochemical behaviour, should be taken into account for future research, highlighting the following aspects: (i) matrices doped with heteroatoms presented better textural properties than the undoped matrices; (ii) UV-visible measurements made it possible to demonstrate the absorption power of ACs over time against a polysulfide solution; (iii) setting an appropriate voltage window is a

key aspect to perform the galvanostatic measurements correctly; (iv) the incorporation of functionalized membranes instead of the traditional Celgard separator led to better electrochemical results; (v) novel electrolyte preparations using ether based solvents led to the manufacturing of safer Li-S cells due to their non-flammable character and showed an adequate electrochemical behaviour; (vi) several studies have confirmed that one of the best routes to obtain activated carbons with excellent properties is through one-step activation with KOH; (vii) the use of coating layers such as PANI, S-PANI or NNH turned out to be fairly successful for sulfur encapsulation; and (viii) the template effect of the silica in the rice husk favorably affected the textural properties of the activated carbons.

### 3.2.2.2 Agri-food residues

The use of agri-food sources for energy storage systems involves two drawbacks: (i) large areas of land are required for its production and (ii) its main use as food for humans and animals is adulterated. A clear example of this problem is the first-generation bioethanol production due to the use of edible feedstocks (corn, wheat, barley, rye, or sugarcane crops). For this reason, the second-generation bioethanol production emerged where the raw materials were not edible [191].

The use of food sources has similar disadvantages in the development of materials for Li-S batteries. For sustainability reasons, the incorporation of edible raw materials in these devices should be limited or focused on raw materials that require small volumes for a very high technical performance. Since 2014, there have been quite a few studies that have used agri-food materials to obtain hierarchically porous carbons (starch [192], sugars [193], watermelon juice [194], yam [195], wheat flour [196,197], popcorn [198] and chickpea [199]) or activated carbons (gelatin [200], rapeseed meal [201], soybean [202], cinnamon sticks [203], Kombucha scoby [204], and puffed rice [205]) with good properties to host sulfur.

To avoid this competition and not generate a conflict of interest in the agri-food sector, dozens of studies have been carried out where the properties of different inedible raw materials have been analyzed to become efficient conductive and sulfur capture matrices. The most relevant investigations over the last five years, which obtained the best electrochemical results using agri-food waste in Li-S batteries, will be discussed below (see Fig. 11 (a) and (b)). In addition, Table 3 shows all the information regarding the electrochemical measurements of the investigations selected in this section.

The activating agents used in this group were the three most conventional (KOH,  $ZnCl_2$ ,  $H_3PO_4$ ) with a clear dominance of KOH. A large range is also observed in terms of calcination temperature, between 550 and 1000 °C, Fig. 11a. In this group of materials, the non-activated carbons show the expected behaviour, with lower  $S_{BET}$  values than the activated ones. The AC35 sample, whose  $S_{BET}$  is more than  $2700\text{ m}^2\text{ g}^{-1}$  but with only  $0.17\text{ cm}^3\text{ g}^{-1}$  of  $V_p$ , stands out [206]. In addition, its S content is high, around 70 %, much higher than that of for example the composite AC22.1b with only 50 % S, but with  $1.72\text{ cm}^3\text{ g}^{-1}$  of  $V_p$  [207]. Undoubtedly the best textural properties were obtained for the AC40 sample with a surface area above  $4000\text{ m}^2\text{ g}^{-1}$  and a total pore volume of  $2.02\text{ cm}^3\text{ g}^{-1}$ , the highest of all carbons in this group (Fig. 11b) [208]. In addition, the derived composite has the highest sulfur loading, with values close to 90 %.

In 2016, Yang and co-workers [209] carried out a study on the preparation of activated carbons from banana peel (AC21, BPC) using different temperatures in the carbonization process (500, 700 and 900 °C). Depending on the carbonization temperature, the ACs were obtained with different surface area and pore volume values; BPC-700 being the one with the highest  $S_{BET}$  ( $2741\text{ m}^2\text{ g}^{-1}$ ) and intermediate pore volume ( $1.23\text{ cm}^3\text{ g}^{-1}$ ). In all cases, the S-BPC composites contained 65 % sulfur in the carbonaceous matrix, but the total S loading in the electrodes was not specified. The S-BPC-700 composite showed the best electrochemical results with an initial capacity of  $1227\text{ mAh g}^{-1}$ . After 100 charge and discharge cycles, the cell had a capacity of  $870\text{ mAh g}^{-1}$  at 0.2C and  $775\text{ mAh g}^{-1}$  at 1 C.

Corn cob waste (W22) has been used in recent years as a carbon source by different researchers. It is worth noting the studies by Zhang et al. on the preparation of carbonaceous matrices derived from corn cob, and their subsequent use as cathodes in Li-S batteries [207,210]. The best electrochemical behaviour was obtained for a carbon activated with KOH and subsequently doped with nitrogen through annealing in an ammonia flow at 800 °C for 3 h (NAC-800, AC22.1). Both studies are very similar in that an acceptable cycling stability of the NAC-800/S composite was found at a moderate current density (0.3C), but for a rather low S loading, particularly that used in Ref. [207] of only  $0.8\text{ mg cm}^{-2}$ . A convincing explanation for the differences in the capacity values for the same composite studied in both references is also still an open question. It does not seem that the difference in S loading used in both cells is the cause of the different capacity retention of the composite, since the expected response should be the opposite, i.e., the cell with less content in S (ref. [207]) should conventionally have a better performance.

The work published in 2019 by Li et al. provided complementary information to researchers interested in the use of corn cob waste (and other biomass residues) as a sulfur host [211]. As shown in Fig. 12, the novelty of this study is based on the formation of an ultra-thin  $Fe_3C$  nanosheet grown on the mesoporous carbon from corn cob waste ( $Fe_3C$ -MC, C22.2), which possesses a strong adsorption and catalytic ability to LiPSs. As a result, the  $Fe_3C$ -MC/S composite delivers a high initial capacity of  $1465\text{ mAh g}^{-1}$  at 0.5 C, and a capacity of  $920\text{ mAh g}^{-1}$  after 1000 cycles for a moderate sulfur loading ( $1.5\text{ mg cm}^{-2}$ ). Nevertheless, Li-S cells with a high sulfur load of  $9.0\text{ mg cm}^{-2}$  were tested at 0.5 C, obtaining values of  $699\text{ mAh g}^{-1}$  after 100 cycles with a fairly good capacity retention.

In the above case, the  $Fe_3C$  nanosheets played a key role in the electronic transmission, adsorption, and conversion of LiPSs in Li-S batteries. However, this is not the only occasion where researchers have added different transition metal species such as metal oxides, sulfides, or complex salts due to their strong adsorption capacity for polysulfides, to improve the cell performance. Within inedible agri-food waste, different polar compounds have been combined with biomass-derived carbon, such as  $TiO_2$  (W23: olive stones) [212],  $MnO_2$  (W23: olive stones and W27: pistachio shell) [213,214],  $CoS_2$  (W37: ginkgo nut) [215] and CoFe-Prussian blue analogues (W28: pomelo peel) [216] (see Table 3).

GACs from coconut shell (W24) has its main application as an adsorbent, and its use in the odour control systems of wastewater treatment plants (WWTP) should be highlighted. In a recent study, these contaminated GACs were regenerated through a simple thermal treatment, allowing the activated carbons to be used for the same application or giving them a second life as cathodes for Li-S cells (AC24.2); thereby, in both cases, reducing their deposition in landfills [218]. Two types of contaminated GACs were analyzed, one from the head pre-treatment point of the water line (WL) and the other from the sludge dewatering point of the sludge line (SL). After thermal regeneration of both samples at low temperature, the values of surface area and total pore volume were very similar, around  $600\text{ m}^2\text{ g}^{-1}$  and  $0.35\text{ cm}^3\text{ g}^{-1}$ , however, the type of porosity displayed significant differences. Although both were mainly mesoporous activated carbons, the SL-ACt3 sample also contained micropores, which favour a homogeneous and efficient distribution of sulfur in the carbonaceous structure and the adsorption of lithium polysulfides (Fig. 13a and b). The SL-ACt3@S composite showed a greater amount of pore sulfur (green line around 280 °C, marked as "S Inside" in Fig. 13c) than surface sulfur (red line around 245 °C, marked as "S Outside"). Therefore, the electrochemical performance of the SL-ACt3@S sample was better than that of the WL-ACt4@S sample, as confirmed in Fig. 13d.

Other inedible residues have been tested in Li-S cells, such as soybean hulls (W25) [219]. After its activation with potassium hydroxide and subsequent pyrolysis at 700 °C for 2 h, the material (AC25; S/porous carbon) acquired a high BET surface area ( $1232\text{ m}^2\text{ g}^{-1}$ ), but a moderate pore volume of  $0.54\text{ cm}^3\text{ g}^{-1}$  that limited the amount of sulfur in the composite to 63 %. The resulting sulfur loading per electrode was  $1.5\text{ mg cm}^{-2}$ , and the specific capacity maintained for 200 cycles at a current density of 0.5C was  $450\text{ mAh g}^{-1}$ . This satisfactory performance could be attributed to its hierarchical porous structure and the somewhat high content of acetylene black (20 %) present in the electrode.

Pistachio shell (W27) is a well-studied agri-food waste in Li-S batteries. The preparation of porous carbons have been carried out in several ways: by pyrolysis under Ar flow at 1000 °C (C27.1) [214], chemical activation with 1.5 M  $ZnCl_2$  pyrolysis at a moderate temperature of 550 °C (AC27.2) [221], or activation with 3 M  $H_3PO_4$  and


subsequent carbonization at 800 °C under a nitrogen flow (AC27.3) [222]. The electrochemical results showed that a PSAC@S composite (AC27.3) containing 70 wt % sulfur and a S loading in the electrode of 2.6 mg cm<sup>-2</sup>, one of the highest values in Table 3, is a good candidate for this application. It delivers 300 cycles, and the cell maintained a reversible specific capacity of 570 mAh g<sup>-1</sup> working in a voltage range of 2.6 to 1.8 V. Two factors positively affected this behaviour: i) the preparation of the electrodes on a carbon substrate or gas diffusion layer (GDL) which, due to its textural properties, enhances the increase in the S loading, the electrolyte impregnation of the electrode, and the kinetics of the reaction between Li and S [239,240]; and ii) the excellent textural properties acquired by the AC27.3 material after its activation ( $S_{\text{BET}} = 1345 \text{ m}^2 \text{ g}^{-1}$  and  $V_p = 0.67 \text{ cm}^3 \text{ g}^{-1}$ ) that favour the preparation of a composite with a high sulfur content and LiPSs adsorption.

The good performance of a carbon from cherry pits activated with phosphoric acid (AC30b, AC-H) in a Li-S cell has recently been used to design of a new S-based Li-ion battery using the AC-H@S composite as cathode and Li<sub>y</sub>SiO<sub>x</sub> as anode [228]. This full-cell exhibited a high initial capacity around 1200 mAh g<sup>-1</sup> at 0.2 C, which retained slightly below 60 % over 500 cycles.

A few studies can be found in the literature on doped activated carbons within the group of inedible agri-food waste. One of them is the use of natural okra shells (W35) activated with KOH and pyrolyzed at 900 °C under an Ar flow, and subsequently doped with nitrogen by a treatment at 600 °C for 1 h in NH<sub>3</sub> atmosphere to form the N-OSCs (AC35) [206]. The activated carbon obtained has a high surface area of 2703 m<sup>2</sup> g<sup>-1</sup>, but surprisingly a small total pore volume ( $V_p = 0.17 \text{ cm}^3 \text{ g}^{-1}$ ) compared to other studies. However, in the preparation of the N-OSC/S composite, its sulfur content was 69.71 wt %, calculated according to the C/H/N/S elements analysis results. The sulfur content can be correlated with pore volume using the formula  $W_s (\%) V = (\rho_s V / (\rho_s V + 1)) \times 100$ , where V is the pore volume of the carbon matrix and  $\rho_s$  is the density of sulfur (~2.07 g cm<sup>-3</sup>) [226,227]. The theoretical amount of S that N-OSC can hold when applying the above formula is 26 wt %, which is markedly lower than the experimental value (~70 wt %). This fact is indicative of an excess of sulfur on the surface of the material, as can also be observed in the SEM images. In this context, thermogravimetric methods – which generally can distinguish between these differently located S domains – appears as an underutilized technique for bringing clarity to the S location on the carbon surface, to avoid doubts in the reported results.

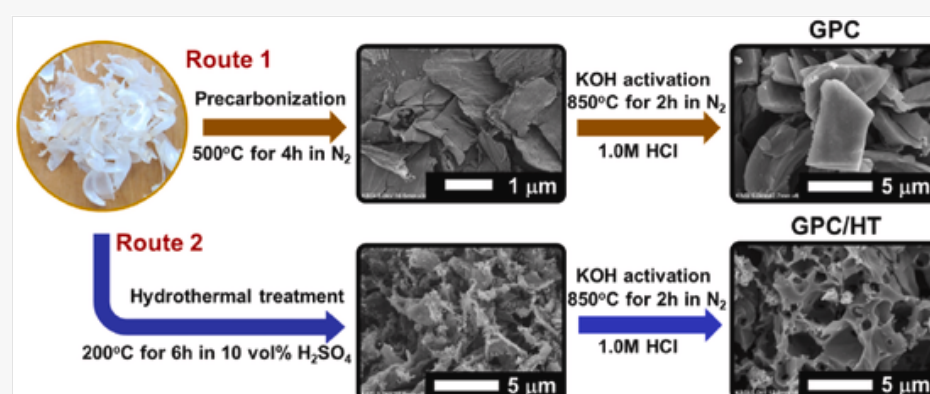
Considering the high production and consumption of palm oil, the residues it generates constitute one of the main sources of biomass residues. Hence, the studies for its application in Li-S batteries are of obvious interest. The work of Han et al. on palm kernel shell (W38) addresses this goal [234]. After the preparation of activated carbon by the most used method for biomass transformation: (1) pre-carbonization at a moderate temperature of 500 °C under a N<sub>2</sub> atmosphere, (2) chemical activation with KOH and (3) carbonization at a high temperature of 900 °C with N<sub>2</sub> flow; AC38 or PAC was obtained with excellent properties of specific surface area and pore volume (Specific Surface Area (SSA): 2760 m<sup>2</sup> g<sup>-1</sup> and  $V_p: 1.6 \text{ cm}^3 \text{ g}^{-1}$ ). Cycling performance of the Li-S cells was assessed by prolonged cycling at 0.48C. After 1000th cycles, the capacity retention was 51 % with only 0.05 % capacity loss per cycle. By adding LiNO<sub>3</sub> to the electrolyte, a further improved performance was observed (capacity loss per cycle, 0.03 %) although cycling was limited to 200 cycles.

Agricultural garlic peelings (W40) were transformed into porous carbons by two routes as shown in Fig. 14, in both cases achieving suitable carbonaceous matrices to infiltrate sulfur [208]. In both routes the carbon activation process is carried out using KOH as the active agent. The use of hydrothermal conditions in the pre-carbonization stage is the main difference between both synthesis methods. The SEM images shown in Fig. 14 indicate that the hydrothermal process favours the increased porosity of the activated carbon, hence the GPC/HT (AC40) sample showed better textural properties and was able to accommodate the higher sulfur content (around 87.6 % S). The best electrochemical properties of this composite were attributed to the high surface area, which made a homogeneous distribution of sulfur in the matrix possible, thus facilitating the Li-ion transfer and provided stability during cycling.

 Images are optimised for fast web viewing. Click on the image to view the original version.

alt-text: Fig. 14

Fig. 14




Scheme for the preparation of carbons based on garlic peels, showing their morphological differences: GPC (route 1) and GPC/HT (route 2). (reprinted from Ref. [208] with permission from Elsevier). In many of these articles there is no clear indication that the cells are being tested at controlled constant temperature. If the room where the charge-discharge tests are carried out is not well acclimatized to a fixed temperature, such variations can seriously affect the cycling stability [165]. This effect can likely be observed in many long-term cycling graphs, in which instead of a progressive loss of capacity throughout the cycles, small increases in reversible capacity are observed between consecutive cycles, which could have been corrected by controlling the external temperature.

### 3.2.3 ACs from aquatic biomass

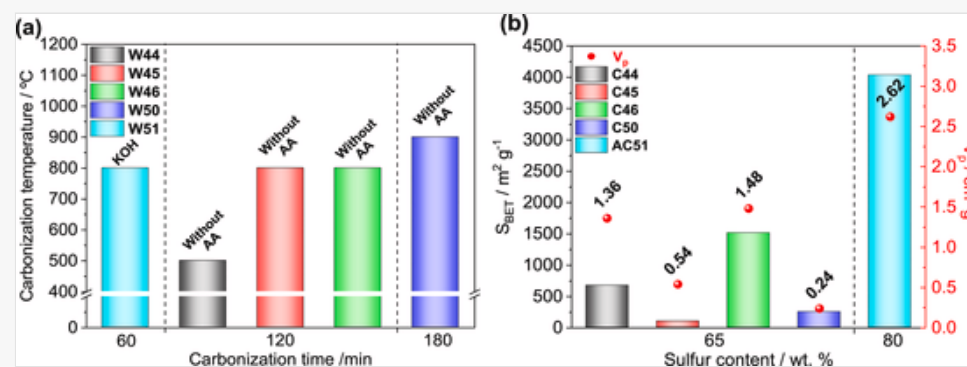
Several marine aqueous plants are excellent and sustainable candidates for producing porous (C) or activated carbons (AC) due to their low cost, high content of carbon, and especially rapid growth. The precursors of this group are mainly non-toxic and easily degradable macro- or microalgae.

In this group, the number of reported articles is smaller and of the five waste products collected in Fig. 15a, only one possess a carbon that has been activated with KOH. The  $S_{\text{BET}}$  and  $V_p$  values are higher than those of the non-activated ones, as is its S content of 80 %. In addition, it is worth noting an unusual residue used by a research group from Shandong University who conducted a study with jellyfish umbrellas (W47) as the precursor biomass [241].

 Images are optimised for fast web viewing. Click on the image to view the original version.

alt-text: Fig. 15

Fig. 15



(a) Pyrolysis conditions set for different wastes (W) from aquatic biomass and the activating agent (AA) used [W44: Microalgae; W45: Green algae; W46: Seaweed; W47: Jellyfish umbrella; W48: Enteromorpha algae; W49: Echinodorus Amazonicus Rataj-EAR waterweed; W50: Nori algae; W51: Red algae] (b) Textural properties of activated carbons (ACs) obtained from the residues shown in Fig. 15 (a). (For interpretation of the references to colour in this figure legend, the reader is referred to the Web version of this article.)

Following the model of previous tables, the most relevant features of the reports published so far on carbons derived from this type of biomass are collected in Table 4. Starting with the group of algae, some of them, such as microalgae (W44) [242] or green algae (W45) [243], have been transformed into porous carbons by a simple carbonization process under Ar atmosphere at 500 °C and 800 °C, respectively, for 2 h; others such as brown seaweed (W46) [244] or Nori algae (W50) [245] were subjected to a previous treatment with NaCl that acted as an exfoliating agent, and were then pyrolyzed in a similar way to the previous examples. Finally, most of these have been chemically activated with KOH to produce ACs. Another positive factor for this type of biomass is that several species contain large amounts of N, S in their structures. These atoms can improve properties of C that are beneficial for Li-S batteries, e.g. electrical conductivity [246], or affinity towards LiPSs [247].

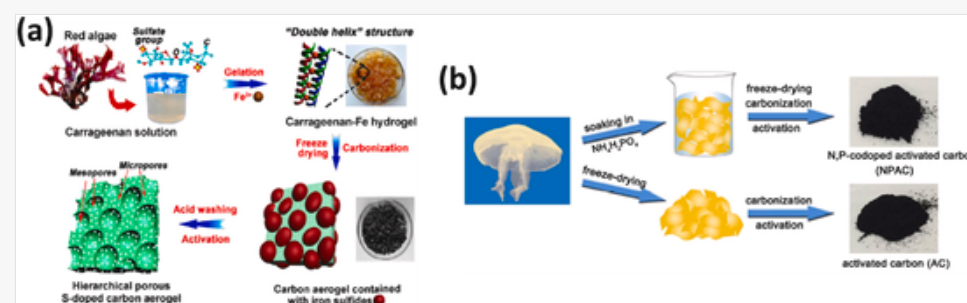
In 2017, Hencz et al. [244] synthesized a hierarchical porous seaweed carbon (C46, abbreviated SWC) for Li-S batteries. Once the SWC was annealed at 800 °C and characterized by XPS, the presence of 2.23 wt % of nitrogen heteroatoms could be confirmed. This was expected because the raw material already had nitrogen atoms in its composition. This simple pyrolysis process gave rise to a carbon with a high surface area ( $1511 m^2 g^{-1}$ ). Moreover, its total pore volume ( $1.48 cm^3 g^{-1}$ ) was appropriate to prepare a SWC-S composite with 66 wt % S. After 300 cycles at 1C the delivered capacity was  $541 mAh g^{-1}$ , a satisfactory value, although the sulfur loading was unfortunately not quantified. The authors argue that the N content of the pristine algae plays an important role in the electrochemical activity of the AC.

Carrageenan comes from a family of linear sulfated polysaccharides that are extracted from red edible seaweeds (W51). Li et al. [248] obtained an AC from a solution of carrageenan mixed with  $Fe^{3+}$  as an agent to generate a hierarchical pore system. Moreover, sulfate pyrolysis introduces S heteroatoms in the carbon lattice (AC51, HPSCA-400, Fig. 16a). The BET specific surface area ( $S_{BET}$ ) of the AC51 is  $4037 m^2 g^{-1}$  and the corresponding total pore volume is  $2.62 cm^3 g^{-1}$ , which are unusually high values for this kind of material. Thus, the S content of the S/HPSCA-400 composite was 80 wt %; the highest content of S collected in Table 4. Unfortunately, the S loading was not specified for this material either, despite being an important parameter to more accurately estimate the potential of the system for practical applications. The composite is able to supply an initial discharge capacity close to  $800 mAh g^{-1}$  at 1C and, after 400 cycles, the reversible capacity value recorded was of  $590 mAh g^{-1}$  with a small capacity decay of 0.07 % per cycle.

Images are optimised for fast web viewing. Click on the image to view the original version.

alt-text: Fig. 16

Fig. 16



Synthesis schemes for the preparation of (a) hierarchical porous S-doped carbon aerogel based on Carrageenan solution (reprinted from Ref. [248] with permission from Elsevier) and (b) activated carbons from jellyfish umbrellas (reproduced from Ref. [241] with permission from John Wiley and Sons).

As previously mentioned, one particular example was the preparation of a N,P-co-doped activated carbon from jellyfish umbrellas through its immersion in a  $NH_4H_2PO_4$  solution as a N and P source, followed by a subsequent activation process by potassium hydroxide (AC47, NPAC, Fig. 16b) [241]. Previously, other authors had used different ammonium phosphates to prepare activated carbons derived from biomass, such as herbaceous plant [251] and wood [252]. In the latter case, they compared the textural properties of wood-derived activated carbons using  $H_3PO_4$  or  $(NH_4)_2HPO_4$  as activating agents, displaying a more effective activation with  $H_3PO_4$  in terms of surface functionality and porosity of the materials. This conclusion is somewhat contradictory with ref. [241] where it is instead argued that the ammonium salt contributes by introducing N and P into the C structure. Doubt remains whether the electrochemical properties listed in Table 4 are due to the introduction of these heteroatoms or simply to the activation of the carbonaceous matrix with KOH. [Instruction: Table 4 should be moved to this section.]

While the weight of S of the electrode is often not specified for the examples in Table 4, two of the works reviewed discuss the electrodes that have a reasonably high S content: around  $3 mg cm^{-2}$ . In both these, the obtained C matrix comprise N [243] or N and S [245] from the algae itself. Although the capacity values and cycling properties are satisfactory, the applied current densities used are low, around 0.1C. Further studies are needed at higher current densities to confirm if these constitute good prospects.

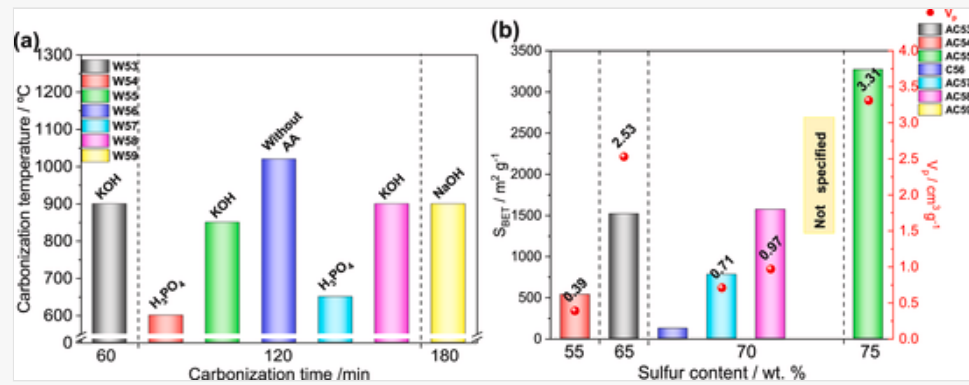
### 3.2.4 ACs from animal and human waste biomass

In this category of wastes, the use of KOH as an activating agent continues to dominate (Fig. 17 a). This approach provides higher values of both  $S_{BET}$  and  $V_p$  compared to those obtained with  $H_3PO_4$ , and also using lower carbonization temperatures (Fig. 17 b). It is also found that the activation of the carbon increases the numerical values of both properties substantially. It should be noted that the C with the highest  $V_p$  values ( $3.3 cm^3 g^{-1}$ ) is also the one with the highest value of S content (75 %). The electrochemical conditions used, and the results obtained are collected in Table 5.

Images are optimised for fast web viewing. Click on the image to view the original version.

alt-text: Fig. 17

Fig. 17



(a) Pyrolysis conditions set for different wastes (W) from animal and human biomass and the activating agent (AA) used [W52: Pig bone; W53: Tuna bone; W54: Goat hair; W55: Bovine bone; W56: Bovine bones ashes; W57: Silk cocoons; W58: Silkworm faeces; W59: Human hair] (b) Textural properties of activated carbons (ACs) obtained from the residues shown in Fig. 17 (a).

Within the section of *animal waste*, an early study dates from 2011 when Wei et al. [30] studied the effect of temperature during the activation process with KOH to obtain activated carbons derived from pig bones (AC52, BHPC). The highest values of specific surface area and pore volume,  $2157 \text{ m}^2 \text{ g}^{-1}$  and  $2.26 \text{ cm}^3 \text{ g}^{-1}$  respectively, were obtained at  $850 \text{ }^\circ\text{C}$ . However, the electrochemical performance in Li-S cells was not as good as one might expect, among other causes because the electrolyte used. The study used  $\text{LiClO}_4$  dissolved in DOL: DME, which has inferior properties than electrolytes based on LiTFSI salt. Later, this same method of preparing activated carbon was used to transform bovine bones (W55) into hierarchical porous carbon with high porosity (AC55, CHPC) [253]. Remarkable textural properties were obtained ( $S_{\text{BET}}$ :  $3273 \text{ m}^2 \text{ g}^{-1}$  and  $V_p$ :  $3.32 \text{ cm}^3 \text{ g}^{-1}$ ), which allowed a high amount of sulfur to be incorporated into the carbonaceous matrix (almost 76 wt %), but with a moderate S loading ( $2.0 \text{ mg cm}^{-2}$ ). The CHPC/S composite showed good electrochemical performance maintaining a specific discharge capacity at almost  $700 \text{ mAh g}^{-1}$  after 250 cycles at 0.2 C, with a small fade rate per cycle of 0.14 %. The performance was improved by incorporating  $\text{CoS}_2$  through a hydrothermal treatment at  $140 \text{ }^\circ\text{C}$  for 12 h. As for several similar examples using transition metal doping, the ability of this compound to anchor to LiPSs reduces the shuttle effect and improves both the specific discharge capacity and cycling properties. A different strategy was used by Wang et al. [254] who used commercial bovine bone ashes (W56) as a template for 3D graphene growth through a synthesis process based on chemical vapour deposition (CVD), and employed it in Li-S cells.

Tuna bone (W53) was used by Ai et al. [242] to obtain activated carbon (AC53, FBPC) with two important features, first the ability to introduce O, N and S in the carbon lattice and second, its use as an interlayer between the cathode and the electrolyte separator to hinder the LiPSs diffusion towards the Li anode. The cells tested provided good electrochemical performance, not least the specific capacity value maintained after a long-term cycling of 700th cycles,  $600 \text{ mAh g}^{-1}$ , and an associated good stability (loss of capacity of 0.07 % per cycle). [Instruction: Table 5 should be moved to this section.]

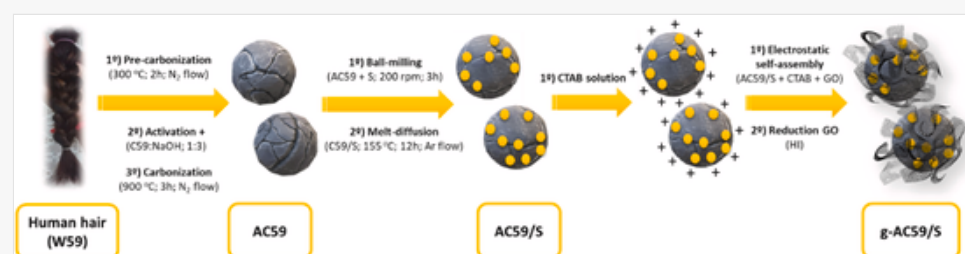
Other residues such as goat hair (W54) [256,257] and silkworm cocoons (W57) [258] have been used, through activation with  $\text{H}_3\text{PO}_4$  to obtain activated carbons co-doped with nitrogen and phosphorus. The latter was used simultaneously as an S host and interlayer. The synergy between both actions was reflected in a clear improvement in the performance of the cell (see Table 5). In addition to silk cocoons, the same research group used silkworm faeces (W58) as a source for preparing N-doped activated carbons due to the inherent nitrogen content in their composition [259]. On this occasion, the carbon matrix was more complex as the authors incorporated different proportions of rGO and CNTs to improve the properties of activated carbon with KOH. The 55-PGC@SFPC/S composite exhibited excellent cycling stability (0.035 % capacity fading per cycle at 3 C) and delivered a good discharge capacity of  $414 \text{ mAh g}^{-1}$  after 1000 cycles for a midrange value of sulfur loading ( $2.35 \text{ mg cm}^{-2}$ ). The outstanding electrochemical performance can be attributed to various factors: (i) the addition of rGO and CNTs increased the conductivity of the electrode, (ii) the hierarchical porous structure obtained allowed to increase the amount of S in the electrode and retain the polysulfides in their cavities and (iii) the presence of heteroatoms favours the trapping of polysulfides, so reducing their dissolution in the electrolyte.

Finally, hair (W59) has been the only human waste used in the manufacture of Li-S batteries [260]. The AC59 matrix was prepared from pre-carbonized hair fibres at  $300 \text{ }^\circ\text{C}$ , further activated with NaOH at  $900 \text{ }^\circ\text{C}$ . S impregnation was carried out by the melt diffusion process. This AC59/S composite was further wrapped with rGO sheets by electrostatic self-assembly (with aqueous solution of cetyltrimethylammonium bromide, CTAB) leading to the so-called g-AC59/S composite in Table 5. The active material that constitutes the cathode electrode was prepared as shown in the scheme of Fig. 18.

Images are optimised for fast web viewing. Click on the image to view the original version.

alt-text: Fig. 18

Fig. 18



Schematic illustration of the morphological evolution process from human hair waste (W59) to the g-AC59/S composite. Adapted from Ref. [260].

Replacement Image: Figure 18.jpg

Replacement Instruction: Replace image requested

Positively, the good cycling properties of the electrode for current densities from 0.2C to 2C deserve to be highlighted; but at the same time, the low value of S loading of the electrode along with the complexity of the composite preparation method needs to be noted.

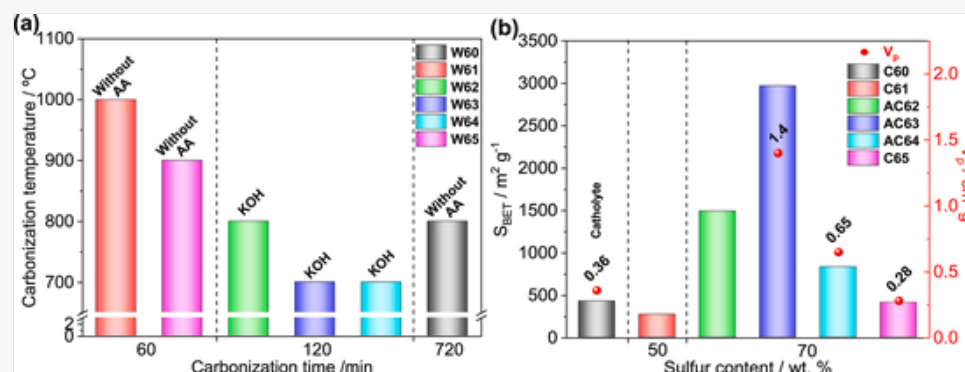
### 3.2.5 ACs from household and industrial wastes

For this group of carbons only KOH was used as the activating agent while the employed time and temperature ranges of carbonization are also wide, Fig. 19 a. Activation, as expected, leads to higher  $S_{\text{BET}}$  and  $V_p$  values, but the composite with the highest S content (70 %) is actually found for a non-activated carbon with the lowest  $V_p$  value, Fig. 19 b.

Images are optimised for fast web viewing. Click on the image to view the original version.

alt-text: Fig. 19

Fig. 19



(a) Pyrolysis conditions set for different wastes (W) from household and industrial biomass and the activating agent (AA) used [W60: eggshell; W61: Recycled paper roll; W62: Ion exchange resin; W63: Paper (lignosulfonate); W64: Tobacco stem; W65: Brewing waste] (b) Textural properties of activated carbons (ACs) obtained from the residues shown in Fig. 19 (a).

This category has been divided in two subgroups, *household* and *industrial wastes*, and the electrochemical conditions and performance of the derived carbons are shown in Table 6. In the first group, we have only found two articles that fit this heading, where residues from eggshells (W60) [261] and recycled paper strips (W61) [262] have been evaluated in Li-S cells. On the other hand, in the *industrial biomass group*, other types of biomass sources have been studied to produce carbonaceous materials, such as exchange resins (W62), paper (W63), tobacco stems (W64) or brewing waste (W65) [263–266].

The Chung and Manthiram cell [261] possessed a particular architecture: free-standing carbonized sucrose-coated eggshell membranes (W60, CSEMs) were used both as a current collector and to form a reservoir for the dissolved  $\text{Li}_2\text{S}_6$  polysulfide catholyte as an active material. This architecture is indeed very different to those used in the other reviewed articles (with Al foil as current collector and S as active material); hence providing some difficulty of comparing the results. Zhang et al. [262] took advantage of the recycled paper capillarity to wrap graphene oxide sheets onto paper fibers. High temperature annealing simultaneously reduced graphene oxide into graphene and converted the paper into activated carbon, forming an activated paper carbon/reduced graphene oxide (APC/graphene) matrix used both as an S host (W61) and a current collector. A moderate S content was deposited (50 %), partially balanced by a high electrode S loading ( $3.6 \text{ mg cm}^{-2}$ ). The initial discharge capacity of the APC-graphene/S electrode was  $1083 \text{ mAh g}^{-1}$  at close to 1C and  $754 \text{ mAh g}^{-1}$  after more than 600 cycles, thereby displaying a very good cycling stability with a capacity recession of as low as 0.05 % per cycle. [Instruction: Table 6 should be moved to this section.]

To finalize this review, a category of *industrial biomass wastes* will be discussed. Some industries over-manufacture by-products that are typically burned to produce electrical energy or become destined for landfills. Several researchers have focused their efforts on the production of energy from these by-products with the aim of minimizing the serious damage to the environment and human health that the massive burning of this waste implies. Specifically, in the bottom of Table 6 the wastes used for the Li-S technology are collected. Li et al. [264] used a by-product generated in large quantities in the paper manufacturing industry: lignosulfonates (W63). After an activation process with KOH, followed by a pyrolysis at  $700 \text{ }^\circ\text{C}$  in an Ar flow for 2 h, an activated carbon (AC63) with good porosity properties was obtained ( $S_{\text{BET}}$ :  $2970 \text{ m}^2 \text{ g}^{-1}$  and  $V_p$ :  $1.4 \text{ cm}^3 \text{ g}^{-1}$ ). Unlike all other composites discussed so far, this was impregnated with two types of S, from the residue itself ( $\sim 35 \%$ ) and commercial ( $\sim 33 \%$ ), origin in the symbols-cap S and + S, respectively. The presence of the latter type of S improves the electrode performance and capacity values and cycling properties, which can be considered satisfactory. Another activated carbon (AC64, a-NOSPC) was prepared under similar conditions as the previous example in its activation process, starting from tobacco stems as a biomass source, which is one of the leftover materials from the cigarette industry and tobacco agriculture [265]. This carbon contains N, O and S impurities (contents quantified from the XPS spectrum in % 14.23, 1.22 and 0.35, respectively) that can favour the presence of electrocatalytic active sites. Electrochemical measurements carried out at 0.5C revealed an initial discharge capacity of  $1122 \text{ mAh g}^{-1}$ , and after 400 cycles  $754 \text{ mAh g}^{-1}$ , i.e. a fading loss per cycle of 0.08 %.

Finally, it is worth noting that one of the latest residues from the agri-food industry that have been treated to obtain porous carbon (C65, ABW-C) and later incorporated as a component of the cathode in Li-S cells is brewing waste (W65, Fig. 20) [266]. The composite prepared from the pyrolysis of the brewing industry waste mixed with elemental sulfur (70 wt %) showed attractive performance as a cathode in Li-S batteries. The ABW-C/S electrode prepared on carbon paper (or GDL) exhibited an initial discharge capacity of  $1375 \text{ mAh g}^{-1}$  at 1C and maintained a good reversible capacity of  $800 \text{ mAh g}^{-1}$  after 450 cycles. The long-term cycling properties were maintained at higher rates, delivering capacities of  $450 \text{ mAh g}^{-1}$  at 2 C and  $270 \text{ mAh g}^{-1}$  at 5 C, after the 625th and 950th charge-discharge cycles, respectively.

Images are optimised for fast web viewing. Click on the image to view the original version.

alt-text: Fig. 20

Fig. 20



Schematic illustration of the process of manufacturing the cathode of a Li-S cell from brewing waste and battery testing (reprinted from Ref. [266] with permission from John Wiley and Sons).

## 4 Summary and outlook



During the last few years, the design, activation, physico-chemical properties, and behaviour of biomass-derived carbons have caused a breakthrough in the development of more sustainable energy storage devices. Here, we have presented an in-depth review on these carbons as a very attractive choice to be used as a matrix for sulfur in positive electrodes of high-energy efficient Li-S batteries. Biomass is a rich source of carbon, and the derived-biocarbons (or biochars) have, a priori, a high specific surface area and pore volume, hierarchical distribution of pore sizes, good conductivity, availability, and simple synthesis methods. Despite the emergence of other designed carbonaceous materials with special morphologies, such as carbon nanotubes, carbon nanofibers, carbon aerogels, graphene, graphene oxide and ordered mesoporous carbons, among others, porous carbons (C) and/or activated carbons (AC) derived from biomass remain promising candidates to meet the challenge of ecological transition through evolution in bioenergy. For example, carbons derived from sawdust and wheat/rice straws have shown remarkable electrochemical results due to their multiple properties of being able to alleviate inherent problems of the Li-S battery technology: low conductivity of electroactive element (sulfur) and discharge products ( $\text{Li}_2\text{S}/\text{Li}_2\text{S}_2$ ), large volume expansion of sulfur during cycles, loss of active materials resulting from the dissolved lithium polysulfides (LiPSs) in the electrolyte (“shuttle effect”), and irreversible  $\text{Li}_2\text{S}/\text{Li}_2\text{S}_2$  deposition on lithium metal. The incorporation of these sustainable materials could be a viable alternative to the use of carbons derived from petrochemical products, which are generally obtained through complex and high-cost processes.

Based on the literature covered in this review, it is difficult to target any clear strategies for which source of biomass that will render a preferable template for Li-S batteries. However, carbons that possess a hierarchical pore structure, high SSA and large pore volume, and with a high concentration of heteroatoms which remain after carbonization or are inserted during activation, seems generally preferable. There are plenty of such materials in the examples covered here, where many display a performance on par with heavily designed carbon structures from synthetic sources. This signals that their clear advantages should exist for this category of materials, especially if they originate from biowaste that is otherwise of little use and has low environmental impact. However, a more systematic approach in finding such AC materials based on their different sources would certainly move this field forward.

In most of the studies analyzed in this review, the authors use activated carbons from biomass as a scaffold to accommodate sulfur. As an activating agent, KOH is commonly used, but the yield of the pyrolysis process is a missing piece of information. Comparative studies related to the effectiveness of the different methods of both physical and chemical activation for this application are also lacking. In addition to all the appropriate characteristics already mentioned for ACs, their eco-friendliness and compatibility with elemental sulfur to prepare efficient and homogeneous AC-S composites should be examined.

Focusing on the electrochemical performance of the materials chosen for application in Li-S batteries, it should be noted that there is a fair degree of homogeneity in the cell construction in the reviewed studies. Generally, the studies employ two-electrodes coin-cells assembled similarly, with the AC-S composite and Li foil as cathode and anode, respectively, a Celgard-type separating membrane and fairly similar electrolyte formulation. Electrochemical measurements were mostly carried out using a sulfur loading on the positive electrode in a range of  $1.0\text{--}2.5\text{ mg cm}^{-2}$ , a voltage window of  $1.7\text{--}2.8\text{ V}$ , and applying a wide range of current densities between  $0.1\text{C}$  and  $1\text{C}$ . The electrochemical performance has been highly variable depending on the origin of the biomass residue and the parameters set during its transformation to the host sulfur matrix. All variations have been detailed throughout this review and some actions have been disapproved in order to point out the strategies for improved conditions in the global process of making better Li-S cells.

Based on the current research progress, it is clearly discernible that Li-S batteries have remarkable potential to serve as an alternative energy storage system to Li-ion batteries in several future applications. Most of the studies reported on the use of biomass-derived carbons as electrodes in Li-S batteries are mainly focused on physicochemical, structural, morphological and electrochemical analysis in lithium cells. Before considering the implementation of these bio-carbons in future Li-S batteries, a series of considerations and additional aspects should be addressed, considering the following aspects:

- (1) Although the raw materials are low-cost since they are residues from biomass, they are quite abundant and, in many cases, they are simply stored in factories or landfills because they do not have any specific application. However, economic studies on their feasibility of applying them in commercial Li-S batteries are lacking, and it is therefore difficult to assess the advantages – if any – as compared to other strategies. The future of this new technology will need to clarify the commercial problems that may arise in this application for biomass wastes.
- (2) The preparation of the AC requires the consumption of activating agents and additional thermal treatment, which implies additional costs and environmental effects. The most used activating agents, KOH or  $\text{H}_3\text{PO}_4$ , are highly corrosive. Therefore, less harmful agents, such as physical activation systems, should preferably be used. On the other hand, some residues intrinsically comprise impurities based on N and other elements that can enhance the absorption of LiPSs, and even the conductivity of the AC, adding advantages to these biomass-derived carbons. This issue requires a knowledge of the elements present and their concentration in the residue prior to its conversion into carbon. The appropriate exploitation of these heteroatoms should certainly also guide the activation strategy.
- (3) Generally, the global availability of biomass residues is not in doubt. However, there exists no quantitative evaluation of the volume of waste that could be destined for this application. As has been shown in this review, there are various categories in which we can classify biomass waste, and the amount of waste generated is different depending on the origin. For example, the volume of waste obtained on a domestic scale or from animals is much lower than that generated after forest pruning, agricultural or agri-food processes, or in industries.
- (4) Within this area, the use of inedible agri-food industrial waste would be an attractive option. As it is industrial waste, it is generated in tons and its reuse would be solving a problem of storage and recycling for manufacturers; and moreover, since it is non-edible agri-food waste, its main use would not be distorted or tempting against the reserves destined for the feeding of society.
- (5) Another point to evaluate would be the industrial scaling of the waste reuse. All studies analyzed in this work are focused on the carbon preparation process (mostly activated carbons) and its application in Li-S coin cells on a laboratory scale. However, there exist little work on larger size electrodes, for example electrodes for pouch-cell types. Advancing these processes would be desirable to truly estimate the impact of this technology area, because full-scale conditions may differ significantly from those at the laboratory scale.
- (6) In search of the environmental sustainability of the global process of producing these batteries, there are certain factors that must be controlled, such as energy efficiency, life cycle, and generation of by-products in each stage, and which will contribute to environmental emissions. However, the industrial preparation of activated carbons is a mature process. The management of by-products that may negatively affect the environment are well known and controlled by different regulations. Hence, the increase in production involved in this new application would likely not drastically affect the sustainable nature of the technology.
- (7) Comparative studies are lacking on how the preparation of S composites with carbons derived from biomass affects the electrode performance. Although the melt diffusion method is the most widely used in fundamental research, this would provide a drawback for a large-scale application due to the cost of heat treatment and the need for an inert atmosphere. Simple grinding methods that homogenize the mixture of the components would constitute an alternative, although studies would be needed to optimize the electrochemical response of such composites.
- (8) There is little uniformity in the methods and conditions used in the articles reviewed, and it is generally applicable to Li-S batteries. We believe that by applying more homogeneous testing criteria, the conclusions drawn from reviews such as this would be of even greater use to the scientific community. Thus, in the measurements of the electrochemical properties, the following could be considered, namely (i) select a potential window in which there is solid

evidence that the measured capacity corresponds to the electrochemical reaction between Li and S and not to secondary reactions, for example 2.6/2.7–1.9/1.8 V; (ii) homogenize the components of the electrodes, composite, additive conductor, and binder; (iii) indicate not only the S content of the composite but also the S loading of the electrode; (iv) the current density in terms of C, referred to as the theoretical capacity and (v) a more precise description of the electrolyte formulation together with the volume used would also be useful information for the reader. More complex is the uniformity in the conditions of preparation of activated carbons, considering the diversity of activating agents, although the most used is KOH. In this case, the following should be homogenized (i) composition in the C/KOH mixture, (ii) carbonization time and temperature, among other conditions.


## Declaration of competing interest

We declare no conflict of interest.

## Acknowledgments

The authors wish to acknowledge the financial support from [Ministerio de Economía y Competitividad \(Project MAT2017-87541-R\)](#) and [Junta de Andalucía \(FQM-175 Group\)](#), [Ministerio de Ciencia e Innovación \(Project PID2020-113931RB-I00\)](#), and [Junta de Andalucía \(Project PY20\\_00432 & FQM-175 Group\)](#). A. Benítez thanks the financial support from Cordoba University (Plan Propio de Investigación 2019; Sub. 2.4.) and Junta de Andalucía (PAIDI 2020 – FSE). J. Amaro-Gahete acknowledges the financial support from [Spanish Ministry of Science, Innovation and Universities](#) [Ministerio de Ciencia, Innovación y Universidades](#) for an FPU teaching and research fellowship (FPU17/03981). D. Brandell and Y.-C. Chien acknowledges support from STandUP for Energy and Batteries Sweden (Vinnova, 2019-00064). Permissions for reproduced graphics have been obtained from the respective journals.

## References

 The corrections made in this section will be reviewed and approved by a journal production editor. The newly added/removed references and its citations will be reordered and rearranged by the production team.

- [1] Haegel N.M., Atwater H., Barnes T., Breyer C., Burrell A., Chiang Y.-M., et al. Terawatt-scale photovoltaics: transform global energy. *Science* 2019. doi:10.1126/science.aaw1845. 80.
- [2] Abas N., Kalair A., Khan N. Review of fossil fuels and future energy technologies. *Futures* 2015;69:31–49. doi:10.1016/j.futures.2015.03.003.
- [3] Ming Z., Shaojie O., Yingjie Z., Hui S. CCS technology development in China: status, problems and countermeasures—based on SWOT analysis. *Renew Sustain Energy Rev* 2014;39:604–616. doi:10.1016/j.rser.2014.07.037.
- [4] Smil V. Examining energy transitions: a dozen insights based on performance. *Energy Res Soc Sci* 2016;22:194–197. doi:10.1016/j.erss.2016.08.017.
- [5] Engler J.-O. Global and regional probabilities of major nuclear reactor accidents. *J Environ Manag* 2020;269:110780. doi:10.1016/j.jenvman.2020.110780.
- [6] European Environment Agency. The European environment - state and outlook 2020: knowledge for transition to a sustainable Europe. 2019. doi:10.2800/96749.
- [7] Scarlet N., Dallemand J.-F., Taylor N., Banja M., Sanchez Lopez J., Avraamides M. Brief on biomass for energy in the European Union. *Publ Off Eur Union*; 2019. p. 1–8. doi:10.2760/546943.
- [8] Paris agreement. United Nations; 2015.
- [9] Eurostat. Share of renewable energy in the EU up to 18.0 %. *Newsrelease*; 2020. 17/2020:32–4.
- [10] Houghton R.A. Biomass. *Encycl. Ecol.*. Elsevier; 2008. p. 448–453. doi:10.1016/B978-008045405-4.00462-6.
- [11] Liu P., Wang Y., Liu J. Biomass-derived porous carbon materials for advanced lithium sulfur batteries. *J Energy Chem* 2019;34:171–185. doi:10.1016/j.jechem.2018.10.005.
- [12] Global W.B.A. Biomass potential towards 2035. vol. 6; 2016.
- [13] Houghton R.A., Hall F., Goetz S.J. Importance of biomass in the global carbon cycle. *J Geophys Res Biogeosci* 2009;114. doi:10.1029/2009JG000935. n/a-n/a.
- [14] Li Y., Liang G., Chang L., Zi C., Zhang Y., Peng Z., et al. Conversion of biomass ash to different types of zeolites: a review. *Energy Sources, Part A Recover Util Environ Eff* 2021;43:1745–1758. doi:10.1080/15567036.2019.1640316.
- [15] Hickman R., Banister D. Looking over the horizon: transport and reduced CO<sub>2</sub> emissions in the UK by 2030. *Transport Pol* 2007;14:377–387. doi:10.1016/j.tranpol.2007.04.005.
- [16] Canals Casals L., Martinez-Laserna E., Amante García B., Nieto N. Sustainability analysis of the electric vehicle use in Europe for CO<sub>2</sub> emissions reduction. *J Clean Prod* 2016;127:425–437. doi:10.1016/j.jclepro.2016.03.120.
- [17] Sakr N., Sadarnac D., Gascher A. A review of on-board integrated chargers for electric vehicles. 2014 16th Eur. Conf. Power electron. Appl. IEEE; 2014. p. 1–10. doi:10.1109/EPE.2014.6910865.

- [18] Nitta N., Wu F., Lee J.T., Yushin G. Li-ion battery materials: present and future. *Mater Today* 2015;18:252–264. doi:10.1016/j.mattod.2014.10.040.
- [19] Li X., Wang Z., Zhang L. Co-estimation of capacity and state-of-charge for lithium-ion batteries in electric vehicles. *Energy* 2019;174:33–44. doi:10.1016/j.energy.2019.02.147.
- [20] Goodenough J.B., Kim Y. Challenges for rechargeable batteries. *J Power Sources* 2011;196:6688–6694. doi:10.1016/j.jpowsour.2010.11.074.
- [21] Manthiram A. Materials challenges and opportunities of lithium ion batteries. *J Phys Chem Lett* 2011;2:176–184. doi:10.1021/jz1015422.
- [22] Huang J.-Q., Zhang Q., Wei F. Multi-functional separator/interlayer system for high-stable lithium-sulfur batteries: progress and prospects. *Energy Storage Mater* 2015;1:127–145. doi:10.1016/j.ensm.2015.09.008.
- [23] Bruce P.G., Freunberger S.A., Hardwick L.J., Tarascon J.-M. Li–O<sub>2</sub> and Li–S batteries with high energy storage. *Nat Mater* 2012;11:19–29. doi:10.1038/nmat3191.
- [24] Carbone L., Greenbaum S.G., Hassoun J. Lithium sulfur and lithium oxygen batteries: new frontiers of sustainable energy storage. *Sustain Energy Fuels* 2017;1:228–247. doi:10.1039/C6SE00124F.
- [25] Fotouhi A., Auger D.J., Propp K., Longo S., Wild M. A review on electric vehicle battery modelling: from Lithium-ion toward Lithium–Sulphur. *Renew Sustain Energy Rev* 2016;56:1008–1021. doi:10.1016/j.rser.2015.12.009.
- [26] Song Y., Cai W., Kong L., Cai J., Zhang Q., Sun J. Rationalizing electrocatalysis of Li–S chemistry by mediator design: progress and prospects. *Adv Energy Mater* 2020. doi:10.1002/aenm.201901075.
- [27] Li G.C., Jing H.K., Su Z., Lai C., Chen L., Yuan C.C., et al. A hydrophilic separator for high performance lithium sulfur batteries. *J Mater Chem* 2015;3:11014–11020. doi:10.1039/C5TA01970B.
- [28] He J., Manthiram A. A review on the status and challenges of electrocatalysts in lithium-sulfur batteries. *Energy Storage Mater* 2019;20:55–70. doi:10.1016/j.ensm.2019.04.038.
- [29] Zhu K., Wang C., Chi Z., Ke F., Yang Y., Wang A., et al. How far away are lithium-sulfur batteries from commercialization? *Front Energy Res* 2019;7. doi:10.3389/fenrg.2019.00123.
- [30] Wei S., Zhang H., Huang Y., Wang W., Xia Y., Yu Z. Pig bone derived hierarchical porous carbon and its enhanced cycling performance of lithium–sulfur batteries. *Energy Environ Sci* 2011;4:736. doi:10.1039/c0ee00505c.
- [31] Moreno N., Caballero A., Hernán L., Morales J. Lithium–sulfur batteries with activated carbons derived from olive stones. *Carbon N Y* 2014;70:241–248. doi:10.1016/j.carbon.2014.01.002.
- [32] Zhang J., Xiang J., Dong Z., Liu Y., Wu Y., Xu C., et al. Biomass derived activated carbon with 3D connected architecture for rechargeable lithium - sulfur batteries. *Electrochim Acta* 2014. doi:10.1016/j.electacta.2013.11.035.
- [33] Ji X., Lee K.T., Nazar L.F. A highly ordered nanostructured carbon–sulphur cathode for lithium–sulphur batteries. *Nat Mater* 2009;8:500–506. doi:10.1038/nmat2460.
- [34] Dutta S., Bhaumik A., Wu K.C.W. Hierarchically porous carbon derived from polymers and biomass: effect of interconnected pores on energy applications. *Energy Environ Sci* 2014;7:3574–3592. doi:10.1039/C4EE01075B.
- [35] Li Q., Liu Y., Wang Y., Chen Y., Guo X., Wu Z., et al. Review of the application of biomass-derived porous carbon in lithium-sulfur batteries. *Ionics* 2020;26:4765–4781. doi:10.1007/s11581-020-03694-3.
- [36] Yuan H., Liu T., Liu Y., Nai J., Wang Y., Zhang W., et al. A review of biomass materials for advanced lithium–sulfur batteries. *Chem Sci* 2019;10:7484–7495. doi:10.1039/C9SC02743B.
- [37] Imtiaz S., Zhang J., Zafar Z.A., Ji S., Huang T., Anderson J.A., et al. Biomass-derived nanostructured porous carbons for lithium-sulfur batteries. *Sci China Mater* 2016;59:389–407. doi:10.1007/s40843-016-5047-8.
- [38] Wang M., Xia X., Zhong Y., Wu J., Xu R., Yao Z., et al. Porous carbon hosts for lithium–sulfur batteries. *Chem Eur J* 2019;25:3710–3725. doi:10.1002/chem.201803153.
- [39] Yan L., Yu J., Houston J., Flores N., Luo H. Biomass derived porous nitrogen doped carbon for electrochemical devices. *Green Energy Environ* 2017;2:84–99. doi:10.1016/j.gee.2017.03.002.
- [40] Yao Y., Wu F. Naturally derived nanostructured materials from biomass for rechargeable lithium/sodium batteries. *Nanomater Energy* 2015;17:91–103. doi:10.1016/j.nanoen.2015.08.004.
- [41] Li Z., Guo D., Liu Y., Wang H., Wang L. Recent advances and challenges in biomass-derived porous carbon nanomaterials for supercapacitors. *Chem Eng J* 2020;397:125418. doi:10.1016/j.cej.2020.125418.
- [42] Vassilev S.V., Baxter D., Andersen L.K., Vassileva C.G. An overview of the chemical composition of biomass. *Fuel* 2010;89:913–933. doi:10.1016/j.fuel.2009.10.022.

- [43] Vassilev S.V., Baxter D., Andersen L.K., Vassileva C.G., Morgan T.J. An overview of the organic and inorganic phase composition of biomass. *Fuel* 2012;94:1–33. doi:10.1016/j.fuel.2011.09.030.
- [44] Vassilev S.V., Baxter D., Andersen L.K., Vassileva C.G. An overview of the composition and application of biomass ash. Part 1. Phase–mineral and chemical composition and classification. *Fuel* 2013;105:40–76. doi:10.1016/j.fuel.2012.09.041.
- [45] Vassilev S.V., Vassileva C.G. Composition, properties and challenges of algae biomass for biofuel application: an overview. *Fuel* 2016;181:1–33. doi:10.1016/j.fuel.2016.04.106.
- [46] Field C.B. Primary production of the biosphere: integrating terrestrial and oceanic components. *Science* 1998;281:237–240. doi:10.1126/science.281.5374.237. 80.
- [47] Couturier M., Ladevèze S., Sulzenbacher G., Ciano L., Fanuel M., Moreau C., et al. Lytic xylan oxidases from wood-decay fungi unlock biomass degradation. *Nat Chem Biol* 2018;14:306–310. doi:10.1038/nchembio.2558.
- [48] Liu S., Lu H., Hu R., Shupe A., Lin L., Liang B. A sustainable woody biomass biorefinery. *Biotechnol Adv* 2012. doi:10.1016/j.biotechadv.2012.01.013.
- [49] Driscoll M.S., Stipanovic A.J., Cheng K., Barber V.A., Manning M., Smith J.L., et al. Ionizing radiation and a wood-based biorefinery. *Radiat Phys Chem* 2014;94:217–220. doi:10.1016/j.radphyschem.2013.05.045.
- [50] Lauri P., Havlík P., Kindermann G., Forsell N., Böttcher H., Obersteiner M. Woody biomass energy potential in 2050. *Energy Pol* 2014;66:19–31. doi:10.1016/j.enpol.2013.11.033.
- [51] Zhu J.Y., Pan X., Zalesny R.S. Pretreatment of woody biomass for biofuel production: energy efficiency, technologies, and recalcitrance. *Appl Microbiol Biotechnol* 2010;87:847–857. doi:10.1007/s00253-010-2654-8.
- [52] Havlík P., Schneider U.A., Schmid E., Böttcher H., Fritz S., Skalský R., et al. Global land-use implications of first and second generation biofuel targets. *Energy Pol* 2011;39:5690–5702. doi:10.1016/j.enpol.2010.03.030.
- [53] Rudakiya D.M., Gupte A. Degradation of hardwoods by treatment of white rot fungi and its pyrolysis kinetics studies. *Int Biodeterior Biodegrad* 2017. doi:10.1016/j.ibiod.2017.02.004.
- [54] Thammasouk K., Tandjo D., Penner M.H. Influence of extractives on the analysis of herbaceous biomass. *J Agric Food Chem* 1997;45:437–443. doi:10.1021/jf960401r.
- [55] Demirbas A. Biofuels from agricultural biomass. *Energy sources. Part A Recover Util Environ Eff* 2009;31:1573–1582. doi:10.1080/15567030802094011.
- [56] Barbieri L., Andreola F., Lancellotti I., Taurino R. Management of agricultural biomass wastes: preliminary study on characterization and valorisation in clay matrix bricks. *Waste Manag* 2013;33:2307–2315. doi:10.1016/j.wasman.2013.03.014.
- [57] Marsh G. Small wonders: biomass from algae. *Renew Energy Focus* 2009;9:74–78. doi:10.1016/S1755-0084(09)70046-8.
- [58] Ward A.J., Lewis D.M., Green F.B. Anaerobic digestion of algae biomass: a review. *Algal Res* 2014;5:204–214. doi:10.1016/j.algal.2014.02.001.
- [59] Dębowski M., Zieliński M., Grala A., Dudek M. Algae biomass as an alternative substrate in biogas production technologies - Review. *Renew Sustain Energy Rev* 2013. doi:10.1016/j.rser.2013.07.029.
- [60] Zhong W., Zhang Z., Luo Y., Qiao W., Xiao M., Zhang M. Biogas productivity by co-digesting Taihu blue algae with corn straw as an external carbon source. *Bioresour Technol* 2012. doi:10.1016/j.biortech.2012.02.111.
- [61] Vergara-Fernandez A., Vargas G., Alarcon N., Velasco A. Evaluation of marine algae as a source of biogas in a two-stage anaerobic reactor system. *Biomass Bioenergy* 2008;32:338–344. doi:10.1016/j.biombioe.2007.10.005.
- [62] Chisti Y. Biodiesel from microalgae. *Biotechnol Adv* 2007. doi:10.1016/j.biotechadv.2007.02.001.
- [63] Raheem A., Prinsen P., Vuppaladadiyam A.K., Zhao M., Luque R. A review on sustainable microalgae based biofuel and bioenergy production: recent developments. *J Clean Prod* 2018;181:42–59. doi:10.1016/j.jclepro.2018.01.125.
- [64] Flecker A.S., Twining C.W., Schmitz O.J., Cooke S.J., Hammerschlag N. Aquatic predators influence micronutrients: important but understudied. *Trends Ecol Evol* 2019. doi:10.1016/j.tree.2019.07.006.
- [65] Bar-On Y.M., Phillips R., Milo R. The biomass distribution on Earth. *Proc Natl Acad Sci Unit States Am* 2018;115:6506–6511. doi:10.1073/pnas.1711842115.
- [66] Hendrichs H. Schafzungen der Huftierbiomasse in der Dornbuschsavanne nordlich und westlich der Serengetisteppe in Ostafrika nach einem neuen Verfahren und Bemerkungen zur Biomasse der anderen pflanzenfressenden Tierarten. *Saugetierkundliche Mitteilungen* 1969;18:237–255.
- [67] Fittkau E.J., Klinge H. On biomass and trophic structure of the central amazonian rain forest ecosystem. *Biotropica* 1973;5:2. doi:10.2307/2989676.
- [68]

- [69] Vassilev S.V., Vassileva C.G. Water-soluble fractions of biomass and biomass ash and their significance for biofuel application. *Energy Fuels* 2019;33:2763–2777. doi:10.1021/acs.energyfuels.9b00081.
- [70] Marsh H., Rodríguez-Reinoso F. *Activated carbon*. Elsevier; 2006. doi:10.1016/B978-0-08-044463-5.X5013-4.
- [71] van Oss C.J. A review of: “active carbon.” R.C. Bansal, J.B. Donnet and F. Stoeckli; marcel Dekker, New York, 1988. pp. 482, \$135.00. *J Dispersion Sci Technol* 1990;11. doi:10.1080/01932699008943255. 323–323.
- [72] Bansal R.C., Goyal M. *Activated carbon adsorption*. 2005. doi:10.1680/bwtse.63341.147.
- [73] Husen A., Siddiqi K.S. *Carbon and fullerene nanomaterials in plant system*. 2014. doi:10.1186/1477-3155-12-16.
- [74] Binnie C., Kimber M., Thomas H. *Activated carbon adsorption. Basic water treat.* ICE Publishing; 2017. p. 147–155. doi:10.1680/bwtse.63341.147.
- [75] Inagaki M., Tascón J.M.D. Chapter 2 Pore formation and control in carbon materials. *Interface Sci. Technol.*; 2006. p. 49–105. doi:10.1016/S1573-4285(06)80011-6.
- [76] Mohamad Nor N., Lau L.C., Lee K.T., Mohamed A.R. Synthesis of activated carbon from lignocellulosic biomass and its applications in air pollution control—a review. *J Environ Chem Eng* 2013;1:658–666. doi:10.1016/j.jece.2013.09.017.
- [77] Sircar S., Golden T.C., Rao M.B. *Activated carbon for gas separation and storage*. Carbon N Y 1996;34:1–12. doi:10.1016/0008-6223(95)00128-X.
- [78] Dąbrowski A., Podkościelny P., Hubicki Z., Barczak M. Adsorption of phenolic compounds by activated carbon—a critical review. *Chemosphere* 2005;58:1049–1070. doi:10.1016/j.chemosphere.2004.09.067.
- [79] Tan X., Liu S., Liu Y., Gu Y., Zeng G., Hu X., et al. Biochar as potential sustainable precursors for activated carbon production: multiple applications in environmental protection and energy storage. *Bioresour Technol* 2017;227:359–372. doi:10.1016/j.biortech.2016.12.083.
- [80] Baccar R., Sarrà M., Bouzid J., Feki M., Blánquez P. Removal of pharmaceutical compounds by activated carbon prepared from agricultural by-product. *Chem Eng J* 2012;211–212:310–317. doi:10.1016/j.cej.2012.09.099.
- [81] Bagheri M., Jafari S.M., Eikani M.H. Development of ternary nanoadsorbent composites of graphene oxide, activated carbon, and zero-valent iron nanoparticles for food applications. *Food Sci Nutr* 2019;7:2827–2835. doi:10.1002/fsn3.1080.
- [82] Shukla P.R., Wang S., Sun H., Ang H.M., Tadó M. Activated carbon supported cobalt catalysts for advanced oxidation of organic contaminants in aqueous solution. *Appl Catal B Environ* 2010;100:529–534. doi:10.1016/j.apcatb.2010.09.006.
- [83] González-García P. Activated carbon from lignocellulosics precursors: a review of the synthesis methods, characterization techniques and applications. *Renew Sustain Energy Rev* 2018;82:1393–1414. doi:10.1016/j.rser.2017.04.117.
- [84] Yin C., Aroua M., Daud W. Review of modifications of activated carbon for enhancing contaminant uptakes from aqueous solutions. *Separ Purif Technol* 2007;52:403–415. doi:10.1016/j.seppur.2006.06.009.
- [85] Shafeeyan M.S., Daud W.M.A.W., Houshmand A., Shamiri A. A review on surface modification of activated carbon for carbon dioxide adsorption. *J Anal Appl Pyrolysis* 2010;89:143–151. doi:10.1016/j.jaap.2010.07.006.
- [86] Jain A., Balasubramanian R., Srinivasan M.P. Hydrothermal conversion of biomass waste to activated carbon with high porosity: a review. *Chem Eng J* 2016;283:789–805. doi:10.1016/j.cej.2015.08.014.
- [87] Maneerung T., Liew J., Dai Y., Kawi S., Chong C., Wang C.-H. Activated carbon derived from carbon residue from biomass gasification and its application for dye adsorption: kinetics, isotherms and thermodynamic studies. *Bioresour Technol* 2016;200:350–359. doi:10.1016/j.biortech.2015.10.047.
- [88] Danish M., Ahmad T. A review on utilization of wood biomass as a sustainable precursor for activated carbon production and application. *Renew Sustain Energy Rev* 2018;87:1–21. doi:10.1016/j.rser.2018.02.003.
- [89] Kobya M., Demirbas E., Senturk E., Ince M. Adsorption of heavy metal ions from aqueous solutions by activated carbon prepared from apricot stone. *Bioresour Technol* 2005;96:1518–1521. doi:10.1016/j.biortech.2004.12.005.
- [90] Srinivasakannan C. Production of activated carbon from rubber wood sawdust. *Biomass Bioenergy* 2004;27:89–96. doi:10.1016/j.biombioe.2003.11.002.
- [91] Şentorun-Shalaby Ç., Uçak-Astarlıođ lu M.G., Artok L., Sarıcı Ç. Preparation and characterization of activated carbons by one-step steam pyrolysis/activation from apricot stones. *Microporous Mesoporous Mater* 2006;88:126–134. doi:10.1016/j.micromeso.2005.09.003.
- [92] Müller B.R. Effect of particle size and surface area on the adsorption of albumin-bonded bilirubin on activated carbon. *Carbon N Y* 2010;48:3607–3615. doi:10.1016/j.carbon.2010.06.011.

- [93] Suhas Carrott P.J.M., Ribeiro Carrott M.M.L. Lignin – from natural adsorbent to activated carbon: a review. *Bioresour Technol* 2007;98:2301–2312. doi:10.1016/j.biortech.2006.08.008.
- [94] Ioannidou O., Zabaniotou A. Agricultural residues as precursors for activated carbon production—a review. *Renew Sustain Energy Rev* 2007;11:1966–2005. doi:10.1016/j.rser.2006.03.013.
- [95] Fitzer E., Mueller K., Schaefer W. Chemistry of the pyrolytic conversion of organic compounds to carbon. *Chem Phys Carbon* 1971.
- [96] Homann K.-H. Chemistry of hydrocarbon combustion. Von D. J. Hucknall. Chapman & Hall, London 1985. VIII, 415 S., geb. £ 39.50. – ISBN 0-412-26110-3. *Angew Chemie*; 1987. doi:10.1002/ange.19870990135.
- [97] Ali I., Asim M., Khan T.A. Low cost adsorbents for the removal of organic pollutants from wastewater. *J Environ Manag* 2012;113:170–183. doi:10.1016/j.jenvman.2012.08.028.
- [98] Ali I. The quest for active carbon adsorbent substitutes: inexpensive adsorbents for toxic metal ions removal from wastewater. *Separ Purif Rev* 2010;39:95–171. doi:10.1080/15422119.2010.527802.
- [99] Heidarinejad Z., Dehghani M.H., Heidari M., Javedan G., Ali I., Sillanpää M. Methods for preparation and activation of activated carbon: a review. *Environ Chem Lett* 2020;18:393–415. doi:10.1007/s10311-019-00955-0.
- [100] Mohammad-Khah A, Ansari R. Activated charcoal: preparation, characterization and applications : a review article. *Int J Chem Tech Res.* 1. [n.d].
- [101] Li W., Yang K., Peng J., Zhang L., Guo S., Xia H. Effects of carbonization temperatures on characteristics of porosity in coconut shell chars and activated carbons derived from carbonized coconut shell chars. *Ind Crop Prod* 2008. doi:10.1016/j.indcrop.2008.02.012.
- [102] Rodriguez-Reinoso F. Preparation and characterization of activated carbons. *NATO ASI Ser Ser E Appl Sci* 1986.
- [103] Rodríguez-Reinoso F. Activated carbon: structure, characterization, preparation and applications. *Introd. to carbon Technol.*; 1997.
- [104] Lizzio A.A., Jiang H., Radovic L.R. On the kinetics of carbon (Char) gasification: reconciling models with experiments. *Carbon N Y* 1990;28:7–19. doi:10.1016/0008-6223(90)90087-F.
- [105] Marsh H., Rand B. The process of activation of carbons by gasification with CO<sub>2</sub>-I. Gasification of pure polyfurfuryl alcohol carbon. *Carbon N Y* 1971;9:47–61. doi:10.1016/0008-6223(71)90143-6.
- [106] Cal M., Strickler B., Lizzio A. High temperature hydrogen sulfide adsorption on activated carbon. *Carbon N Y* 2000;38:1757–1765. doi:10.1016/S0008-6223(00)00010-5.
- [107] Zhang T., Walawender W., Fan L., Fan M., Daugaard D., Brown R. Preparation of activated carbon from forest and agricultural residues through CO activation. *Chem Eng J* 2004;105:53–59. doi:10.1016/j.cej.2004.06.011.
- [108] Mak S.M., Tey B.T., Cheah K.Y., Siew W.L., Tan K.K. The effect of mechanical grinding on the mesoporosity of steam-activated palm kernel shell activated carbons. *J Chem Technol Biotechnol* 2009;84:1405–1411. doi:10.1002/jctb.2235.
- [109] Nowicki P., Pietrzak R., Wachowska H. Sorption properties of active carbons obtained from walnut shells by chemical and physical activation. *Catal Today* 2010;150:107–114. doi:10.1016/j.cattod.2009.11.009.
- [110] Plaza M.G., Rubiera F., Pis J.J., Pevida C. Ammoxidation of carbon materials for CO<sub>2</sub> capture. *Appl Surf Sci* 2010;256:6843–6849. doi:10.1016/j.apsusc.2010.04.099.
- [111] Molina-Sabio M., Rodriguez-Reinoso F. Role of chemical activation in the development of carbon porosity. *Colloids Surfaces A Physicochem Eng Asp* 2004;241:15–25. doi:10.1016/j.colsurfa.2004.04.007.
- [112] Kalderis D., Bethanis S., Paraskeva P., Diamadopoulos E. Production of activated carbon from bagasse and rice husk by a single-stage chemical activation method at low retention times. *Bioresour Technol* 2008;99:6809–6816. doi:10.1016/j.biortech.2008.01.041.
- [113] Wang J., Kaskel S. KOH activation of carbon-based materials for energy storage. *J Mater Chem* 2012;22:23710. doi:10.1039/c2jm34066f.
- [114] Yahya M.A., Al-Qodah Z., Ngah C.W.Z. Agricultural bio-waste materials as potential sustainable precursors used for activated carbon production: a review. *Renew Sustain Energy Rev* 2015. doi:10.1016/j.rser.2015.02.051.
- [115] Alslaibi T.M., Abustan I., Ahmad M.A., Foul A.A. A review: production of activated carbon from agricultural byproducts via conventional and microwave heating. *J Chem Technol Biotechnol* 2013;88:1183–1190. doi:10.1002/jctb.4028.
- [116] Maciá-Agulló J.A., Moore B.C., Cazorla-Amorós D., Linares-Solano A. Activation of coal tar pitch carbon fibres: physical activation vs. chemical activation. *Carbon N. Y.*; 2004. doi:10.1016/j.carbon.2004.01.013.
- [117] Purnomo C.W., Salim C., Hinode H. Effect of the activation method on the properties and adsorption behavior of bagasse fly ash-based activated carbon. *Fuel Process Technol* 2012;102:132–139. doi:10.1016/j.fuproc.2012.04.037.
- [118] Mohd Din A.T., Hameed B.H., Ahmad A.L. Batch adsorption of phenol onto physiochemical-activated coconut shell. *J Hazard Mater* 2009;161:1522–1529. doi:10.1016/j.jhazmat.2008.05.009.

- [119] Hu C.-C., Wang C.-C., Wu F.-C., Tseng R.-L. Characterization of pistachio shell-derived carbons activated by a combination of KOH and CO<sub>2</sub> for electric double-layer capacitors. *Electrochim Acta* 2007;52:2498–2505. doi:10.1016/j.electacta.2006.08.061.
- [120] Košir U., Kralj Cigić I., Markelj J., Drvarič Talian S., Dominko R. Polysulfide species in various electrolytes of Li-S batteries – a chromatographic investigation. *Electrochim Acta* 2020;363:137227. doi:10.1016/j.electacta.2020.137227.
- [121] He Q., Freiberg A.T.S., Patel M.U.M., Qian S., Gasteiger H.A. Operando identification of liquid intermediates in lithium–sulfur batteries via transmission UV–vis spectroscopy. *J Electrochem Soc* 2020;167:080508. doi:10.1149/1945-7111/ab8645.
- [122] Hagen M., Schiffels P., Hammer M., Dörfler S., Tübke J., Hoffmann M.J., et al. In-situ Raman investigation of polysulfide formation in Li-S cells. *J Electrochem Soc* 2013;160:A1205–A1214. doi:10.1149/2.045308jes.
- [123] Wujcik K.H., Wang D.R., Teran A.A., Nasybulin E., Pascal T.A., Prendergast D., et al. Determination of redox reaction mechanisms in lithium–sulfur batteries. *Electrochem. Eng.* John Wiley & Sons, Ltd; 2018. p. 41–74. doi:10.1002/9783527807215.ch3.
- [124] Wild M., O'Neill L., Zhang T., Purkayastha R., Minton G., Marinescu M., et al. Lithium sulfur batteries, a mechanistic review. *Energy Environ Sci* 2015;8:3477–3494. doi:10.1039/C5EE01388G.
- [125] Walus S., Barchasz C., Colin J.-F., Martin J.-F., Elkaïm E., Leprêtre J.-C., et al. New insight into the working mechanism of lithium–sulfur batteries: in situ and operando X-ray diffraction characterization. *Chem Commun* 2013;49:7899. doi:10.1039/c3cc43766c.
- [126] Cuisinier M., Cabelguen P., Evers S., He G., Kolbeck M., Garsuch A., et al. Sulfur speciation in Li – S batteries determined by operando X - ray absorption spectroscopy. *J Phys Chem Lett* 2013;4:3227–3232. doi:10.1021/jz401763d.
- [127] Varzi A., Thanner K., Scipioni R., Di Lecce D., Hassoun J., Dörfler S., et al. Current status and future perspectives of lithium metal batteries. *J Power Sources* 2020;480:228803. doi:10.1016/j.jpowsour.2020.228803.
- [128] Pope M.A., Aksay I.A. Structural design of cathodes for Li-S batteries. *Adv Energy Mater* 2015;5:1–22. doi:10.1002/aenm.201500124.
- [129] Fotouhi A., Auger D., O'Neill L., Cleaver T., Walus S. Lithium-sulfur battery technology readiness and applications—a review. *Energies* 2017;10:1937. doi:10.3390/en10121937.
- [130] Bonnick P., Muldoon J. The Dr Jekyll and mr Hyde of lithium sulfur batteries. *Energy Environ Sci* 2020;13:4808–4833. doi:10.1039/D0EE02797A.
- [131] Strubel P., Thieme S., Biemelt T., Helmer A., Oschatz M., Brückner J., et al. ZnO hard templating for synthesis of hierarchical porous carbons with tailored porosity and high performance in lithium-sulfur battery. *Adv Funct Mater* 2015;25:287–297. doi:10.1002/adfm.201402768.
- [132] Yang C.-P., Yin Y.-X., Ye H., Jiang K.-C., Zhang J., Guo Y.-G. Insight into the effect of boron doping on sulfur/carbon cathode in lithium–sulfur batteries. *ACS Appl Mater Interfaces* 2014;6:8789–8795. doi:10.1021/am501627f.
- [133] Dörfler S., Strubel P., Jaumann T., Troschke E., Hippauf F., Kency C., et al. On the mechanistic role of nitrogen-doped carbon cathodes in lithium-sulfur batteries with low electrolyte weight portion. *Nanomater Energy* 2018;54:116–128. doi:10.1016/j.nanoen.2018.09.065.
- [134] Xie J., Li B., Peng H., Song Y., Zhao M., Chen X., et al. Implanting atomic cobalt within mesoporous carbon toward highly stable lithium–sulfur batteries. *Adv Mater* 2019;31:1903813. doi:10.1002/adma.201903813.
- [135] Liang X., Kwok C.Y., Lodi-Marzano F., Pang Q., Cuisinier M., Huang H., et al. Tuning transition metal oxide-sulfur interactions for long life lithium sulfur batteries: the “goldilocks” principle. *Adv Energy Mater* 2016;6:1–9. doi:10.1002/aenm.201501636.
- [136] Lacey M.J., Jeschull F., Edström K., Brandell D. Functional, water-soluble binders for improved capacity and stability of lithium-sulfur batteries. *J Power Sources* 2014;264:8–14. doi:10.1016/j.jpowsour.2014.04.090.
- [137] Lacey M.J., Jeschull F., Edström K., Brandell D. Why PEO as a binder or polymer coating increases capacity in the Li–S system. *Chem Commun* 2013;49:8531–8533. doi:10.1039/c3cc44772c.
- [138] Lacey M.J., Jeschull F., Edström K., Brandell D. Porosity blocking in highly porous carbon black by PVdF binder and its implications for the Li-S system. *J Phys Chem C* 2014;118:25890–25898. doi:10.1021/jp508137m.
- [139] Lacey M.J., Österlund V., Bergfelt A., Jeschull F., Bowden T., Brandell D. A robust, water-based, functional binder framework for high-energy lithium-sulfur batteries. *ChemSusChem* 2017;10:2758–2766. doi:10.1002/cssc.201700743.
- [140] Xue W., Miao L., Qie L., Wang C., Li S., Wang J., et al. Gravimetric and volumetric energy densities of lithium-sulfur batteries. *Curr Opin Electrochem* 2017;6:92–99. doi:10.1016/j.coelec.2017.10.007.
- [141] Fan F.Y., Carter W.C., Chiang Y.-M. Mechanism and kinetics of Li<sub>2</sub>S precipitation in lithium-sulfur batteries. *Adv Mater* 2015;27:5203–5209. doi:10.1002/adma.201501559.
- [142] Strubel P., Thieme S., Weller C., Althues H., Kaskel S. Insights into the redistribution of sulfur species during cycling in lithium-sulfur batteries using physisorption methods. *Nanomater Energy* 2017;34:437–441. doi:10.1016/j.nanoen.2017.03.018.

- [143] Chien Y.-C., Menon A.S., Brant W.R., Brandell D., Lacey M.J. Simultaneous monitoring of crystalline active materials and resistance evolution in lithium–sulfur batteries. *J Am Chem Soc* 2020;142:1449–1456. doi:10.1021/jacs.9b11500.
- [144] Mistry A., Mukherjee P.P. Precipitation–microstructure interactions in the Li-sulfur battery electrode. *J Phys Chem C* 2017;121:26256–26264. doi:10.1021/acs.jpcc.7b09997.
- [145] Shen C., Andrei P., Zheng J.P. Stable cycling of lithium-sulfur batteries by optimizing the cycle condition. *Electrochim Acta* 2019;326:134948. doi:10.1016/j.electacta.2019.134948.
- [146] Zheng J., Gu M., Wang C., Zuo P., Koech P.K., Zhang J.-G., et al. Controlled nucleation and growth process of Li<sub>2</sub>S<sub>2</sub>/Li<sub>2</sub>S in lithium-sulfur batteries. *J Electrochem Soc* 2013;160:A1992–A1996. doi:10.1149/2.032311jes.
- [147] Lin Y., Chen D., Wang S., Han D., Xiao M., Meng Y. Addressing passivation of a sulfur electrode in Li–S pouch cells for dramatically improving their cyclic stability. *ACS Appl Mater Interfaces* 2020;12. doi:10.1021/acsami.0c05385. acsami.0c05385.
- [148] Tang X., Xu Z., Sun Z., Zhou J., Wu X., Lin H., et al. Factors of kinetics processes in lithium–sulfur reactions. *Energy Technol* 2019;1900574:1900574. doi:10.1002/ente.201900574.
- [149] Rana M., Ahad S.A., Li M., Luo B., Wang L., Gentle I., et al. Review on areal capacities and long-term cycling performances of lithium sulfur battery at high sulfur loading. *Energy Storage Mater* 2019;18:289–310. doi:10.1016/j.ensm.2018.12.024.
- [150] Yuan H., Liu T., Liu Y., Nai J., Wang Y., Zhang W., et al. A review of biomass materials for advanced lithium-sulfur batteries. *Chem Sci* 2019. doi:10.1039/c9sc02743b.
- [151] Jozwiuk A., Sommer H., Janek J., Brezesinski T. Fair performance comparison of different carbon blacks in lithium-sulfur batteries with practical mass loadings - simple design competes with complex cathode architecture. *J Power Sources* 2015;296:454–461. doi:10.1016/j.jpowsour.2015.07.070.
- [152] Xu J., Zhou K., Chen F., Chen W., Wei X., Liu X.-W., et al. Natural integrated carbon architecture for rechargeable lithium–sulfur batteries. *ACS Sustainable Chem Eng* 2016;4:666–670. doi:10.1021/acssuschemeng.5b01258.
- [153] Luo C., Zhu H., Luo W., Shen F., Fan X., Dai J., et al. Atomic-layer-deposition functionalized carbonized mesoporous wood fiber for high sulfur loading lithium sulfur batteries. *ACS Appl Mater Interfaces* 2017. doi:10.1021/acsami.7b01205.
- [154] Garapati M.S., AP V.S., Sundara R. Synergy between partially exfoliated carbon nanotubes-sulfur cathode and nitrogen rich dual function interlayer for high performance lithium sulfur battery. *Carbon N Y* 2019;147:364–376. doi:10.1016/j.carbon.2019.03.007.
- [155] Zhang S.S. Role of LiNO<sub>3</sub> in rechargeable lithium/sulfur battery. *Electrochim Acta* 2012;70:344–348. doi:10.1016/j.electacta.2012.03.081.
- [156] Shim J., Ko T.J., Yoo K. Study for an effect of LiNO<sub>3</sub> on polysulfide multistep reaction in Li/S battery. *J Ind Eng Chem* 2019;80:283–291. doi:10.1016/j.jiec.2019.08.006.
- [157] Chulliyote R., Hareendrakrishnakumar H., Raja M., Gladis J.M., Stephan A.M. Sulfur-immobilized nitrogen and oxygen Co-doped hierarchically porous biomass carbon for lithium-sulfur batteries: influence of sulfur content and distribution on its performance. *ChemistrySelect* 2017;2:10484–10495. doi:10.1002/slct.201702061.
- [158] Schneidermann C., Kensy C., Otto P., Oswald S., Giebeler L., Leistenschneider D., et al. Nitrogen-doped biomass-derived carbon formed by mechanochemical synthesis for lithium–sulfur batteries. *ChemSusChem* 2019;12:310–319. doi:10.1002/cssc.201801997.
- [159] Zhu Q., Deng H., Su Q., Du G., Yu Y., Ma S., et al. A free-standing nitrogen-doped porous carbon foam electrode derived from melaleuca bark for lithium-sulfur batteries. *Electrochim Acta* 2019;293:19–24. doi:10.1016/j.electacta.2018.10.017.
- [160] Xia P., Chen F., Lei W., Pan Y., Ma Z. Long cycle performance folium cycas biochar/S composite material for lithium-sulfur batteries. *Ionics* 2020;26:183–189. doi:10.1007/s11581-019-03169-0.
- [161] Xia P., Lei W., Wang X., Luo Z., Pan Y., Ma Z. Simple synthesis of Ni/high porosity biomass carbon composites with enhanced electrochemical performance of lithium–sulfur battery. *J Alloys Compd* 2020;832:153692. doi:10.1016/j.jallcom.2020.153692.
- [162] Guo D., Zheng C., Deng W., Chen X., Wei H., Liu M., et al. Nitrogen-doped porous carbon plates derived from fallen camellia flower for electrochemical energy storage. *J Solid State Electrochem* 2017;21:1165–1174. doi:10.1007/s10008-016-3474-2.
- [163] Zhao Y., Ren J., Tan T., Babaa M.-R., Bakenov Z., Liu N., et al. Biomass waste inspired highly porous carbon for high performance lithium/sulfur batteries. *Nanomaterials* 2017;7:260. doi:10.3390/nano7090260.
- [164] Yan Y., Chen S., Fan C., Lin J., Fan H., Feng Z., et al. Effects of activation process on catkin derived carbon materials and its electrochemical performance as matrix in cathode of Li-S battery. *ChemistrySelect* 2020;5:12020–12027. doi:10.1002/slct.202003118.
- [165] Fan L., Li Z., Kang W., Cheng B. Biomass-derived tube-like nitrogen and oxygen dual-doped porous carbon in the sulfur cathode for lithium sulfur battery. *Renew Energy* 2020;155:309–316. doi:10.1016/j.renene.2020.03.153.
- [166] Wang Z., Zhang X., Liu X., Zhang Y., Zhao W., Li Y., et al. High specific surface area bimodal porous carbon derived from biomass reed flowers for high performance lithium-sulfur batteries. *J Colloid Interface Sci* 2020;569:22–33. doi:10.1016/j.jcis.2020.02.062.



- [167] Muttakin M., Mitra S., Thu K., Ito K., Saha B.B. Theoretical framework to evaluate minimum desorption temperature for IUPAC classified adsorption isotherms. *Int J Heat Mass Tran* 2018;122:795–805. doi:10.1016/j.ijheatmasstransfer.2018.01.107.
- [168] Yamin H., Peled E. Electrochemistry of a nonaqueous lithium/sulfur cell. *J Power Sources* 1983;9:281–287. doi:10.1016/0378-7753(83)87029-3.
- [169] Barchasz C., Leprêtre J.-C., Patoux S., Alloin F. Electrochemical properties of ether-based electrolytes for lithium/sulfur rechargeable batteries. *Electrochim Acta* 2013;89:737–743. doi:10.1016/j.electacta.2012.11.001.
- [170] Carbone L., Gobet M., Peng J., Devany M., Scrosati B., Greenbaum S., et al. Comparative study of ether-based electrolytes for application in lithium–sulfur battery. *ACS Appl Mater Interfaces* 2015;7:13859–13865. doi:10.1021/acsami.5b02160.
- [171] Carbone L., Peng J., Agostini M., Gobet M., Devany M., Scrosati B., et al. Carbon composites for a high-energy lithium–sulfur battery with a glyme-based electrolyte. *ChemElectroChem* 2017. doi:10.1002/celec.201600586.
- [172] Benítez A., Di Lecce D., Caballero Á., Morales J., Rodríguez-Castellón E., Hassoun J. Lithium sulfur battery exploiting material design and electrolyte chemistry: 3D graphene framework and diglyme solution. *J Power Sources* 2018;397. doi:10.1016/j.jpowsour.2018.07.002.
- [173] Gu X., Wang Y., Lai C., Qiu J., Li S., Hou Y., et al. Microporous bamboo biochar for lithium-sulfur batteries. *Nano Res* 2015;8:129–139. doi:10.1007/s12274-014-0601-1.
- [174] Yan Y., Shi M., Wei Y., Zhao C., Carnie M., Yang R., et al. Process optimization for producing hierarchical porous bamboo-derived carbon materials with ultrahigh specific surface area for lithium-sulfur batteries. *J Alloys Compd* 2018;738:16–24. doi:10.1016/j.jallcom.2017.11.212.
- [175] Wei Y., Yan Y., Zou Y., Shi M., Deng Q., Zhao N., et al. The ternary PANI@BDC/S composite cathode with enhanced electrochemical performance in lithium-sulfur batteries. *J Electroanal Chem* 2019;839:149–159. doi:10.1016/j.jelechem.2019.03.014.
- [176] Wei Y., Yan Y., Zou Y., Shi M., Deng Q., Zhao N., et al. Sulfonated polyaniline coated bamboo-derived biochar/sulfur cathode for Li-S batteries with excellent dual conductivity and polysulfides affinity. *Electrochim Acta* 2019. doi:10.1016/j.electacta.2019.04.067.
- [177] Xu J., Dai L., Gui Y., Yuan L., Ma J., Zhang C. Towards a waste-free biorefinery: a cascade valorization of bamboo for efficient fractionation, enzymatic hydrolysis and lithium-sulfur cathode. *Ind Crop Prod* 2020;149:112364. doi:10.1016/j.indcrop.2020.112364.
- [178] Chen M., Jiang S., Huang C., Wang X., Cai S., Xiang K., et al. Honeycomb-like nitrogen and sulfur dual-doped hierarchical porous biomass-derived carbon for lithium-sulfur batteries. *ChemSusChem* 2017;10:1803–1812. doi:10.1002/cssc.201700050.
- [179] Cui Y., Zhang Q., Wu J., Liang X., Baker A.P., Qu D., et al. Developing porous carbon with dihydrogen phosphate groups as sulfur host for high performance lithium sulfur batteries. *J Power Sources* 2018;378:40–47. doi:10.1016/j.jpowsour.2017.12.027.
- [180] Chen S., Wu Z., Luo J., Han X., Wang J., Deng Q., et al. Constructing layered double hydroxide fences onto porous carbons as high-performance cathodes for lithium–sulfur batteries. *Electrochim Acta* 2019;312:109–118. doi:10.1016/j.electacta.2019.04.113.
- [181] Yan S., Wu J., Dai Y., Pan Z., Sheng W., Xu J., et al. Excellent electrochemical application of Ni-based hydroxide/biomass porous carbon/sulfur composite cathode on lithium-sulfur batteries. *Colloids Surfaces A Physicochem Eng Asp* 2020;591:124513. doi:10.1016/j.colsurfa.2020.124513.
- [182] Rybarczyk M.K., Peng H.-J., Tang C., Lieder M., Zhang Q., Titirici M.-M. Porous carbon derived from rice husks as sustainable bioresources: insights into the role of micro-/mesoporous hierarchy in hosting active species for lithium–sulfur batteries. *Green Chem* 2016;18:5169–5179. doi:10.1039/C6GC00612D.
- [183] Jin C., Sheng O., Zhang W., Luo J., Yuan H., Yang T., et al. Sustainable, inexpensive, naturally multi-functionalized biomass carbon for both Li metal anode and sulfur cathode. *Energy Storage Mater* 2018;15:218–225. doi:10.1016/j.ensm.2018.04.001.
- [184] Li J.-T., Wu J.-H., Zhang T., Huang L. Preparation of biochar from different biomasses and their application in the Li-S battery. *Acta Phys Chim Sin* 2017;33:968–975. doi:10.3866/PKU.WHXB201702093.
- [185] Chen K., Xue D. Multiple functional biomass-derived activated carbon materials for aqueous supercapacitors, lithium-ion capacitors and lithium-sulfur batteries. *Chin J Chem* 2017. doi:10.1002/cjoc.201600785.
- [186] Chen F., Ma L., Ren J., Zhang M., Luo X., Li B., et al. Wheat straw-derived N-, O-, and S-Tri-doped porous carbon with ultrahigh specific surface area for lithium-sulfur batteries. *Materials* 2018;11:989. doi:10.3390/ma11060989.
- [187] Zhang J., You C., Wang J., Guo S., Zhang W., Yang R., et al. Synergistic catalytic effect of ion tunnels with polar dopants to boost the electrochemical kinetics for high-performance sulfur cathodes. *ChemElectroChem* 2019;6:5051–5059. doi:10.1002/celec.201901360.
- [188] Wang S., Zou K., Qian Y., Deng Y., Zhang L., Chen G. Insight to the synergistic effect of N-doping level and pore structure on improving the electrochemical performance of sulfur/N-doped porous carbon cathode for Li-S batteries. *Carbon N Y* 2019;144:745–755. doi:10.1016/j.carbon.2018.12.113.
- [189] Wang S., Liu X., Zou K., Deng Y., Chen G. Toward a practical Li-S battery enabled by synergistic confinement of a nitrogen-enriched porous carbon as a multifunctional interlayer and sulfur-host material. *J Electroanal Chem* 2020;858:113797. doi:10.1016/j.jelechem.2019.113797.
- [190] Zhang S.S. Heteroatom-doped carbons: synthesis, chemistry and application in lithium/sulphur batteries. *Inorg Chem Front* 2015;2:1059–1069. doi:10.1039/C5QI00153F.

- [191] Aditya H.B., Mahlia T.M.I., Chong W.T., Nur H., Sebayang A.H. Second generation bioethanol production: a critical review. *Renew Sustain Energy Rev* 2016;66:631–653. doi:10.1016/j.rser.2016.07.015.
- [192] Li J., Qin F., Zhang L., Zhang K., Li Q., Lai Y., et al. Mesoporous carbon from biomass: one-pot synthesis and application for Li–S batteries. *J Mater Chem* 2014;2:13916. doi:10.1039/C4TA02154A.
- [193] Schipper F., Vizintin A., Ren J., Dominko R., Fellingner T.-P. Biomass-derived heteroatom-doped carbon aerogels from a salt melt sol-gel synthesis and their performance in Li-S batteries. *ChemSusChem* 2015;8:3077–3083. doi:10.1002/cssc.201500832.
- [194] Yu Q., Lu Y., Peng T., Hou X., Luo R., Wang Y., et al. Construction of tubular polypyrrole-wrapped biomass-derived carbon nanospheres as cathode materials for lithium–sulfur batteries. *J Phys D Appl Phys* 2017;50:115002. doi:10.1088/1361-6463/aa5ade.
- [195] Chabu J.M., Li Y., Liu Y. Biomass-derived N, O, and S-tridoped hierarchically porous carbon as a cathode for Lithium–Sulfur batteries. *ChemNanoMat* 2019;5:612–618. doi:10.1002/cnma.201800662.
- [196] Gao Z., Song N., Zhang Y., Schwab Y., He J., Li X. Carbon nanotubes derived from yeast-fermented wheat flour and their energy storage application. *ACS Sustainable Chem Eng* 2018;6:11386–11396. doi:10.1021/acssuschemeng.8b01292.
- [197] Hong X., Liu Y., Fu J., Wang X., Zhang T., Wang S., et al. A wheat flour derived hierarchical porous carbon/graphitic carbon nitride composite for high-performance lithium–sulfur batteries. *Carbon N Y* 2020;170:119–126. doi:10.1016/j.carbon.2020.08.032.
- [198] Wang W., Zhao Y., Zhang Y., Liu N., Bakenov Z. Nickel embedded porous macrocellular carbon derived from popcorn as sulfur host for high-performance lithium-sulfur batteries. *J Mater Sci Technol* 2021;74:69–77. doi:10.1016/j.jmst.2020.09.032.
- [199] Faheem M., Li W., Ahmad N., Yang L., Tufail M.K., Zhou Y., et al. Chickpea derived Co nanocrystal encapsulated in 3D nitrogen-doped mesoporous carbon: pressure cooking synthetic strategy and its application in lithium-sulfur batteries. *J Colloid Interface Sci* 2021;585:328–336. doi:10.1016/j.jcis.2020.11.050.
- [200] Qu Y., Zhang Z., Zhang X., Ren G., Lai Y., Liu Y., et al. Highly ordered nitrogen-rich mesoporous carbon derived from biomass waste for high-performance lithium–sulfur batteries. *Carbon N Y* 2015;84:399–408. doi:10.1016/j.carbon.2014.12.001.
- [201] Xia L., Song Z., Zhou L., Lin D., Zheng Q. Nitrogen and oxygen dual-doped hierarchical porous carbon derived from rapeseed meal for high performance lithium–sulfur batteries. *J Solid State Chem* 2019;270:500–508. doi:10.1016/j.jssc.2018.12.031.
- [202] Wen X., Lu X., Xiang K., Xiao L., Liao H., Chen W., et al. Nitrogen/sulfur co-doped ordered carbon nanoarrays for superior sulfur hosts in lithium-sulfur batteries. *J Colloid Interface Sci* 2019;554:711–721. doi:10.1016/j.jcis.2019.07.057.
- [203] Thangavel R., Kannan A.G., Ponraj R., Kaliyappan K., Yoon W.-S., Kim D.-W., et al. Cinnamon-derived hierarchically porous carbon as an effective lithium polysulfide reservoir in lithium–sulfur batteries. *Nanomaterials* 2020;10:1220. doi:10.3390/nano10061220.
- [204] Kalaiappan K., Rengapillai S., Marimuthu S. Clout of carbon in polyacrylonitrile/sulfur composite cathode via solution processing technique for lithium-sulfur batteries. *J Porous Mater* 2020;27:1837–1845. doi:10.1007/s10934-020-00963-4.
- [205] Wu D., Chen J., Zhang W., Liu W., Li J., Cao K., et al. Sealed pre-carbonization to regulate the porosity and heteroatom sites of biomass derived carbons for lithium-sulfur batteries. *J Colloid Interface Sci* 2020;579:667–679. doi:10.1016/j.jcis.2020.06.068.
- [206] Li Y., Liu L., Shi R., Yang S., Zhao C., Shi Y., et al. Natural okra shells derived nitrogen-doped porous carbon to regulate polysulfides for high-performance lithium–sulfur batteries. *Energy Technol* 2019. doi:10.1002/ente.201900165.
- [207] Li B., Xie M., Yi G., Zhang C. Biomass-derived activated carbon/sulfur composites as cathode electrodes for Li–S batteries by reducing the oxygen content. *RSC Adv* 2020;10:2823–2829. doi:10.1039/C9RA09610H.
- [208] Lee S.-Y., Choi Y., Kim J.-K., Lee S.-J., Bae J.S., Jeong E.D. Biomass-garlic-peel-derived porous carbon framework as a sulfur host for lithium-sulfur batteries. *J Ind Eng Chem* 2021;94:272–281. doi:10.1016/j.jiec.2020.10.046.
- [209] Yang K., Gao Q., Tan Y., Tian W., Qian W., Zhu L., et al. Biomass-derived porous carbon with micropores and small mesopores for high-performance lithium-sulfur batteries. *Chem Eur J* 2016;22:3239–3244. doi:10.1002/chem.201504672.
- [210] Geng Z., Xiao Q., Wang D., Yi G., Xu Z., Li B., et al. Improved electrochemical performance of biomass-derived nanoporous carbon/sulfur composites cathode for lithium-sulfur batteries by nitrogen doping. *Electrochim Acta* 2016;202:131–139. doi:10.1016/j.electacta.2016.03.176.
- [211] Li H., Ma S., Cai H., Zhou H., Huang Z., Hou Z., et al. Ultra-thin Fe<sub>3</sub>C nanosheets promote the adsorption and conversion of polysulfides in lithium-sulfur batteries. *Energy Storage Mater* 2019;18:338–348. doi:10.1016/j.ensm.2018.08.016.
- [212] Moreno N., Caballero Á., Morales J., Rodríguez-Castellón E. Improved performance of electrodes based on carbonized olive stones/S composites by impregnating with mesoporous TiO<sub>2</sub> for advanced Li–S batteries. *J Power Sources* 2016;313:21–29. doi:10.1016/j.jpowsour.2016.02.061.
- [213] Luna-Lama F., Hernández-Rentero C., Caballero A., Morales J. Biomass-derived carbon/ $\gamma$ -MnO<sub>2</sub> nanorods/S composites prepared by facile procedures with improved performance for Li/S batteries. *Electrochim Acta* 2018;292:522–531. doi:10.1016/j.electacta.2018.09.176.
- [214]

- [215] Liu J., Xiao S.H., Zhang Z., Chen Y., Xiang Y., Liu X., et al. Naturally derived honeycomb-like N,S-codoped hierarchical porous carbon with MS<sub>2</sub> (M = Co, Ni) decoration for high-performance Li-S battery. *Nanoscale* 2020;12:5114–5124. doi:10.1039/C9NR10419D.
- [216] Jing S., Ding P., Zhang Y., Liang H., Yin S., Tsiakaras P. Lithium-sulfur battery cathodes made of porous biochar support CoFe@NC metal nanoparticles derived from Prussian blue analogues. *Ionics* 2019. doi:10.1007/s11581-019-03065-7.
- [217] Chen Z.-H., Du X.-L., He J.-B., Li F., Wang Y., Li Y.-L., et al. Porous coconut shell carbon offering high retention and deep lithiation of sulfur for lithium-sulfur batteries. *ACS Appl Mater Interfaces* 2017;9:33855–33862. doi:10.1021/acsami.7b09310.
- [218] Benítez A., Márquez P., Martín M.Á., Caballero A. Simple and sustainable preparation of cathodes for Li-S batteries: regeneration of granular activated carbon from the odor control system of a wastewater treatment plant. *ChemSusChem* 2021;14:1–12. doi:10.1002/cssc.202101231.
- [219] Zhu Y., Xu G., Zhang X., Wang S., Li C., Wang G. Hierarchical porous carbon derived from soybean hulls as a cathode matrix for lithium-sulfur batteries. *J Alloys Compd* 2017;695:2246–2252. doi:10.1016/j.jallcom.2016.11.075.
- [220] Selvan R.K., Zhu P., Yan C., Zhu J., Dirican M., Shanmugavani A., et al. Biomass-derived porous carbon modified glass fiber separator as polysulfide reservoir for Li-S batteries. *J Colloid Interface Sci* 2018;513:231–239. doi:10.1016/j.jcis.2017.11.016.
- [221] Chen H., Xia P., Lei W., Pan Y., Zou Y., Ma Z. Preparation of activated carbon derived from biomass and its application in lithium-sulfur batteries. *J Porous Mater* 2019. doi:10.1007/s10934-019-00720-2.
- [222] Benítez A., Morales J., Caballero Á. Pistachio shell-derived carbon activated with phosphoric acid: a more efficient procedure to improve the performance of Li-S batteries. *Nanomaterials* 2020;10:840. doi:10.3390/nano10050840.
- [223] Liu D., Li Q., Hou J., Zhao H. Porous 3D graphene-based biochar materials with high areal sulfur loading for lithium-sulfur batteries. *Sustain Energy Fuels* 2018;2:2197–2205. doi:10.1039/C8SE00343B.
- [224] Xiao Q., Li G., Li M., Liu R., Li H., Ren P., et al. Biomass-derived nitrogen-doped hierarchical porous carbon as efficient sulfur host for lithium-sulfur batteries. *J Energy Chem* 2020;44:61–67. doi:10.1016/j.jechem.2019.09.004.
- [225] Zhu L., Jiang H., Ran W., You L., Yao S., Shen X., et al. Turning biomass waste to a valuable nitrogen and boron dual-doped carbon aerogel for high performance lithium-sulfur batteries. *Appl Surf Sci* 2019;489:154–164. doi:10.1016/j.apsusc.2019.05.333.
- [226] Benítez A., González-Tejero M., Caballero Á., Morales J. Almond shell as a microporous carbon source for sustainable cathodes in lithium-sulfur batteries. *Materials* 2018;11:1428. doi:10.3390/ma11081428.
- [227] Hernández-Rentero C., Córdoba R., Moreno N., Caballero A., Morales J., Olivares-Marín M., et al. Low-cost disordered carbons for Li/S batteries: a high-performance carbon with dual porosity derived from cherry pits. *Nano Res* 2018;11:89–100. doi:10.1007/s12274-017-1608-1.
- [228] Marangon V., Hernández-Rentero C., Olivares-Marín M., Gómez-Serrano V., Caballero Á., Morales J., et al. A stable high-capacity lithium-ion battery using a biomass-derived sulfur-carbon cathode and lithiated silicon anode. *ChemSusChem* 2021;14:3333–3343. doi:10.1002/cssc.202101069.
- [229] Fawaz W., Mosavati N., Abdelhamid E., Simon Ng K.Y. Synthesis of activated carbons derived from avocado shells as cathode materials for lithium-sulfur batteries. *SN Appl Sci* 2019;1:289. doi:10.1007/s42452-019-0300-3.
- [230] Leng S., Chen C., Liu J., Wang S., Yang J., Shan S., et al. Optimized sulfur-loading in nitrogen-doped porous carbon for high-capacity cathode of lithium-sulfur batteries. *Appl Surf Sci* 2019;487:784–792. doi:10.1016/j.apsusc.2019.05.206.
- [231] Chen X., Du G., Zhang M., Kalam A., Su Q., Ding S., et al. Nitrogen-doped hierarchical porous carbon derived from low-cost biomass pomegranate residues for high performance lithium-sulfur batteries. *J Electroanal Chem* 2019;848:113316. doi:10.1016/j.jelechem.2019.113316.
- [232] Arie A.A., Kristianto H., Cengiz E.C., Demir-Cakan R. Activated porous carbons originated from the Indonesian snake skin fruit peel as cathode components for lithium sulfur battery. *Ionics* 2019;25:2121–2129. doi:10.1007/s11581-018-2712-2.
- [233] Kim B., Park J., Baik S., Lee J.W. Spent coffee derived hierarchical porous carbon and its application for energy storage. *J Porous Mater* 2020;27:451–463. doi:10.1007/s10934-019-00826-7.
- [234] Han X.-R., Guo X.-T., Xu M.-J., Pang H., Ma Y.-W. Clean utilization of palm kernel shell: sustainable and naturally heteroatom-doped porous activated carbon for lithium-sulfur batteries. *Rare Met* 2020;39:1099–1106. doi:10.1007/s12598-020-01439-9.
- [235] Arie A.A., Kristianto H., Cengiz E.C., Demir-Cakan R. Waste tea-based porous carbon-sulfur composite cathodes for lithium-sulfur battery. *Ionics* 2020;26:201–212. doi:10.1007/s11581-019-03196-x.
- [236] Rojas M. del C., Nieva Lobos M.L., Para M.L., González Quijón M.E., Cámara O., Barraco D., et al. Activated carbon from pyrolysis of peanut shells as cathode for lithium-sulfur batteries. *Biomass Bioenergy* 2021;146:105971. doi:10.1016/j.biombioe.2021.105971.
- [237] Arie A.A., Kristianto H., Susanti R.F., Lee J.K. Rambutan peel derived porous carbons for lithium sulfur battery. *SN Appl Sci* 2021;3:541. doi:10.1007/s42452-021-04540-5.

- [238] Xue M., Xu H., Tan Y., Chen C., Li B., Zhang C. A novel hierarchical porous carbon derived from durian shell as enhanced sulfur carrier for high performance Li-S batteries. *J Electroanal Chem* 2021;893:115306. doi:10.1016/j.jelechem.2021.115306.
- [239] Benítez A., Caballero Á., Rodríguez-Castellón E., Morales J., Hassoun J. The role of current collector in enabling the high performance of Li/S battery. *ChemistrySelect* 2018;3:10371–10377. doi:10.1002/slct.201802529.
- [240] Benítez A., Luna-Lama F., Caballero A., Rodríguez-Castellón E., Morales J. Contribution to the understanding of the performance differences between commercial current collectors in Li-S batteries. *J Energy Chem* 2021;62:295–306. doi:10.1016/j.jechem.2021.03.014.
- [241] Han J., Chen X., Xi B., Mao H., Feng J., Xiong S. High-surface-area nitrogen/phosphorus dual-doped hierarchical porous carbon derived from biochar for sulfur holder. *ChemistrySelect* 2018;3:10175–10181. doi:10.1002/slct.201802296.
- [242] Xia Y., Fang R., Xiao Z., Huang H., Gan Y., Yan R., et al. Confining sulfur in N-doped porous carbon microspheres derived from microalgae for advanced lithium-sulfur batteries. *ACS Appl Mater Interfaces* 2017;9:23782–23791. doi:10.1021/acsami.7b05798.
- [243] Zhao Y., Zhang X., He Y., Liu N., Tan T., Liang C. Biomass derived nitrogen-doped highly porous carbon material with a hierarchical porous structure for high-performance lithium/sulfur batteries. *Materials* 2017;10:1158. doi:10.3390/ma10101158.
- [244] Hencz L., Gu X., Zhou X., Martens W., Zhang S. Highly porous nitrogen-doped seaweed carbon for high-performance lithium-sulfur batteries. *J Mater Sci* 2017. doi:10.1007/s10853-017-1288-y.
- [245] Huang M., Yang J., Xi B., Mi K., Feng Z., Liu J., et al. Enhancing kinetics of Li-S batteries by graphene-like N,S-codoped biochar fabricated in NaCl non-aqueous ionic liquid. *Sci China Mater* 2019;62:455–464. doi:10.1007/s40843-018-9331-x.
- [246] Ma L., Lin H., Zhang W., Zhao P., Zhu G., Hu Y., et al. Nitrogen-doped carbon nanotube forests planted on cobalt nanoflowers as polysulfide mediator for ultralow self-discharge and high areal-capacity lithium-sulfur batteries. *Nano Lett* 2018;18:7949–7954. doi:10.1021/acs.nanolett.8b03906.
- [247] Shi J., Kang Q., Mi Y., Xiao Q. Nitrogen-doped hollow porous carbon nanotubes for high-sulfur loading Li-S batteries. *Electrochim Acta* 2019;324:134849. doi:10.1016/j.electacta.2019.134849.
- [248] Li D., Chang G., Zong L., Xue P., Wang Y., Xia Y., et al. From double-helix structured seaweed to S-doped carbon aerogel with ultra-high surface area for energy storage. *Energy Storage Mater* 2019;17:22–30. doi:10.1016/j.ensm.2018.08.004.
- [249] Ji S., Imtiaz S., Sun D., Xin Y., Li Q., Huang T., et al. Coralline-like N-doped hierarchically porous carbon derived from Enteromorpha as a host matrix for lithium-sulfur battery. *Chem Eur J* 2017;23:18208–18215. doi:10.1002/chem.201703357.
- [250] Liang C., Zhang X., Zhao Y., Tan T., Zhang Y., Chen Z. Preparation of hierarchical porous carbon from waterweed and its application in lithium/sulfur batteries. *Energies* 2018;11:1535. doi:10.3390/en11061535.
- [251] Li G., Wang M., Huang J., Bao N., Xue J., Liu Q., et al. Preparation of activated carbon from *Iris tectorum* with different ammonium phosphates activation and removal of nickel from aqueous solution. *J Taiwan Inst Chem Eng* 2016;59:341–347. doi:10.1016/j.jtice.2015.08.013.
- [252] Benaddi H., Badosz T., Jagiello J., Schwarz J., Rouzaud J., Legras D., et al. Surface functionality and porosity of activated carbons obtained from chemical activation of wood. *Carbon N Y* 2000;38:669–674. doi:10.1016/S0008-6223(99)00134-7.
- [253] Zhang X.Q., Cui Y.L., Zhong Y., Wang D.H., Tang W.J., Wang X.L., et al. Cobalt disulfide-modified cellular hierarchical porous carbon derived from bovine bone for application in high-performance lithium-sulfur batteries. *J Colloid Interface Sci* 2019;551:219–226. doi:10.1016/j.jcis.2019.04.079.
- [254] Wang K., Shi L., Wang M., Yang H., Liu Z., Peng H. Biomass hydroxyapatite-templated synthesis of 3D graphene. *Acta Phys Chim Sin* 2019;35:1112–1118. doi:10.3866/PKU.WHXB201805032.
- [255] Ai F., Liu N., Wang W., Wang A., Wang F., Zhang H., et al. Heteroatoms-doped porous carbon derived from Tuna bone for high performance Li-S batteries. *Electrochim Acta* 2017;258:80–89. doi:10.1016/j.electacta.2017.10.076.
- [256] Ren J., Xia L., Zhou Y., Zheng Q., Liao J., Lin D. A reduced graphene oxide/nitrogen, phosphorus doped porous carbon hybrid framework as sulfur host for high performance lithium-sulfur batteries. *Carbon N Y* 2018;140:30–40. doi:10.1016/j.carbon.2018.08.026.
- [257] Ren J., Zhou Y., Wu H., Xie F., Xu C., Lin D. Sulfur-encapsulated in heteroatom-doped hierarchical porous carbon derived from goat hair for high performance lithium-sulfur batteries. *J Energy Chem* 2019;30:121–131. doi:10.1016/j.jechem.2018.01.015.
- [258] Song Z., Lu X., Hu Q., Ren J., Zhang W., Zheng Q., et al. Synergistic confining polysulfides by rational design a N/P co-doped carbon as sulfur host and functional interlayer for high-performance lithium-sulfur batteries. *J Power Sources* 2019;421:23–31. doi:10.1016/j.jpowsour.2019.03.003.
- [259] Ren M., Lu X., Chai Y., Zhou X., Ren J., Zheng Q., et al. A three-dimensional conductive cross-linked all-carbon network hybrid as a sulfur host for high performance lithium-sulfur batteries. *J Colloid Interface Sci* 2019;552:91–100. doi:10.1016/j.jcis.2019.05.042.
- [260] Yu M., Li R., Tong Y., Li Y., Li C., Hong J.-D., et al. A graphene wrapped hair-derived carbon/sulfur composite for lithium-sulfur batteries. *J Mater Chem* 2015;3:9609–9615. doi:10.1039/C5TA00651A.
- [261]

Chung S.-H., Manthiram A. Carbonized eggshell membrane as a natural polysulfide reservoir for highly reversible Li-S batteries. *Adv Mater* 2014;26:1360–1365. doi:10.1002/adma.201304365.

[262] Zhang Y., Gao Z., Li X. Capillarity composited recycled paper/graphene scaffold for lithium-sulfur batteries with enhanced capacity and extended lifespan. *Small* 2017;13:1701927. doi:10.1002/sml.201701927.

[263] Lai Y., Wang P., Li J., Zhang K., Zhang Z. Chemically tailoring porosity carbon foam with oxygen-containing functional groups to restrain polysulfide for lithium-sulfur batteries. *J Electroanal Chem* 2017;805:120–125. doi:10.1016/j.jelechem.2017.09.065.

[264] Li L., Huang L., Linhardt R.J., Koratkar N., Simmons T. Repurposing paper by-product liginosulfonate as a sulfur donor/acceptor for high performance lithium–sulfur batteries. *Sustain Energy Fuels* 2018;2:422–429. doi:10.1039/C7SE00394C.

[265] Zhong M., Guan J., Sun J., Guo H., Xiao Z., Zhou N., et al. Carbon nanodot-decorated alveolate N, O, S tridoped hierarchical porous carbon as efficient electrocatalysis of polysulfide conversion for lithium-sulfur batteries. *Electrochim Acta* 2019. doi:10.1016/j.electacta.2019.01.024.

[266] Tesio A.Y., Gómez-Cámer J.L., Morales J., Caballero A. Simple and sustainable preparation of nonactivated porous carbon from brewing waste for high-performance lithium–sulfur batteries. *ChemSusChem* 2020;13:3439–3446. doi:10.1002/cssc.202000969.

---

## Highlights

- The use of biomass and biowaste in Li-S batteries is reviewed.
- Carbonaceous and activated carbons are discussed as sulfur hosts.
- Woody, agricultural, aquatic, animal and industrial biomass waste is evaluated.
- Critical parameters are defined for further progress in the field.

---

## Queries and Answers

Q1

**Query:** Please confirm that the provided **emails** “daniel.brandell@kemi.uu.se, q62betao@uco.es” are the correct address for official communication, else provide an alternate e-mail address to replace the existing one, because private e-mail addresses should not be used in articles as the address for communication.

**Answer:** Reviewed

Q2

**Query:** Note: The author's **telephone/fax number** has been removed as these are not published in journal articles.

**Answer:** Done

Q3

**Query:** Have we correctly interpreted the following funding source(s) and country names you cited in your article: Ministry of Science, Innovation and Universities, Spain; Ministerio de Economía y Competitividad, Spain?

**Answer:** The acknowledgments section has been corrected. Finally, it will appear as: "Ministerio de Ciencia, Innovación y Universidades

Q4

**Query:** Please confirm that **given names and surnames** have been identified correctly and are presented in the desired order and please carefully verify the spelling of all authors' names.

**Answer:** Reviewed

Q5

**Query:** Your article is registered as a regular item and is being processed for inclusion in a regular issue of the journal. If this is NOT correct and your article belongs to a Special Issue/Collection please contact d.perumal@elsevier.com immediately prior to returning your corrections.

**Answer:** The article is a regular issue

**Query:** For figure(s) 13,18, The supplied source image has very low resolution (not enough pixels for the print size) and the visual quality is not sufficient. Please provide us with an image that has a minimum resolution of 300 dpi and with a proper print size (typically we need 900 pixels wide for an image that fits a single column). For more information, refer to <https://www.elsevier.com/authors/author-schemas/artwork-and-media-instructions/artwork-sizing>.

**Answer:** The resolution of Figures 13 and 18 has been improved. In addition, other figures have been replaced by others of higher quality.